VAPEX Experiments
in an Annular Packing of Glass Beads
and the Numerical Simulation of VAPEX using Comsol®

by

Sindy Pui Yin Tam

A thesis

presented to the University of Waterloo

in fulfilment of the

thesis requirement for the degree of

Master of Applied Science

in

Chemical Engineering

Waterloo , Ontario, Canada, 2007

I hereby declare that I am the sole author of this thesis. This is a true copy of the thesis, including any required final revisions, as accepted by my examiners.

I understand that my thesis may be made electronically available to the public.

Abstract

Vapour Extraction (VAPEX) is an in-situ bitumen recovery technique that utilizes light hydrocarbons to reduce the viscosity of bitumen. The mechanism of VAPEX is governed by the mass transfer of light hydrocarbons into bitumen and gravity drainage. The focus of this research is three-fold: 1) to validate a new annulus apparatus design 2) to investigate the effect of connate water and solvent condensation on live oil and bitumen production rates, solvent chamber growth, and solvent requirements, and 3) to develop a numerical model to simulate the solvent chamber growth of VAPEX under isothermal conditions and constant pressure operation.

The new annulus apparatus design has a pay zone of 1 m height with 0.64cm annular opening /width. The new design is a two-sided production apparatus with approximately 10 cm depth each side. The cylindrical "visual cell" design offers superior pressure handling capability and allows for a clear visualization of the pay zone to study the production rate and the solvent chamber growth of VAPEX. The solvent was distributed using an injection tube as a line source to mimic the pathway created during the chamber rising phase, i.e. once communication between the injection well an top of the pay zone is established. Production histories from the new apparatus agreed within 16% to that predicted from Oduntan's scale up model, verifying the feasibility of the apparatus in replicating data from previous experiments.

Four experiments were conducted using unconsolidated porous media with permeabilities of 1.123×10^{-9} m^2 and 3×10^{-10} m^2 and butane as the solvent to study the effect of low percentage volume of connate water on the production histories, the solvent chamber growth and the solvent requirements in VAPEX. The butane supply was maintained 1-2^{o}C below ambient temperature to avoid solvent condensation and asphaltene precipitation. Production histories indicated that the difference in the live oil and the bitumen production rates between the experiments with and without connate water was less then 15%. Furthermore, the interface profiles traced during the experiments showed that the effect of connate water on the average horizontal interface advancement velocity was less than 10%, which is insignificant. Live oil samples indicated the solvent mass fraction in live oil increased as permeability decreased,

due to the extended exposure time for butane to diffuse into bitumen during lower gravity drainage rate in low permeability systems.

In addition to the VAPEX experiments described above, a warm VAPEX experiment was conducted using the annulus apparatus. The solvent supply vessel was maintained at 2-3^{o}C above the ambient temperature to enhance solvent condensation in the apparatus. The live oil production rate doubled in the warm VAPEX experiment compared to that of the normal VAPEX experiment, and the average horizontal interface velocity increased by over 30%. Furthermore, asphaltene precipitation was observed during the experiment, indicating in-situ upgrading of bitumen.

A new numerical model for VAPEX was developed to address certain limitations of the existing numerical simulation models. Instead of separating the bitumen and the live oil into two liquid phases by solvent concentration, the new model considered them as one oil phase. As a result, the new model does not require a predefined moving boundary condition to act as the bitumen solvent interface.

The numerical model of VAPEX was developed using Comsol® 3.3, which is a commercial finite element numerical simulation software with predefined engineering and mathematical equations. The new model used the convection diffusion equation for a variable saturation system and Darcy's equation to evaluate both the liquid saturation and the solvent chamber growth of the control volume. Comparisons of the numerical simulation results and the results from the experiment indicated that the discrepancy in the bitumen production rate and the horizontal interface velocity was less than 12%. This difference is not significant. It is concluded that the numerical model was successful in simulating the production history and the solvent chamber growth of the VAPEX experiment.

Acknowledgements

I would like to thank all those who helped me throughout my master's studies. Special thanks go to:

- Dr. John Chatzis, my supervisor and my mentor, for his continuous guidance and support throughout my master's studies.
- Dr. Mario Ioannidis for his motivation and guidance in the development of the VAPEX numerical model.
- Dr. Ehsan Toyserkani for sharing his knowledge and his expertise in Comsol 3.3
- The Chemical Engineering staff, Liz Bevan, Pat Anderson, Bert Habicher, Ralph Dickhout, Ravindra Singh and Dennis Herman, for their help and advice in all administrative and technical issues
- The Mechanical Engineering Machine Shop for manufacturing my apparatus
- Nima Rezaie and Lesley James, my friends and colleagues, for their assistance with the experiments and the numerical simulations, and for their motivational support.
- Last but not least, my parents, for loving me, for believing in me and for supporting me in pursuit of my dreams

Nomenclature

Symbol	Definition	Units
a_i	Specific interfacial area	m^{-1}
c_s	Mass concentration of solvent in bitumen	kg/m^3, g/cm^3
C_{vB}, C_{vS}	Volume fraction of bitumen and solvent respectively	
C_p	Storage term	
D	downward distance of model	m
D_m	Molecular diffusivity	m^2/s
D_L, D_T	Longitudinal and transverse dispersion	m^2/s
D_i, D_{SB}	Mechanic and hydrodynamic dispersion	m^2/s
D_{ap}, D_{eff}	Apparent and effective diffusivity	m^2/s
D_p	Particles diameter	m
f_s, f_B	Compositional factor for solvent and bitumen respectively	
g	Acceleration by gravity	m/s^2
h	Height	m
H_p	Capillary pressure head	m
J_m	Mass transfer correlation	
k	Absolute permeability	m^2
k_{rg}, k_{ro}, k_{rs}	Relative permeability of oil, gas and solvent	
K_m	Mass transfer coefficient	m/s
L	Length of payzone	m
m_B, m_s, m_w	Mass of bitumen, solvent and water, respectively	g
N_{LO}	Cumulative production of live oil	m^3, cm^3
N_B	Cumulative production of bitumen	g
Ns	VAPEX parameter (Butler and Mokrys, 1989)	
Pc	Capillary pressure	Pa
Pe	Peclet number	
P_o	Pressure of oil phase	Pa
Q_{LO}	Live oil production rate	cm^3/min
Q_B	Bitumen production rate	g/min
Re`	Interstitial Reynolds number	
R_o	Radius of the apparatus outer cylinder	cm
R_s	Average radius of the apparatus slit	cm
S_o, S_s, S_g	Saturation of oil, solvent and gas respectively	
S_L	Average liquid phase saturation of the control volume	
S_{eo}, S_{eg}	Effective saturation of oil and gas respectively	
Sh*	Modified Sherwood number	
t	time	s
u	Horizontal velocity of fluid flow	m/s
v	Vertical velocity of fluid flow	m/s
v_{pv}, v_{pvx}, v_{pvy}	Interstitial velocity. Interstitial velocity in the x and y	m/s

	directions.	
v_H	Horizontal interface velocity	cm/min
v_{HO}	Horizontal interface velocity observed from the outer cylinder	cm/min
V_i	Initial volume of oil in control volume	cm^3, m^3
V_{N2}	Volume of nitrogen	cm^3, m^3
V_{pv}	Pore volume	cm^3, m^3
V_t	Total volume of the apparatus	cm^3, m^3

*Note: SI base unit (kg, m^3, s) are used for the numerical simulation and the cgs system is generally used for experiments with the exception of minutes instead of seconds are used.

Greek Symbols

Symbol	Definition	Units
α_L, α_T	Longitudinal and transverse dispersion coefficient	m, cm
ΔS_o	Change in saturation	
γ	Interfacial tension	Dynes/cm
ϕ	Porosity	
μ	Viscosity	kg/m.s
ρ	density	kg/m^3 , g/cm^3
Ω	Cementation factor	
θ	Fluid fraction	
ω	Mass fraction	
$\delta_{st}, \delta_k, \delta_Q,$	Time scaling factor, flux scaling factor and source scaling factor	

Subscripts

Symbol	Description
B	Bitumen
eff	effective
g	Gas
L	Longitudinal
LO	Live oil
mix	mixture
o	Oil
pv	Pore volume
s	Solvent
T	Transverse
w	Water
x	x- direction
y	y- direction

Table of Contents

List of Figures:

List of Tables

1.0 Introduction

Heavy oil and bitumen are defined as crude oil with high viscosity and low ^{o}API gravity. In general, crude oil with a viscosity (μ) $\geq$ 1 kg/m.s or ^{o}API $\leq$ 20 is classified as heavy oil, and crude oil with $\mu \geq$10 kg/m.s and ^{o}API $\leq$10 is classified as bitumen. (Singhal et. al.,1996). As the world's reserves for sweet crude oil decline rapidly and demands for petroleum resources continue to increase, the role of heavy oil and bitumen is crucial to the future of the world's petroleum supply.

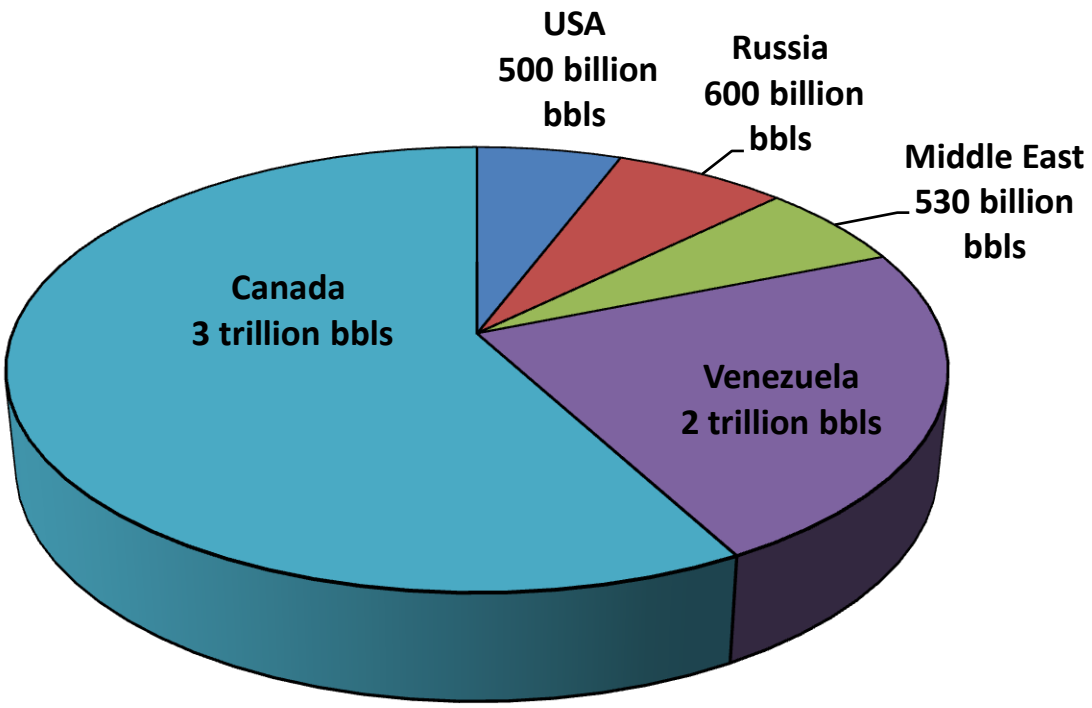

Figure 1-1: Distribution of the world's heavy oil reserves (Sedaee Sola and Rashidi, 2006)

The world's proven reserves for non-conventional oil are approximately 8 trillion barrels, approximately 3 times larger than the world's reserves of conventional oil (Dusseault, 2006). As techniques in heavy oil recovery improve over time, the world's proven reserves for non conventional oil are expected to increase as well. Out of the total 8 trillion barrels of non

conventional oil reserves, Canada and Venezuela possess 3 trillion and 2 trillion barrels respectively. Even though Canada has most of the heavy oil reserves in the world, the high in-situ viscosity and the low ^{o}API gravity makes their recovery a challenge.

1.1 Recovery of Heavy oil

The world's reserves of non-conventional oil are approximately 3 times that of conventional oil, but only 13% of the world's crude oil production is non-conventional oil. The high capital investment and high operation cost in heavy oil recovery are the reasons. In Canada, in order to sustain an economical heavy oil production operation, the price of crude oil must remain well above $25 per barrel (Dusseault, 2006).

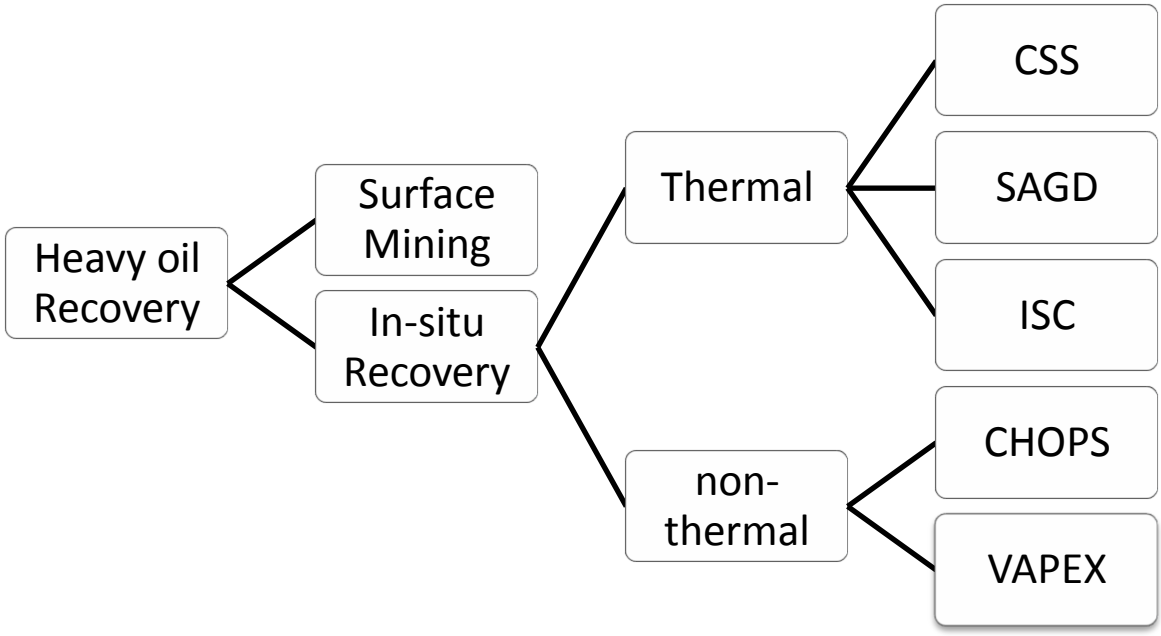

Figure 1-2: Heavy oil exploration techniques

Techniques in heavy oil and bitumen recovery can be divided into two main categories: surface mining and in-situ. Surface mining can recover up to 75% of the bitumen; however, it is only applicable to reservoirs of less than 75 m deep from the surface. Only 5-10% of the Canadian heavy oil reserves can be recovered using this technique.

The development of new in-situ heavy oil recovery techniques have emerged quickly over the past several decades. Progress is fuelled by the improvement in oil field technologies

such as the drilling of horizontal wells and the invention of progressive cavity pumps. Cold heavy oil production yields approximately 1-5% OOIP (original oil in place) under ideal circumstance. Water flooding may improve the recovery by 1-2%, but the high mobility ratio between water and heavy oil results in early water breakthrough and uneconomical water cut (Dusseault, 2006).

Cold heavy oil production with sand (CHOPS) is a common recovery technique for heavy oil reservoirs. Traditionally, sand production is undesirable in conventional oil production. Production data from heavy oil fields indicate the recovery of heavy oil increasing from 1-5% OOIP for cold production wells to 10-20% for CHOPS wells. In addition, the production rate of CHOPS wells increases from 5-10 b/day (cold production) to 100-400 b/day (CHOPS). Evidence indicates CHOPS is most suitable for reservoirs with a pay zone less than 15 m and with no free bottom water.

Cyclic steam stimulation (CSS), steam assisted gravity drainage (SAGD) and in-situ combustion (ISC) all use thermal energy in reducing the viscosity of the heavy oil. CSS and SAGD are the most commonly used in-situ heavy oil recovery techniques. They require an injection of steam into the reservoir to reduce the viscosity of bitumen. The major concern with steam injection techniques is the energy efficiency and recovery factor. CSS uses one thermal resistance vertical well for both steam injection and oil production. The process for a CSS operation is divided into three steps: 1) Steam injection 2) steam soaking 3) heated oil production.

CSS is a pressure driven process. The recovery factor of CSS rarely exceeds 20% OOIP due to high energy consumption and possible gas coning. The ideal conditions for CSS operations are reservoirs with pay zone > 15 m and with no free bottom water. On the other hand, SAGD is a continuous steam injection operation that is driven by gravity drainage (Figure 1-4). Steam injected into the reservoir rises to the top of the formation and the heated bitumen is produced by gravity. The recovery factor in SAGD operation depends on the steam oil ratio. In the best scenario, the recovery factor of SAGD can exceed 70% OOIP. However, the disadvantage of SAGD is the huge capital investment. In addition to the steam generation plant, a pair of thermal resistance horizontal wells is needed for SAGD operation (one for steam injection and one for bitumen production). The distance between SAGD wells

pair depends on the thickness of the pay zone. For example, in a reservoir with 20 m pay zone, SAGD well pairs are drilled every 80 m apart. The thinner the pay zone, the more horizontal well pairs are needed for SAGD operations; therefore, SAGD is generally recommended for reservoirs with at least 20 m of pay zone.

In-situ combustion is an emerging heavy oil recovery technique. The concept is to start a combustion front in the reservoir by injecting O_2 or air into the formation. Theoretically, this concept is ideal because no additional energy is required, unlike SAGD and CSS. The process burns part of the oil in reservoir and produces the rest of it. In reality, almost all of the ISC field trials failed because of gravity segregation of the gas injected. Injected gas tends to rise to the top of the reservoir. This encourages gas channelling near the top of the reservoir. Lack of control in the combustion front results in early gas breakthrough and a low recovery factor.

VAPEX is a non thermal miscible technique for enhancing heavy oil recovery. Light hydrocarbon gas is injected into the reservoir to reduce the viscosity of the bitumen and the diluted oil is produced by gravity. The main advantage of VAPEX is the low energy requirement; therefore, VAPEX is highly desirable in thinner reservoirs where SAGD and CSS are uneconomical. Details of the VAPEX mechanism are discussed in later sections.

1.2 Mechanisms of VAPEX

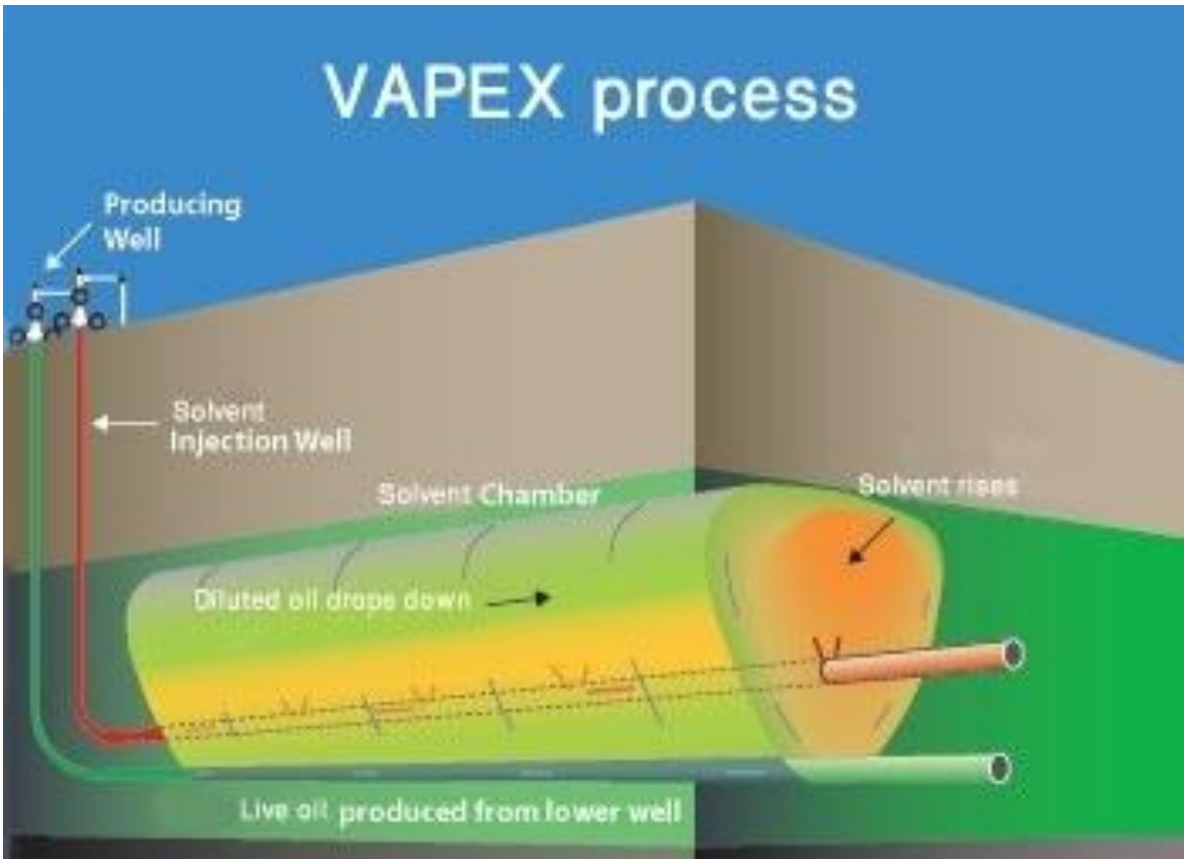

Figure 1-3: Schematic of the VAPEX process. Picture modified from CONNACHER oil and gas Limited. (2007)

VAPEX is a solvent analogue of SAGD. It uses light hydrocarbon as solvent instead of heat to reduce the viscosity of bitumen. Both processes share similar concepts and configurations. They both use two horizontal wells, one for solvent or steam injection and one for oil production. In VAPEX, light hydrocarbons are injected for reduction of bitumen viscosity and voidage replacement. Theoretically, the VAPEX process can be separated into four phases as show in figure 1-4:

a) Communication path (Figure 1-4a and Figure 1-4b)

The first step in VAPEX is to create communication between the injection and the production wells. This can be accomplished in different ways, including: 1) by heating the bitumen around the wellbores, 2) by injecting solvent into the wellbores to dilute the bitumen around it, and/or 3) by circulating steam between the two wells.

b) Rising chamber phase (Figure 1-4c)

After communication between the two wells is established, solvent is injected into the reservoir through the injection well. The injected solvent penetrates the viscous bitumen as it rises to the top of the reservoir and dilutes the bitumen. Diluted oil is then drained by gravity against the current of solvent vapour. The counter current flow of solvent and bitumen results in a high oil production rate.

The counter current flow of VAPEX is applicable to reservoirs with free bottom water. The idea is to have both injection and production wells drilled inside the water zone and utilize the high mobility of water to distribute the solvent vapour along the bitumen water interface. This results in maintaining counter current flow of bitumen and solvent in the whole production cycle of VAPEX.

c) Chamber spreading phase (Figure 1-4d)

Once the solvent reaches the top of the formation, the bitumen solvent interface begins to spread sideways at a constant velocity. The production rate of bitumen is constant during this period of time as the VAPEX process enters a pseudo steady state. It has been observed that the production rate during the chamber spreading phase was 2-3 times lower than that of the chamber raising phase (Butler and Mokrys, 1991). The chamber spreading phase is very important to VAPEX as it accounts for 80-90% of the production time in VAPEX (Oduntan, 2001). This phenomenon ends once the interface reaches the boundary of the reservoirs and the chamber falling phase begins.

d) Chamber falling phase (Figure 1-4e and Figure 1-4f)

As the bitumen solvent interface reaches the boundary of the reservoir, the reservoir is depleted vertically. The production rate begins to decline slowly until the production is uneconomical (Zhang et. al. ,2006).

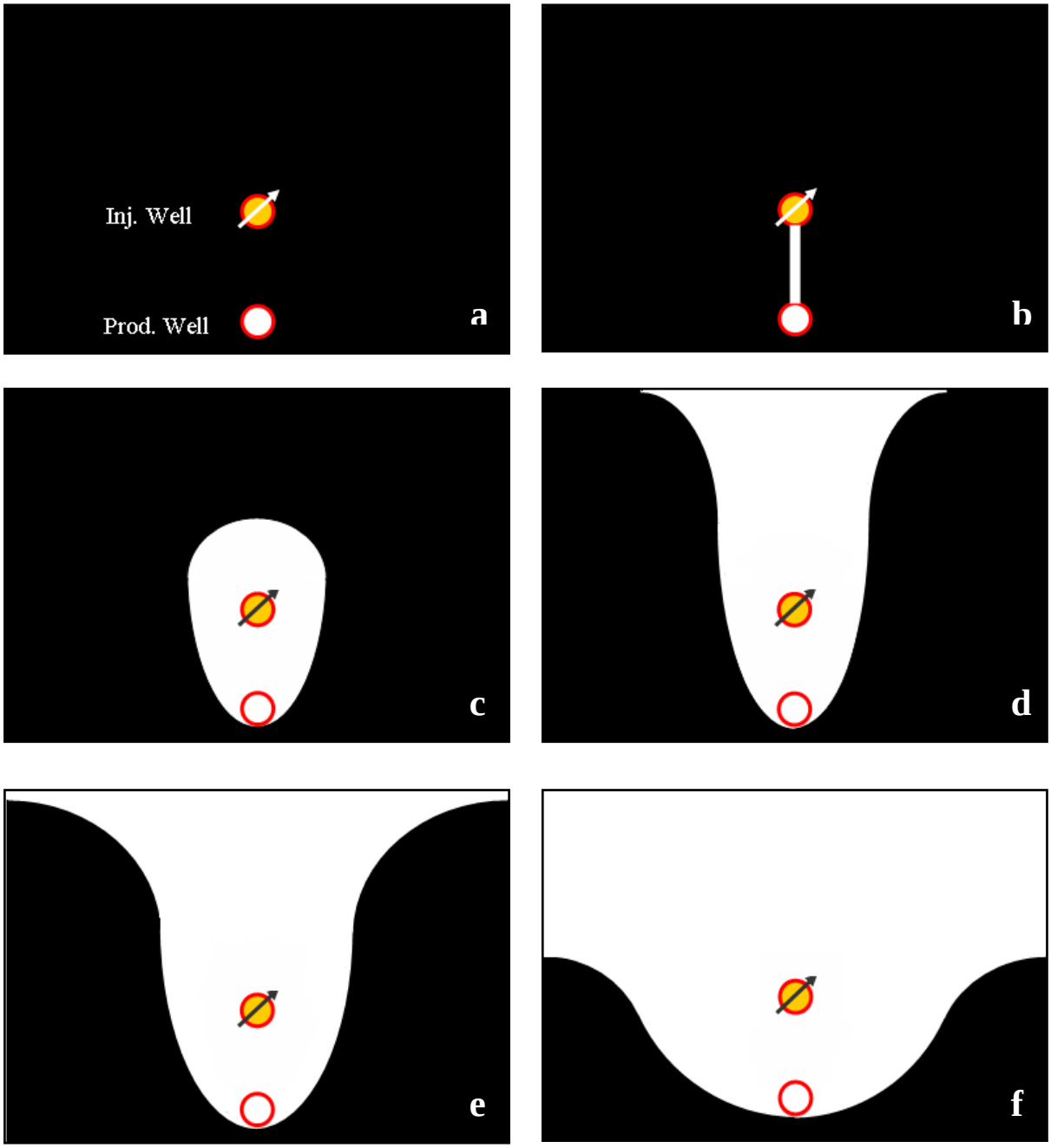

Figure 1-4: Schematic of the progress in a typical VAPEX process: (a) well configurations, (b) communication phase, (c) rising chamber, (d) spreading chamber, (e) falling chamber, and (f) depleted reservoir

1.3 Objectives of Study

VAPEX is a very effective and energy efficient EOR technique for in-situ heavy oil recovery; however, many of the mechanics of VAPEX require further understanding. The objectives of this research are:

1) To validate a new apparatus design for VAPEX experiments by comparing the experimental results to those of Oduntan's (2001). The packing with bitumen is placed in the annulus between two concentric cylindrical vessels and a vertical line source is used for vapour injection.
2) To investigate the effect of connate water and solvent condensation on: live oil production, horizontal interface advancement, and net solvent requirement in VAPEX
3) To develop a numerical model using Comsol® 3.3 to simulate the VAPEX experiments using macroscopic Darcy's law for gravity drainage coupled with the mass transfer of vapour into bitumen with capillary pressure terms and variable dispersion coefficients in the convection - diffusion equation.

2.0 Literature Review

Vapour Extraction (VAPEX) is an enhanced heavy oil recovery technique that uses light hydrocarbon as solvent to reduce viscosity of bitumen. The diluted oil is then drained by gravity.

The mass transfer mechanism is explained in Figure 2-1. For VAPEX using a pure solvent, the solvent concentration is constant within the solvent chamber. Vapour solvent diffuses into the bitumen at the bitumen-solvent interface, generating a concentration gradient in the boundary layer. The diluted oil is then drained and exposes a new bitumen solvent interface. Occasionally, non condensable gas (NCG) is mixed with solvent to avoid solvent condensation. The mass transfer mechanism of NCG VAPEX is very similar to that of VAPEX with pure solvent, with the exception of solvent concentration in the solvent chamber, which is a function of horizontal location.

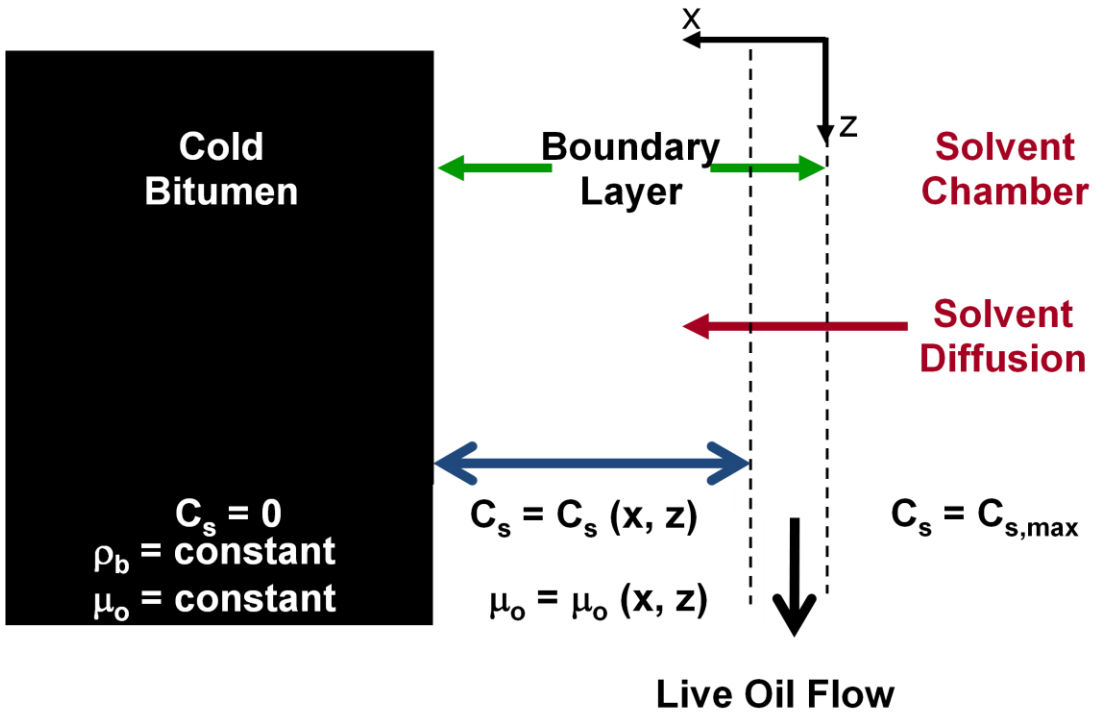

Figure 2-1: Schematic of VAPEX mechanism (Friedrich, 2005)

where c_s is the concentration of solvent, ρ_o and μ_o are the density and viscosity of oil.

This literature review section is divided into the following topics: 1) early development of VAPEX 2) experimental techniques used in VAPEX research 3) diffusion and dispersion mechanisms in VAPEX, 4) viscosity reduction and asphaltene precipitation, and 5) numerical modeling of VAPEX.

2.1 Early Development of VAPEX

Butler and Mokrys (1989) first published the idea of solvent analog of SAGD in 1989. The experiments were conducted with a Hele Shaw cell. Liquid toluene was used to study the recovery of Athasbasca and Suncor bitumen. Butler and Mokrys (1989) observed that at low permeability, the bitumen production rate was proportional to the square root of the height and the permeability; however, in high permeability system, the production rate was independent of permeability of the pay zone. They revealed that in high permeability, the restriction of flow was viscous force from the wall of the glass plates instead of the cell permeability. An analytical model of VAPEX was developed in analogy with the SAGD production model to predict the production rate of bitumen per length. They assumed the horizontal velocity of the bitumen solvent interface was constant during the chamber spreading phase, and neglected dispersion and convection mass transfer in VAPEX. A key result of their model is the following equation:

$$Q = 2\sqrt{2kg\emptyset\Delta S_o h N_s} \qquad (2\text{-}1)$$

where Q is the production rate, k is permeability, ϕ is porosity, g is the acceleration due to gravity, ΔS_o is change in oil saturation, h is height of pay zone, and N_s is the VAPEX parameter. The VAPEX parameter is a description of the mass transfer coefficient of the system. The computation of the VAPEX parameter is very complicated because both the intrinsic diffusivity (D_s) and the viscosity (μ) are functions of solvent concentration (C_s). N_s is defined by:

$$N_s = \int_{C_{min}}^{c_s=1} \frac{\Delta\rho D_s(1-c_s)}{\mu c_s}\, dc_s \qquad (2\text{-}2)$$

The above two equations neglect other VAPEX phenomena such as asphaltene precipitation. According to the experimental results and the values predicted from the analytical model, Butler and Mokrys concluded that the production rate of VAPEX using liquid solvent is

uneconomical for field operations. They suggested other potential factors that could improve the economics of VAPEX: 1) Using vapour solvent instead of liquid solvent 2) possible in-situ upgrading using light hydrocarbon 3) Coupling of SAGD and VAPEX, and 4) only applying VAPEX to reservoirs with lower viscosity heavy oil ($\mu \leq 10000$cP).

2.2 Experimental Techniques in VAPEX Research

2.2.1 Hele Shaw Cells

A Hele Shaw cell is constructed using two glass plates separated by thin spacers. The permeability (k) of a Hele Shaw cell is calculated by $k=b^2/12$, where b is the width of spacing. In addition to the initial VAPEX experiments described previously (Butler and Mokrys, 1989), Butler and Mokrys (1993) studied the effect of counter current VAPEX for reservoirs with free bottom water, and Das (1995) examined the effect of asphaltene precipitation using a Hele Shaw cell. The major advantages of a Hele Shaw cell are the simplicity in construction and set up, while providing reasonable qualitative results.

2.2.2 Unconsolidated Porous Media

Unconsolidated porous media are constructed by random packing of glass beads or sand. The porosity of a homogeneous unconsolidated glass bead model is approximately 36-40% (Chatzis, 2005). The advantages of an unconsolidated porous medium include simplicity in construction and close resemblance to the oil sand reservoirs.

Das (1995) conducted a set of VAPEX experiments using rectangular unconsolidated "visual cell" to study the feasibility of VAPEX in an unconsolidated porous medium with 100% bitumen saturation. They confirmed that the production rate of VAPEX is proportional to the square root of permeability; however, the extraction rate of VAPEX in the porous medium is 5-10 times greater than that of the Hele Shaw cell and that predicted by the analytical model by Butler and Mokrys (1989). Das and Butler (1998) attributed the increase in production rate due to surface renewal, capillary imbibition and the substantial increase in the length of the bitumen solvent interface.

The interface of the oil phase in a Hele Shaw cell has a curvature with a radius of approximately half of the width of the Hele Shaw cell. The ratio of the interfacial area to the

cross section area is $\pi/2 = 1.57$. In a bundle of capillary tubes, the ratio of the interface area to the cross section area increases to 2 (surface area of a half sphere/cross section area). With the same cross section area, the interfacial area of a bundle of capillary tubes is $4/\pi$ times greater than that of the Hele Shaw cell. The interfacial area is very important to VAPEX. Increase in the interfacial area enlarges the area available for mass transfer. Figure 2-2 shows that the interfacial area increases substantially in the sand pack. This explains the substantial increase in the bitumen production rate observed by Das (1995).

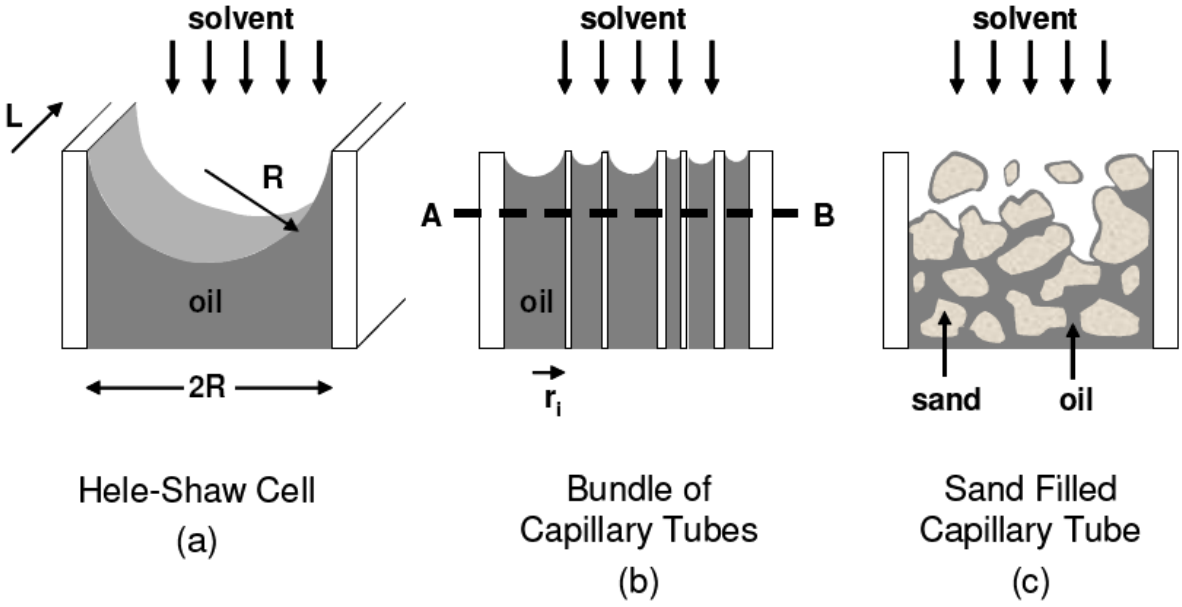

Figure 2-2: Interfacial contact area in porous media (Friedrich, 2005)

Das (1998) updated the analytical model by introducing apparent diffusivity (D_{ap}) and effective diffusivity to accommodate the increase in the interfacial area for mass transfer in a porous medium.

$$D_{ap} = D_s \emptyset^{\Omega} \qquad (2\text{-}3)$$

where D_s is intrinsic diffusivity and Ω is the cementation factor of the porous media, and ϕ is porosity. The effective diffusivity (D_{eff}) incorporates the increase of the interfacial area.

$$D_{eff} = \frac{A_d}{A_f} D_{ap} \qquad (2\text{-}4)$$

A_d is the interfacial area for diffusion and A_f is the area for fluid flow, where A_d is perpendicular to A_f. The following is the modified Butler and Mokrys's VAPEX model for a porous medium:

$$Q = 2\sqrt{2kg\emptyset^{\Omega}\Delta S_o h N_s} \tag{2-5}$$

$$N_s = \int_{c_{min}}^{c_{max}} \frac{\Delta\rho D_{eff}(1-c_s)}{\mu c_s} dc_s \tag{2-6}$$

Furthermore, Das (1995) investigated the effect of residual water saturation on VAPEX. The experiments were conducted in systems with 12.9% and 18% residual water saturation. Only trace amount of water was found in the produced bitumen samples. The stabilized production rate in systems with residual water saturation is slightly lower than in systems with no residual water saturation. Das (1995) suggested that the difference in production rate is due to the changes in the effective permeability of the system described in the following equation:

$$\frac{Q_1}{Q_2} = \frac{L_1}{L_2}\sqrt{\frac{K_1\emptyset_1^{\Omega}\Delta S_{o1}}{K_2\emptyset_2^{\Omega}\Delta S_{o2}}} \tag{2-7}$$

where Q is bitumen production rate, h is the height of horizontal well, and ΔS_o is overall change in oil saturation.

Oduntan (2001) investigated the effect of the length of pay zone on the live oil production rate using a long rectangular channel apparatus (Figure 2-3). The major advantage of this design is the short experiment run time. He conducted experiments with system heights of 21 cm to 247 cm and permeability of 1.36×10^{-10} m^2 at 45° dip angle. The results indicated that the live oil production rate was proportional to the square root of the length of pay zone. Oduntan also observed that the live oil production rate (Q_{LO}) remained constant until 80-90% of the cumulative oil was produced, and recovery was as high as 85-92% OOIP.

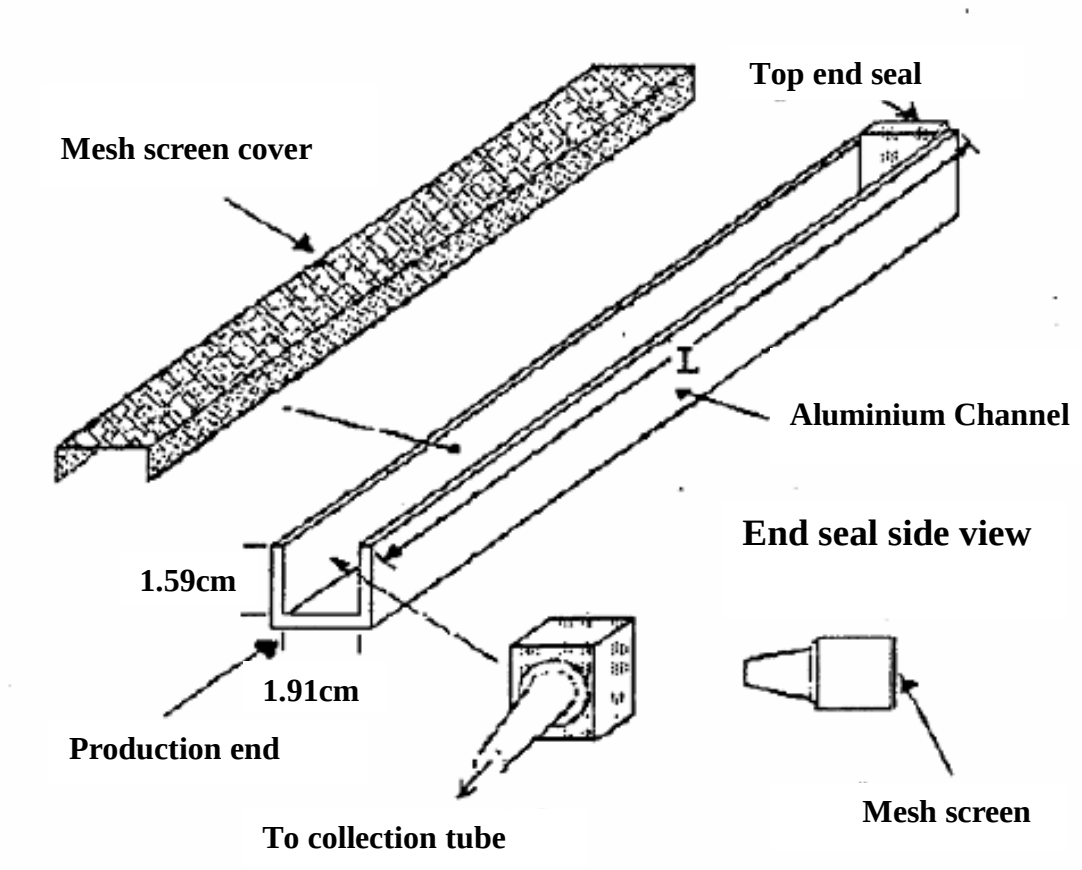

Figure 2-3: Rectangular channel apparatus used by Oduntan (2001)

Using an 84 cm long rectangular channel, Oduntan (2001) investigated the effect on production rate in various configurations of layered systems with permeability of $55x10^{-12}m^2$ and $1.92x10^{-10}$ m^2 respectively. He observed that the sequences of the layered systems may have an impact on the production rate. Experimental results indicated that systems with a higher number of layers would have lower production rate when compared to systems with identical average permeability with a fewer number of layers. He concluded this phenomenon is caused by capillary retention at the boundary of a low permeability layer above a high permeability layer.

Yazdani and Maini (2004) carried out experiments with butane to investigate the effect of the permeability and the height of the system on the production rate using a new annulus apparatus design. The new apparatus used the annulus space between two cylindrical pipes as housing for the packing of unconsolidated media. This design offered supreme pressure

handling capability; hence, a larger model design is feasible under the same operating conditions. They combined the experimental results obtained using the new apparatus with the results from Karmaker and Maini (2003), and concluded that the scale up model of VAPEX should be

$$\frac{Q_f}{Q_m} = \left(\frac{h_f}{h_m}\right)^{\lambda} \frac{\left(\sqrt{K_1 \emptyset_1^{\Omega}}\right)_f}{\left(\sqrt{K_2 \emptyset_2^{\Omega}}\right)_m} \tag{2-8}$$

where h_f and h_m are the pay zone height of the field and the model, respectively. They suggested λ is approximately in the range of $1.1 \leq \lambda \leq 1.3$. This contradicted the analytical model presented by Butler and Mokrys's (1989) and experimental observations by Oduntan (2001). Yazdani and Maini (2006) concluded such a discrepancy is the result of a thicker mixing zone in a longer payzone system. The additional apparatus height extended the exposure path and exposure time of the bitumen to solvent.

2.2.3 Consolidated Porous media

James (2003) investigated the effect of the model height and dip angle on live oil production from consolidated glass beads saturated with bitumen using butane as solvent. A higher residual oil saturation was observed in the consolidated models compared to the unconsolidated models. James (2003) concluded that the live oil production rate was proportional to the length of the consolidated porous media compared to the square root of the length of payzone for VAPEX in the unconsolidated porous media.

$$\frac{(Q_{LO})_f}{(Q_{LO})_m} = \frac{(LW)_f}{(LW)_m} \sqrt{\frac{\left(k_f \emptyset_f \Delta S_{of}\right)}{(k_m \emptyset_m \Delta S_{om})}} \tag{2-9}$$

where L and W are the length and width of the consolidated porous medium.

2.2.4 Pore Scale Phenomena

The experimental technique discussed in the previous sections focused on investigating the macroscopic phenomena in VAPEX. The microscopic phenomena involved in VAPEX was unknown until Jin (1999), Chatzis (2002), James & Chatzis (2004), and Friedrich (2006), used glass micromodels to examine the pore scale phenomena in the VAPEX process.

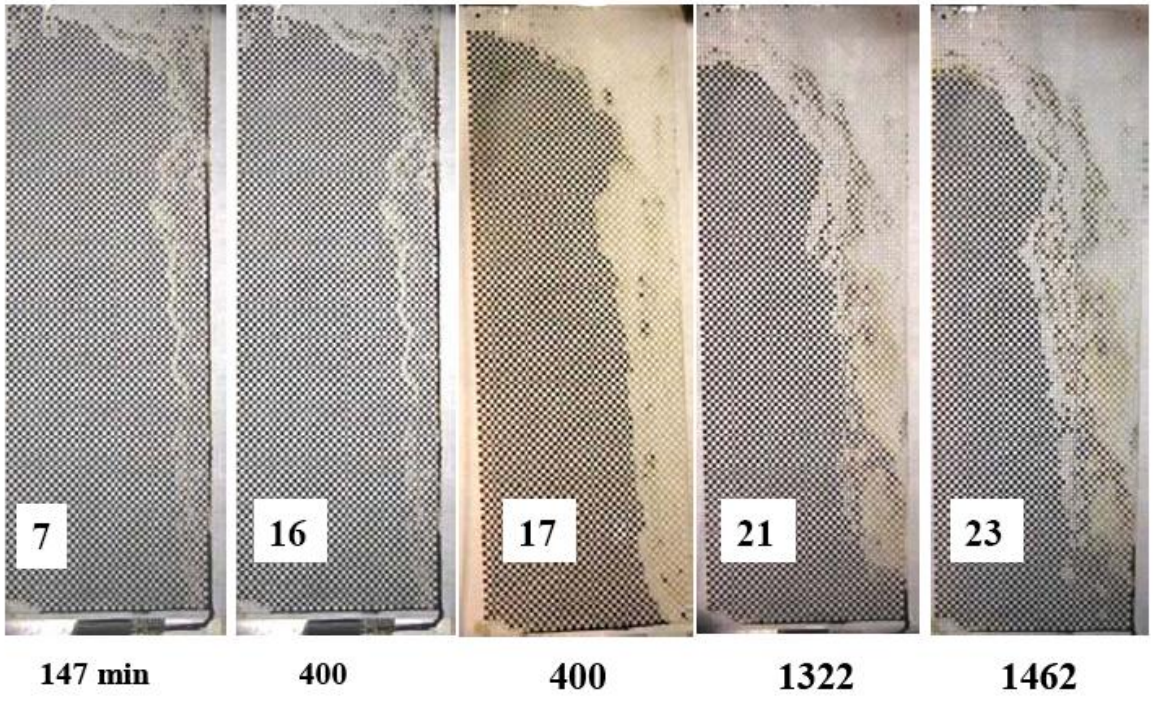

Figure 2-4: VAPEX interface in a glass micromodel with pore aligned at 45^{o} (Chatzis, 2002)

Chatzis (2002), James and Chatzis (2004) investigated the pore scale phenomena of VAPEX using different configurations of glass micromodels. They concluded that the rate of interface advancement was constant throughout the experiments and the velocity of interface advancement was a function of the configurations of the pore body, such as pore throat length, aspect ratio and orientation of the pore throats. The diluted oil drained in the direction of gravity around the grain. The motion of the diluted oil flow enhanced the mixing of oil. Furthermore, drainage occurred in one or two pores at a time. If the pore below was filled with vapour, instead of being drained to the pore below as a continuous film, the diluted oil would swell and drain in the direction opposite to the pore invasion. The redirection of diluted oil could valleys and peaks at the interface. This phenomenon extended the surface area for mass transfer. Other pore scale mechanisms observed in glass micromodels were snap off mechanisms and formation of localized oil films away from the bitumen-solvent interface. Snap off mechanisms occurred because of capillary instability at the advancing interface (Chatzis and Dullien, 1983). The snap off can cause small vapour

bubbles to be entrapped by the oil. The interactions between the vapour bubble and the surrounding oil enhance pore scale mixing.

Localized (closed loop) oil films, formed away from the interface, could not be drained until the oil overcame the capillary and viscous force. It was observed that as the oil film drained as the solvent concentration increased. Although the contribution to live oil production from close loop oil films was small compared to the production due to surface renewal; the phenomenon cannot be neglected.

James and Chatzis (2007) conducted experiments using glass micromodels and butane as solvent, to investigate the effect of solvent condensation on the horizontal interface advancement velocity of VAPEX. They observed that the horizontal interface velocity in experiment with solvent condensation is four times faster than in VAPEX with no solvent condensation. They suggested the enhancement is because of pore scale mixing between liquid butane and bitumen.

2.3 Viscosity and Asphaltene Precipitation

The key idea in VAPEX is to reduce the viscosity of bitumen using a solvent in the gaseous phase. This can be achieved in two ways, 1) by increasing the solvent concentration in the bitumen and 2) by asphaltene precipitation. The theoretical viscosity reduction of bitumen as a result of the increase in solvent concentration can be calculated using Ladiner's equation Wen and Kantzas, 2006):

$$\mu_{mix} = \mu_s^{f_s} \mu_B^{f_B} \tag{2-10}$$

where

$$f_B = \frac{\alpha C_{VB}}{\alpha C_{VB} + \alpha C_{VS}} \tag{2-11}$$

$$f_s + f_B = 1$$

$$C_{VB} + C_{VB} = 1$$

where $\mu_{om,}$ μ_s and μ_B are the viscosity of oil mixture, solvent and bitumen respectively, C_{VS} and C_{VB} are the volume fraction of solvent and bitumen, respectively. α is an empirical

parameter that can be calculated using Shu's correlation for mixture of bitumen with light hydrocarbon:

$$\alpha = \frac{17.04\Delta\rho^{0.5237}\rho_B^{3.2745}\rho_s^{1.6316}}{\ln\left(\frac{\mu_B}{\mu_s}\right)} \qquad (2\text{-}12)$$

where

$$\Delta\rho = \rho_B - \rho_s$$

ρ_B and ρ_s are the density of bitumen and solvent respectively.

Jin (1999) and Ramakrishnan (2003) measured the viscosity of the diluted oil experimentally and proposed an empirical correlation for viscosity of bitumen using butane and propane as solvents respectively is shown is Figure 2-5 The correlation is only applicable to solvent concentrations greater than 0.

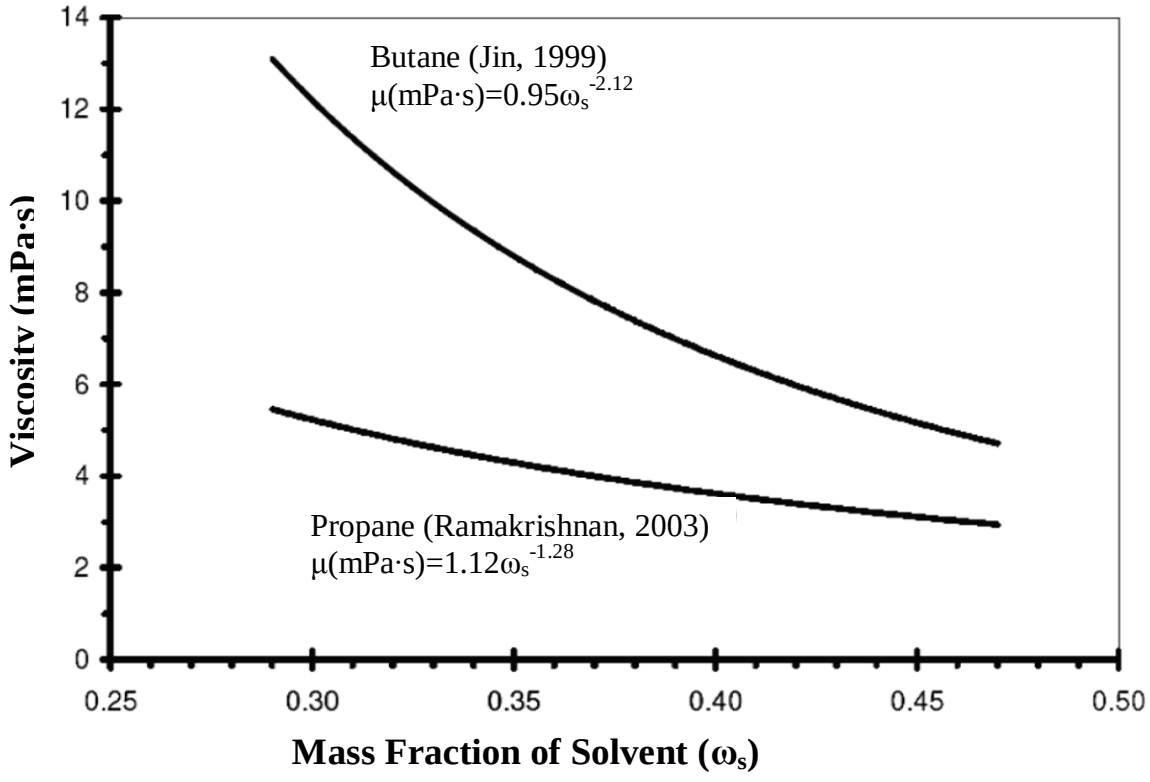

Figure 2-5: Effect of solvent mass fraction on bitumen viscosity (Friedrich, 2005)

Wen and Kantzas (2006) used four different bitumen samples: Peace River, Cold Lake, Edam, and Altene Bufflo (670, 130, 14, and 6 kg/m.s) to measure the viscosity of the

mixture as a function of solvent concentration at 25^{o}C using Nuclear Magnetic Resonance (NMR). Kerosene, toluene, naphtha, hexane and pentane were added to the bitumen at different concentrations. The viscosity measurements were compared to the theoretical values calculated using Cragoe's and Shu's correlation. Wen and Kantzas (2006) concluded that the values calculated using Shu's correlation matched the viscosity data measured by the NMR, which is more accurate than the values calculated from Cragoe's model.

Asphaltene precipitation is critical to the viscosity reduction of bitumen. In a sample of bitumen the asphaltene content may be as high as 22 wt%. Deasphalting takes place when the solvent concentration exceeds critical conditions near the dew point of the vapour solvent (Das, 1998). Asphaltene contains a high concentration of heavy metal like V, Ni, Fe. Deasphalting disposes the heavy metal in the reservoir. This is believed to be beneficial to the downstream refining operations (Das, 1995).

Luo and Guo (2006) studied the effect of asphaltene on bitumen viscosity by measuring the viscosity of bitumen at different concentrations of asphaltenes. First, they created a maltene mixture from a bitumen sample with an original asphaltene content of 14.5wt%. Different amounts of asphaltenes were added to the maltene mixture. The viscosity of the prepared samples was then measured at atmospheric pressure and atmospheric temperature using a cone and plate viscometer. They came to the conclusion that the viscosity of bitumen increased exponentially as the asphaltene content increased. Furthermore, they found that the equilibrium concentration of propane decreased as wt% of asphaltene increased. The macromolecular asphaltenes present in heavy oil prevented the small molecules of propane from penetrating into heavy oil.

Disadvantages of deasphalting include possible permeability reduction and restriction of diluted oil flow because of blockages of flow path by precipitated asphaltene. Das (1994) showed using a Hele Shaw Cell that the asphaltene precipitation did not restrict the flow of diluted oil. They stated that deasphalting occurred at the bitumen solvent interface where the solvent concentration was at its maximum. The precipitated asphaltene formed fringes at the wall of the glass plates and the production rate of live oil was unaffected. The experimental results showed that deasphalting increased the production rate by 30-52%, indicating that asphaltene precipitation is beneficial in VAPEX operation.

2.4 Diffusion and Dispersion

Diffusion and dispersion of solvent into bitumen plays a major role in the VAPEX process. Diffusion is the analog of conduction in heat transfer. The diffusion coefficient describing the rate of solvent diffusing into bitumen has been the focus of many studies (Zhang et al., 2000; Upreti and Mehrotra, 2000; Butler and Mokrys, 1989; Boustani and Maini, 2001).

James (2003) used a direct measurement technique to determine the diffusivity of butane into bitumen, where the uptake of butane and swelling of bitumen was measured. Using a 1-D diffusion model, the numerical results calculated using different configurations of diffusivity were compared to the experimental measurements. James (2003) concluded that the diffusion coefficient of butane into bitumen is a linear function of solvent concentration.

Pore scale mixing of fluid occurs when two miscible fluids are pumped to the porous media simultaneously. Essentially, this is dispersion. Previous literature indicates that it plays a major role in VAPEX (Boustani and Maini, 2001). The longitudinal dispersion coefficient (D_L) is dispersion in the direction of fluid flow, while the transverse dispersion (D_T) coefficient is dispersion perpendicular to the direction of fluid flow. The experimental measurement of dispersion is described using (D_L/D_m) versus Peclet number. The Pelect number is a dimensionless number that describes the ratio of the rate of mass transfer by convection to the rate of mass transfer by molecular diffusion.

$$Pe = \frac{v_{pv} D_p}{D_m} \tag{2-13}$$

$$D_L = \alpha_L v_{pv} \tag{2-14}$$

where v_{pv} is the fluid pore velocity, D_m is molecular diffusion and D_p is the average particle diameter of the particles. Blackwell (1962) found that the typical ratio of longitudinal dispersion to transverse dispersion is approximately 24. Dispersion in 2-D flow system is expressed as follows (Donaldson et al., 1998):

$$D_{xx} = \frac{\alpha_L \vec{u} + \alpha_T \vec{v}}{\sqrt{\vec{u} + \vec{v}}} + D_m \tag{2-15}$$

$$D_{yy} = \frac{\alpha_L \vec{v} + \alpha_T \vec{u}}{\sqrt{\vec{u} + \vec{v}}} + D_m \qquad (2\text{-}16)$$

$$D_{xy} = \frac{(\alpha_L - \alpha_T)\vec{u}\vec{v}}{\sqrt{\vec{u} + \vec{v}}} + D_m \qquad (2\text{-}17)$$

where α_L and α_T are the dispersivities for longitudinal dispersion and transverse dispersion respectively. D_{xx} is the dispersion coefficient in x direction, D_{yy} is the dispersion coefficient in y direction and D_{xy} is the dispersion coefficient in xy direction. At low velocity, diffusion dominates and at high velocity dispersion dominates.

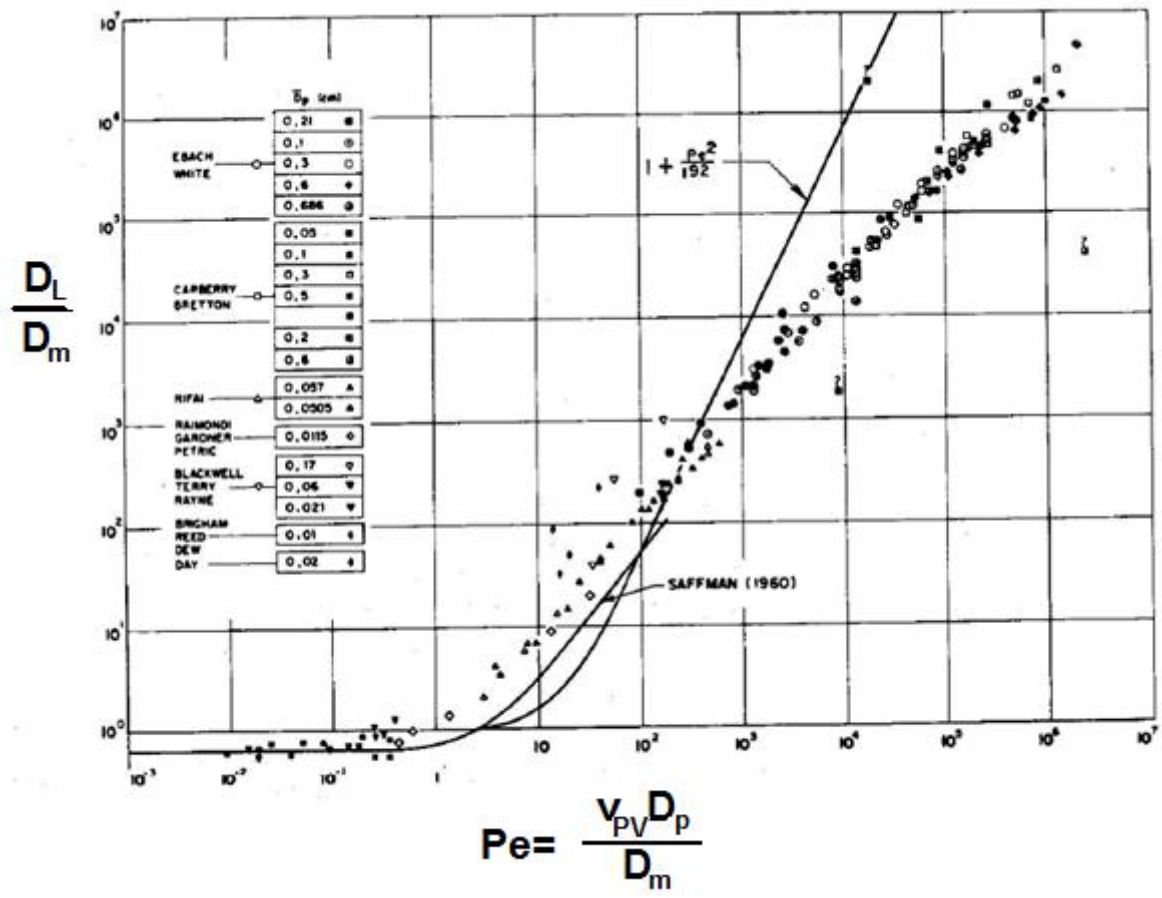

Figure 2-6: (D_L/D_m) versus Peclet number correlation (Dullien, 1992)

2.5 Numerical Simulation of VAPEX

Several researchers have attempted to model the VAPEX process using different numerical tools (Das, 2005 ; Azin et. al., 2005). The most common tool is a commercial software that specialized in reservoir simulation, CMG-STARS®. It is a leading software for thermal process reservoir simulations. The disadvantages of VAPEX simulation using reservoir simulation software are the lack of control and lack of understanding of the governing equations of the system. This resulted in unrealistic input values in order to match the production history of experiments.

Azin et. al. (2005) developed a mechanistic model in simulating the VAPEX process in porous media. The model consisted of the 2-D convective – diffusion equation for a constant variable system and the simplified 2-D Brinkmann equation for the flow of diluted oil. The two equations were coupled by the continuity equation. The Brinkmann equation is an extension of Darcy law that includes the dissipation of the kinetic energy by viscous shear in porous media flow. The system of equations neglected the capillary effect and the relative permeability within the system. They explained the calculation of the dispersion coefficient using the Perkins-Johnston correlation (Perkins and Johnston, 1963). However, they did not address the boundary condition of the system, the correlation used for viscosity reduction, or the molecular diffusion coefficient used in the simulation; nor did they mention the method used to distinguish the difference in physical properties between bitumen and dilute oil. The mechanistic model developed by Azin et. al. (2005) was never used in the numerical simulation. The numerical simulation was simply conducted using CMG-STARS. Azin et. al. (2005) verified the numerical model by comparing the simulation results to the production data of Butler and Jiang (2000); however, they did not address the advancement of the interface and the shape of the bitumen- solvent interface.

Kapadia et. al. (2006) used a different approach in modelling the VAPEX process. They divided the system into blocks of bitumen. As the blocks absorbed the solvent, the live oil drained from the bottom of the block and the blocks shrunk. They used the 2-D convection diffusion equation for a constant saturation system to describe the mass transfer mechanism in VAPEX and the Darcy's Law for gravity drainage of the diluted oil. The mathematical model assumed 1) constant density throughout the system, 2) no convective mass transfer in

horizontal direction, 3) no diffusion in vertical direction, and 4) omission of capillary effect and relative permeability. They used Jin's correlation for viscosity reduction and neglected the velocity effect in the dispersion coefficient.

The model was compared to the experimental results of Oduntan (2001). Although the model matched the production rate of Oduntan's experimental results, there are still some fundamental problems with the input values used and numerical results produced. The dispersion coefficient used was a constant value from 0.0194 cm^2/s to 1.39 cm^2/s, which was unreasonably high for a gas liquid mass transfer system. Second, The height of block versus width (bitumen and solvent interface) of the numerical simulation results (Figure 2-7) contradicted the shape of the VAPEX interface observed in laboratory scale experiments Butler and Mokrys (1989), Chatzis (2000), James and Chatzis (2004).

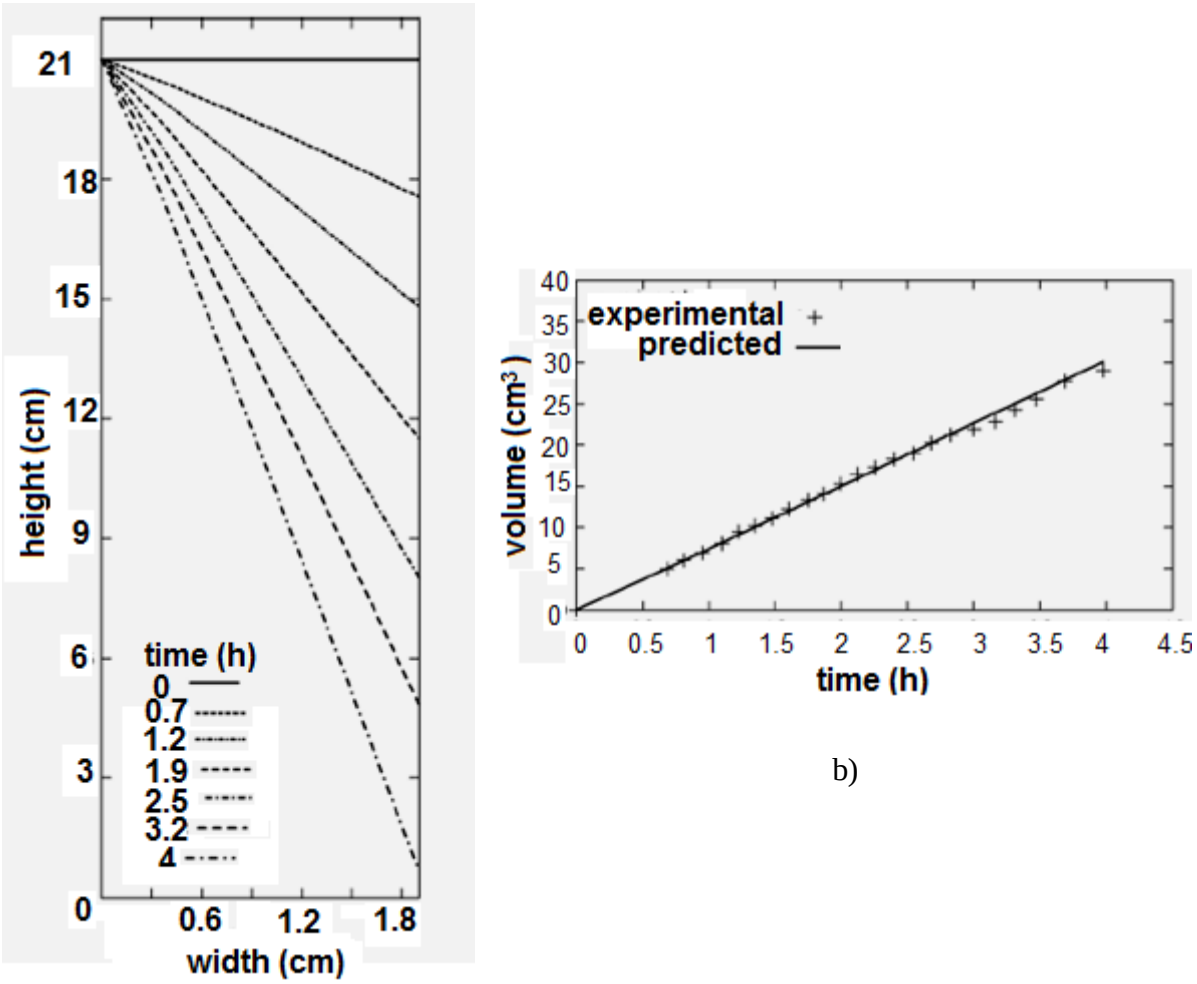

Figure 2-7: Results from numerical modeling of Kapadia et. al. (2006) a) The height of block versus width at different times b) experimental and model predicted production of live oil versus time

3.0 Experiment Setup and Procedure:

3.1 Experimental Apparatus Design

The design of an annular-type experimental model was first introduced by Yazdani and Maini (2005). An annular space was created between two concentric cylinder tubes of different radii as the housing for the unconsolidated glass beads packing. The major advantage of this design is the ability to withstand high operating pressure while maintaining a uniform slit thickness. The experimental apparatus of Yazdani and Maini was made of aluminium, which resulted in the loss of visibility of porous medium and it did not allow tracking of the solvent-bitumen interface. Moreover, it was very time consuming to saturate the model with bitumen and also to clean up the model after each run.

Table 3-1: Properties of Apparatus

OD of outer cylinder	3″ (76.2 mm)
ID of outer cylinder	2½″ (63.5 mm)
Material of outer cylinder	3″ (76.2 mm) OD Plexiglas® tube with ¼” thickness
OD of inner cylinder	2″ (50.8 mm)
Material of inner cylinder	2″ (50.8 mm) OD Plexiglas® rod
Height of the slit	39.4″ (1 m)
Material of gas tube	¼″ (6.4 mm) OD stainless steel tube with 2 perforated hole 180^{o} apart per cm
Material for Collecting cylinder	1½″ (38.1 mm) OD Plexiglas® with ¼” thickness
Length of collecting cylinder	12″ (304.8 mm)
Overall volume of slit	1154 cm^3

A new design was constructed using Plexiglas® material to provide a visibility to the porous medium. Each component of the apparatus can be disassembled for ease of saturation and clean up. The design followed by Oduntan et. al. (2001) aimed for smaller depth to reduce

the time required for each experimental run. Table 1 summarizes the dimension and material requirement of each component in the apparatus in this thesis.

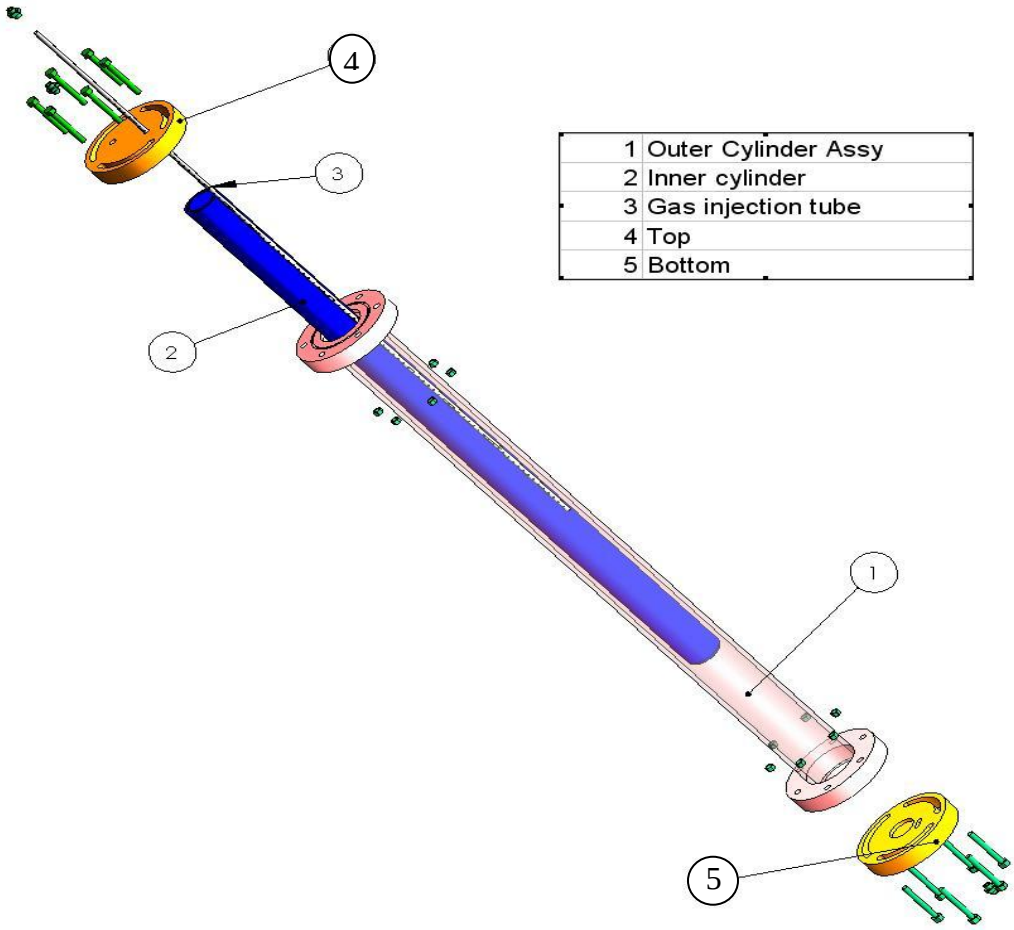

Figure 3-1: Details Experimental Apparatus

According to detailed calculations (appendix A) conducted on the design, the maximum allowable pressure of the apparatus exceeds 70 psig and the maximum operating temperature is 90^{o}C. The dimension of the slit is approximately 20 by 0.064 by 101 cm, which provides an overall volume of approximately 1154 cm^{3}. The solvent was distributed in the porous medium using a ¼″ OD stainless steel tube with holes of 1 mm diameter, perforated 180^{o} apart per cm length of the tube.

The top and bottom plates were attached to the apparatus using 12 nuts and bolts. The top plate consisted of two openings. Opening #1 was used for solvent injection and opening #2 was used for the saturation of the apparatus. The diluted live oil was drained by gravity and

produced from opening 3 of the bottom plate. The apparatus was sealed using two o-rings on each side. The opening 3 was connected to a live oil collection cylinder that operated under the same pressure as the apparatus, to measure the volume of live oil produced under reservoir conditions.

3.2 Bitumen and Solvent Properties

All experiments were conducted using Cold Lake bitumen and instrumental grade n-butane. The properties of these materials are shown in Table 3-2.

Table 3-2: Properties of bitumen and butane used in experiments (Friedrich, 2005)

Properties	Bitumen	n-Butane
Purity	n/a	Instrumental grade
Asphaltene Content (wt %)	18.3	n/a
Molecular Weight (kg/kmol)	400	58.1
Liquid Density (kg/m^3)	980	573
Liquid Viscosity (kg/m.s)	23.2	0.171 x10^{-3}
Gas density (kg/m^3)	n/a	2.01

3.3 Saturation of the Packing in the Annulus

Four experiments were conducted using this new apparatus to investigate the effect of connate water and solvent condensation to the live oil production rate and the advancement of solvent bitumen interface. The experiments with and without connate water were saturated using 2 different methods.

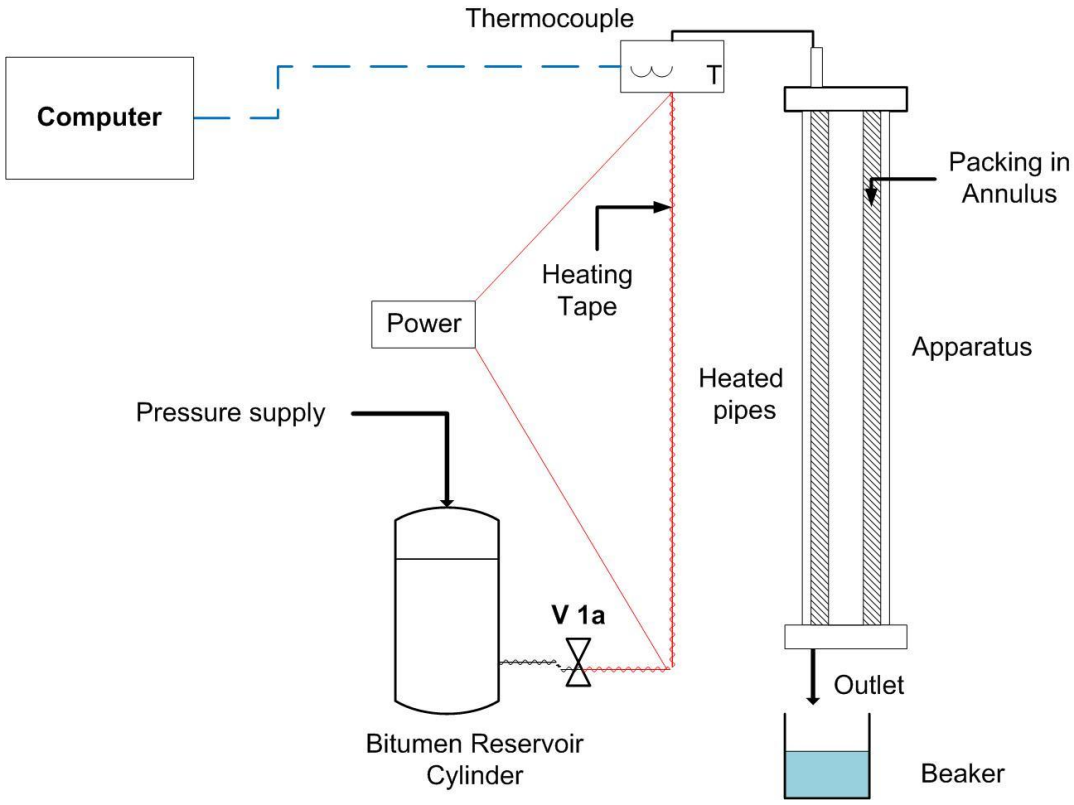

Figure 3-2: Apparatus saturation assembly

The saturation method for experiments with and with no connate water was similar to the method used by Das (1995). First the apparatus was packed with glass beads and leak tested by applying 20 psig of nitrogen before saturating it with bitumen. CO_2 was then used to remove the trapped air from the porous medium. Low flow rate of CO_2 was applied to the system for 5-10 minutes from opening #3 (see Figure 3-3) to displace the air and nitrogen from the porous medium. Diluted NaOH solution made using deaerated water would then be slowly pumped into the porous medium by opening #3 in Figure 3-1 (or V3 in Figure 3-3). This procedure was intended to completely remove the CO_2 gas in the porous medium and to establish a 100% liquid saturation within the porous medium. A relatively large volume of fresh deaerated water was injected to the model to replace the NaOH solution.

The bitumen reservoir assembly, shown in Figure 3-2 included:

- A ¼″ stainless steel tubing, heated by an electrical heating tape, connected the reservoir cylinder to Opening 2 of the apparatus
- A cylindrical reservoir

- A T- type thermocouple at the end of the ¼″ stainless steel tubing to monitor and maintain the temperature of bitumen at a desired level (below 60 C), as it is entering the model

Pressure of 30-40 psig was applied to the reservoir cylinder to force the bitumen through the heated ¼″ tubing into the apparatus. The ¼″ tubing was wrapped with an electrical heating tape to heat the flowing bitumen to approximately 60^{o}C. The heat decreased the viscosity of the bitumen and improved the efficiency of the oil saturation. The water displaced by bitumen was collected from the bottom and measured to calculate the volume of connate water in the porous medium.

Water flooding before saturation was inapplicable to the system with no connate water; therefore, butane gas instead of CO_2 gas was applied to the porous medium to displace the air out of the apparatus. Butane was applied because:

Butane is more soluble in bitumen than CO_2 and air. If a small amount of butane is trapped in the porous media during saturation, the butane can diffuse into the bitumen to achieve 100% bitumen saturation. The viscosity reduction due to trapped butane is negligible because the volume of trapped butane is negligible compared to the volume of bitumen in the system. Butane was utilized as the solvent for heavy oil extraction in all the experiments. The trapped butane left over during saturation would not affect the overall mass transfer mechanism of the experiment, unlike air and CO_2.

The rest of the oil saturation procedure was identical to experiments with connate water.

3.4 Experiments Setup and Procedures:

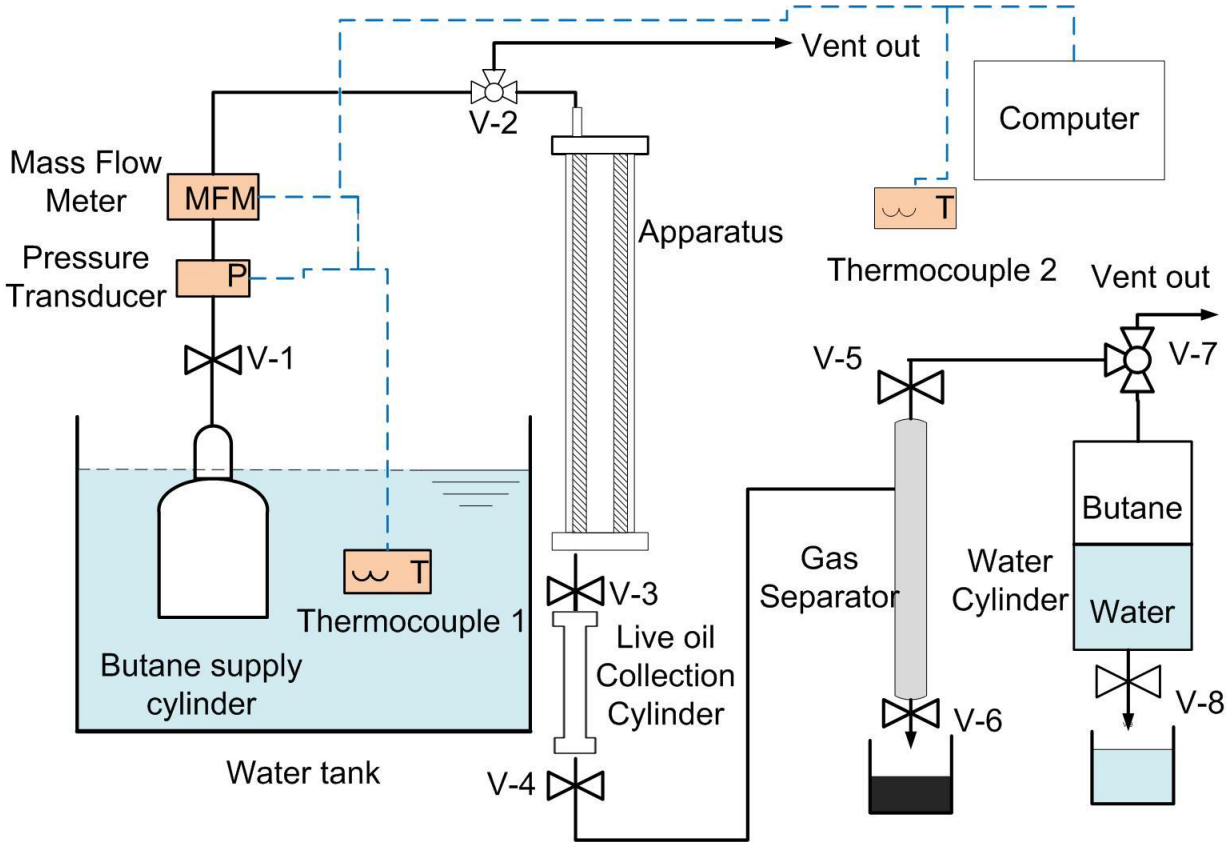

Figure 3-3: Experiment setup for experiments #1-#4

The complete experimental setup, is shown in Figure 3-3: Experiment setup. The experiment set up consists of two parts: 1) the solvent injection components that connected the solvent supply to the apparatus 2) the production components that collected the live oil, bitumen and solvent produced during the experiments. The solvent injection consisted of a water bath, a butane supply cylinder, a mass flow meter, a pressure transducer and 2 thermocouples.

A 2 L stainless steel cylinder with maximum operating pressure of 3000 psig was used as the butane supply cylinder. It was submerged in the water bath maintained at 1-2°C below the ambient temperature. This setup was to ensure that the operating pressure stayed below the dew point pressure of solvent and to avoid condensation of butane vapour during experiments. The uptake of butane was driven by pressure depletion in the apparatus due to the diffusion of solvent into bitumen. The free uptake of butane was proven to be a very effective method by the University of Waterloo Porous Media Research Group (Oduntan,

2001; Ramakrishnan, 2003; James, 2003). The butane cylinder was connected to a 3 way valve (V2). An Omega FMA-3107 gas mass flow meter and an Omega PX-304 pressure transducer were attached to the solvent injection line to measure the butane uptake and the operating pressure of the apparatus. Two T-type thermocouples were used to monitor the water bath and ambient temperature.

The solvent injection tube was then flushed by butane for 5-10 minutes in order to remove the air in the piping and the connections. After flushing, valve V2 was switched to the gas injection tube, with valve V3 opened to the atmosphere. The pressure difference between the butane supply and the atmospheric pressure displaced the bitumen out of the solvent injection tube. Experiments began once communication between the gas injection tube and the production outlet (opening #3) was established.

The production line consisted of a 150 cm^3 collection cylinder, a bitumen solvent separator, and a graduated water cylinder. The collection cylinder, constructed of clear Plexiglas®, was used to measure the volume of live oil production during the experiments. V3 was then opened and V4 was shut off during experiment to collect the produced live oil. Occasionally the collection cylinder was emptied. V4, V5, V7 and V8 were opened while V3 and V6 were closed. The pressure difference between the collection cylinder (reservoir pressure) and the separator (atmospheric pressure) drove the live oil toward the separator. V3 was closed when emptying the collecting cylinder to reduce the effect of pressure depletion on the butane uptake. In addition, a small amount of live oil was retained in the collecting cylinder during the emptying process to avoid depressurization of the collecting cylinder.

A 0.5 L stainless steel flush vessel was used to flush a part of dissolved solvent in the live oil. The vessel was heated up to 70°C using a heating tape to flush the solvent out from the live oil. The liberated solvent was then collected in a 6 L graduated water cylinder. Once all the solvent was liberated from the live oil, the mass of water drained from the graduated water cylinder and the mass of the bitumen produced were weighed to calculate the mass fraction of solvent in the live oil. The collected bitumen samples were reweighed after they were left at atmospheric condition for days to vent out the remaining solvent. This extra step was to ensure all of the solvent was vented out from the bitumen.

The experiment continued until the packed column was completely swept. Then, valves V1 and V2 were closed to cut off the butane supply to the porous medium. Finally, a blowdown process was followed to recover the excess solvent remaining in the porous medium. During the blowdown process, valves V3, V4, V5, V7, and V8 were opened. The remaining solvent flowed from the apparatus to the graduated water cylinder. The volume of solvent recovered during the experiment and blowdown process were used to calculate the net solvent requirement for the VAPEX experiments.

3.5 VAPEX Experiments with Solvent Condensation

The procedure for the conventional VAPEX experiments, where the solvent remains at the vapour stage in the chamber was described in the previous section. In experiments with no solvent condensation, the water bath temperature was adjusted at 1-2^{o}C below the ambient temperature to avoid condensation inside the apparatus. James and Chatzis (2007) observed that the washing effect created by condensed solvent at the bitumen solvent interface enhanced the production rate of VAPEX. They found that in a glass micromodel type of porous medium was used; the horizontal sweeping velocity for bitumen-solvent interface was four times faster then for the case of non-condensing VAPEX.

In another attempt, a condensing VAPEX experiment was conducted in unconsolidated packed model. Butane was used as solvent in 1.19 mm diameter glass beads ($k = 1.123 \times 10^{-9}$ m^2) to investigate the live oil production enhancement, due to solvent condensation. Properties of the porous medium for the condensing VAPEX experiment were identical to experiment 1 described previously. The system was saturated as system with no connate water described in section 3.3. The same procedure was used to reduce the discrepancy between the two runs.

3.5.1 Experimental Setup

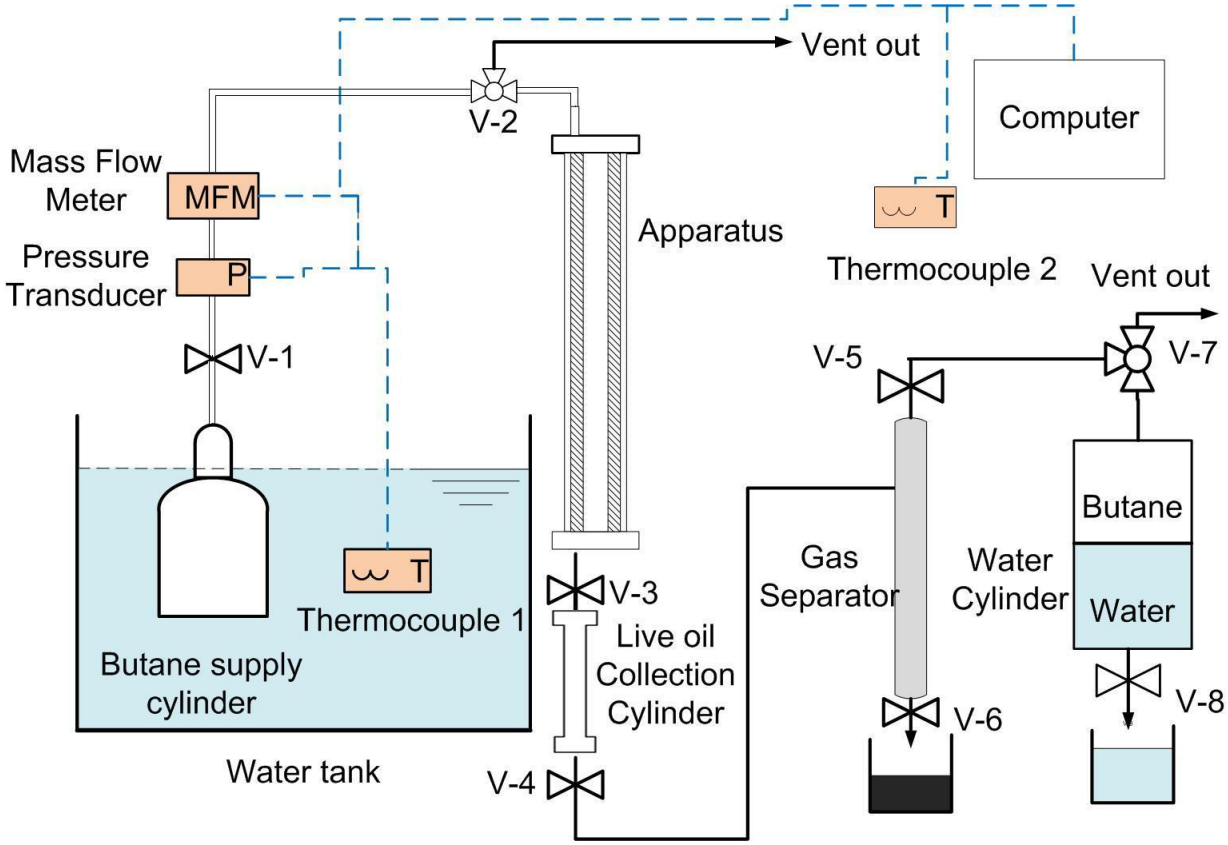

Figure 3-4: Experimental set up for experiment #5

The experimental setup for VAPEX experiment with condensation is shown in Figure 3-4. The water bath was maintained at 2-3^{o}C above ambient temperature to ensure that the pressure of the system was greater than the dew point pressure of solvent; thus, the solvent would condense at the bitumen-solvent interface. In addition, the tubing connected the butane cylinder and the apparatus (highlighted by double line) was heated to approximately 2-5^{o}C above ambient temperature using heating tapes to avoid solvent condensation inside the solvent injection piping. The procedure for running this experiment was exactly the same as for the previous runs.

3.6 Experimental Measurements and Analysis Methods

3.6.1 Porosity and Permeability

Porosity is defined as a fraction of bulk volume of porous sample occupied by pore or void space (Dullien, 1992). In general, the porosity of homogeneous unconsolidated porous media ranges from 0.36 to 0.40 depending on the quality of the packing (Chatzis, 2005).

$$\emptyset = \frac{V_{pv}}{V_t} \tag{3-1}$$

Where V_{pv} is the pore volume of the system and V_t is the total volume of the system.

Permeability is defined as the conductivity of the porous medium with respect to permeation by Newtonian fluid (Dullien, 1992). For the homogeneous unconsolidated porous media used in the experiments, the permeability is estimated using the Carman-Kozeny correlation:

$$k = \frac{D_p^2 \emptyset^3}{180(1-\emptyset)} \tag{3-2}$$

where k is permeability and D_p is the particle size diameter.

3.6.2 Live Oil Production

The collection cylinder was used to collect and measure the produced live oil under reservoir pressure. It was designed in such a way that 1 cm of live oil production in the collection cylinder corresponded to 5 ml of live oil produced. The measurement error of the reading was approximately +/- 0.25 ml. The cumulative live oil production was plotted against time to calculate the steady state live oil production rate during chamber spreading phase.

3.6.3 Bitumen and Solvent Production

The collection cylinder was connected to the separator and water cylinder. Occasionally, the collection cylinder was emptied and the live oil flow into the separator heated to approximately 70^{o}C under atmospheric pressure. The heat would then accelerate the ventilation of butane from the bitumen. The released butane flowed into the graduated water cylinder and displaced the water from the water cylinder. The weight of water displaced

corresponds to the amount of liquid butane released from the live oil. Once the majority of butane was released from the bitumen, the bitumen was produced for V6 of the separator (Figure 3-3). The produced bitumen was weighed and used to calculate the mass fraction of solvent in the live oil.

$$m_S = \frac{m_w/\rho_s}{22400} \tag{3-3}$$

$$\omega_s = \frac{m_s}{m_s + m_B} \tag{3-4}$$

where m_w and m_s are mass of water and solvent, ρ_s is the liquid density of butane, and ω_s is the mass fraction of solvent in live oil.

3.6.4 Interface Tracking

One of the objectives of the experiments carried out was to observe the growth of solvent chamber. During the experiments, the bitumen-solvent interface was manually traced on a clear transparency placed on the outer surface of the cylinder housing. Later, interface profiles were scanned into a computer for further analysis. The horizontal advancement velocities as well as the length of interfaces were analyzed from it. The horizontal location of the bitumen solvent interface during chamber spreading phase was plotted against time to evaluate the horizontal interface advancing velocity at specific vertical locations. The interface advancement was compared among various different vertical locations, permeability and fluid saturation. An important note about interface tracking in an annulus apparatus is that the horizontal interface velocity calculated must be scaled to the average perimeter of the annulus slit where the unconsolidated porous medium is placed. During the experiments, the interface profiles were traced according to the perimeter of the outer cylinder, which is 25% larger than the average perimeter of the slit. The following relationship is used to scale the horizontal interface velocities in the analysis:

$$v_H = \frac{r_s}{r_o}\, v_{Ho} = 0.75 v_{Ho} \tag{3-5}$$

where v_H is the horizontal interface velocity of the unconsolidated porous medium, v_{Ho} is the horizontal interface velocity observed at the outer cylinder, r_s is the average radius of the slit,

r_o is the average radium of the outer cylinder. For this apparatus, the ratio of the average radius of the slit to the ratio of the radius of the outer cylinder is 0.75.

The length of the interface profile at different times was measured using Scion Image software (Scion Image, Scion Corporation). The interface profiles were manually traced on the transparency; this introduced uncertainty and affected the precision of the measured length.

3.7 Data Acquisition System

The experimental setup described in the previous sections included a pressure transducer, a mass flow meter, and two thermocouples to record the system condition automatically. The devices were connected to a personal computer by two circuit boards via two 9 pins cables. The readings of each device were recorded and monitored by the customized program developed in LABVIEW 6.0 as shown Figure 3-5, Figure 3-6, Figure 3-7 and Figure 3-8. Figure 3-5 is the graphic interface used in LABVIEW. It records and displays the pressure, temperature and the mass flow rate of the system every 30s. Figure 3-6, Figure 3-7 and Figure 3-8 are the logical used by LABVIEW. The calibration curves converted the output voltage of each device to the proper readings.

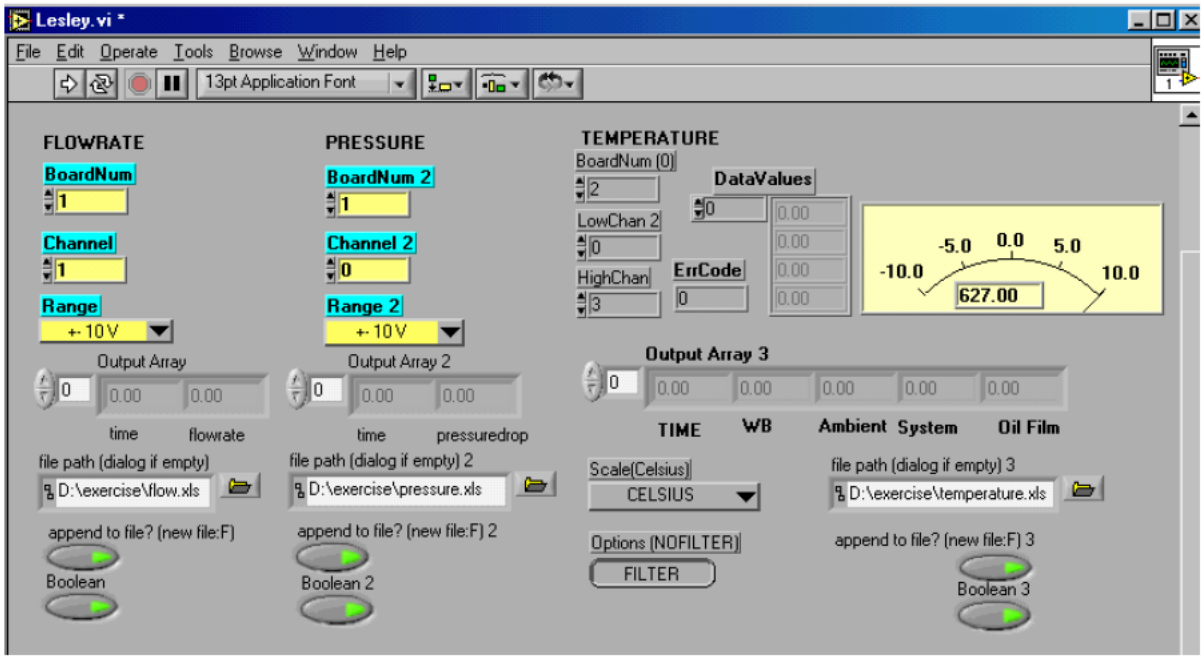

Figure 3-5: User graphic interface of LABVIEW 6.0

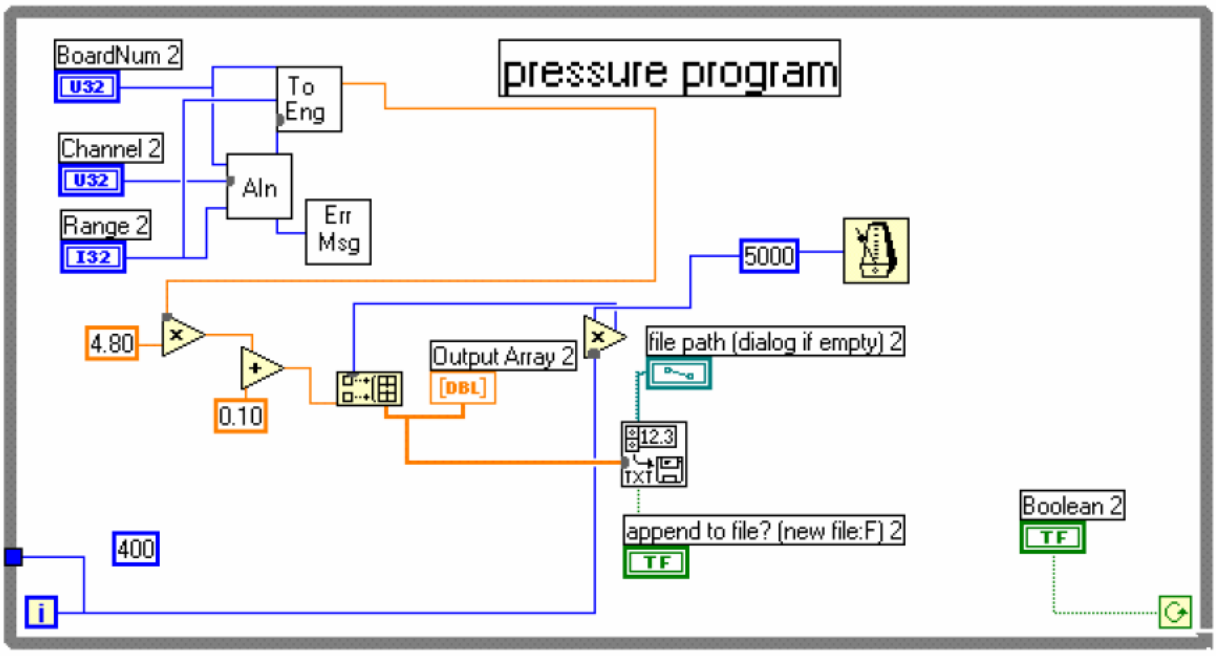

Figure 3-6: LABVIEW logical flow diagram for pressure readings

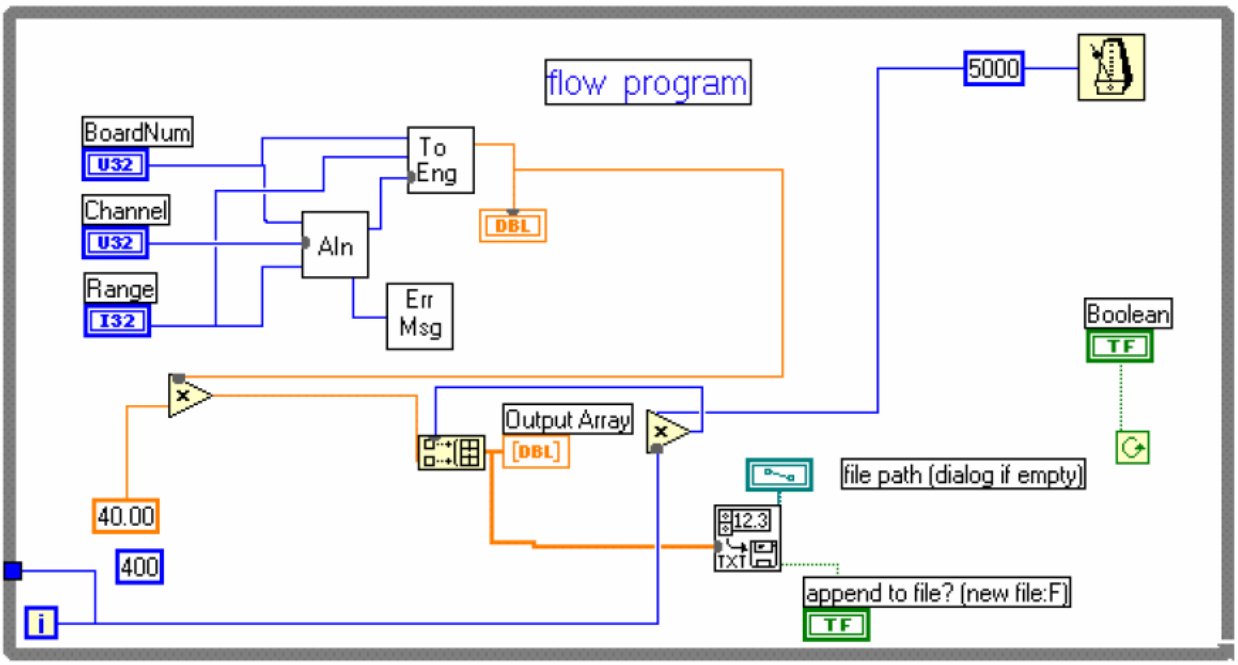

Figure 3-7: LABVIEW logical flow diagram for flow readings

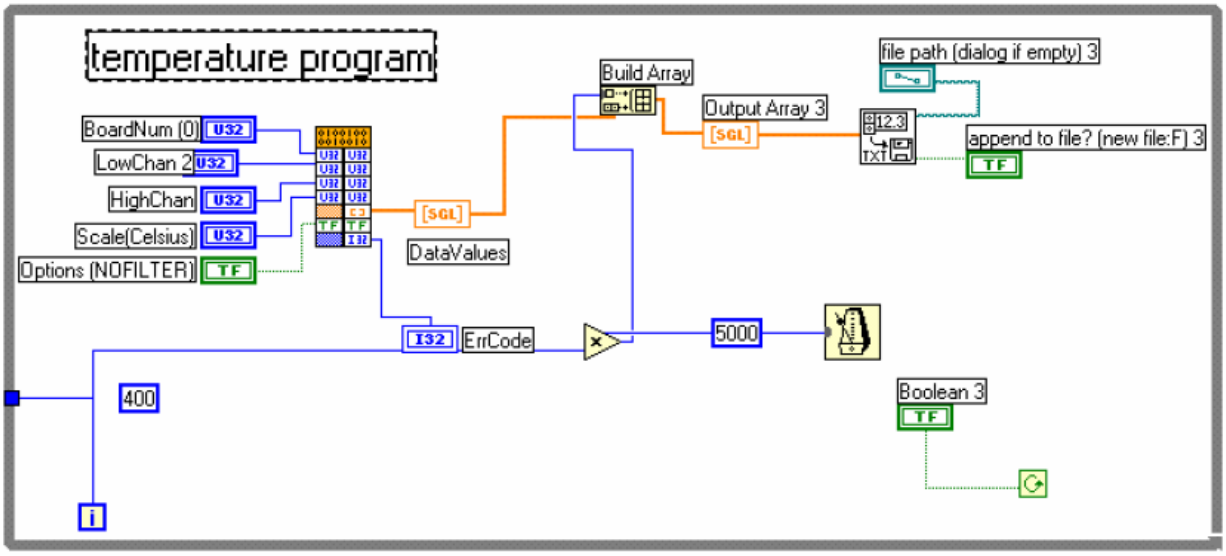

Figure 3-8: LABVIEW logical flow diagram for temperature readings

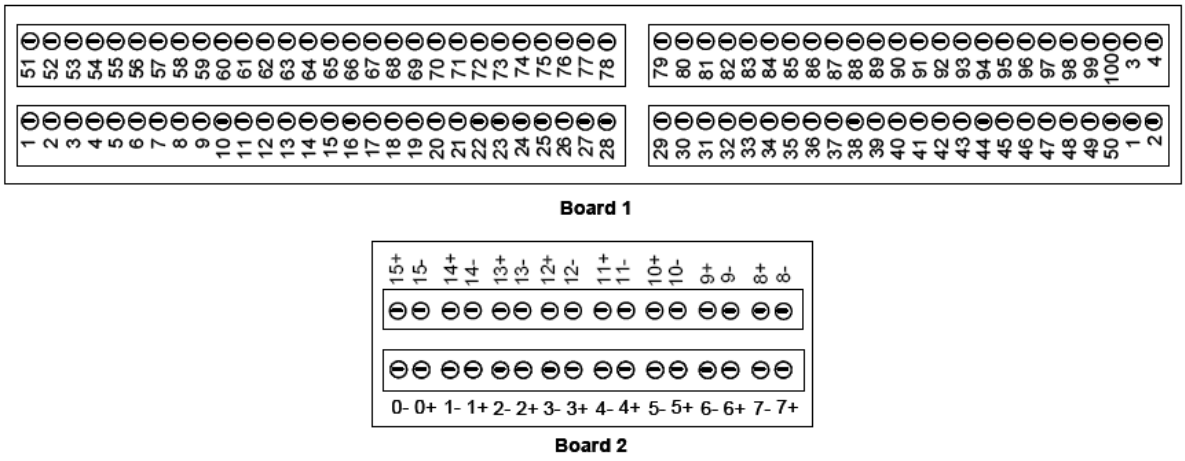

Figure 3-9: Schematic of circuit boards 1 and 2 used in the experiments

The pressure transducer and mass flow meter were connected to circuit board 1. The negative wires of both devices were connected to pin "1" and the positive wires were connected every other pin starting pin "2". For this research, the positive wires of the pressure transducer and the mass flow meter were connected to pin "2" and pin "6" respectively. This corresponded to channel 1 and channel 3 in the LABVIEW program. The thermocouples were connected to circuit board 2. The configuration of circuit board 2 is slightly different from circuit board 1. Each pin in circuit board 2 is numbered according to the channel number starting from channel 0. The negative wires were connected to the negative pins "-0, -1, -2…etc." and the positive wires were connected to the positive pins "+0, +1, +2…etc".

The specifications of the pressure transducer, mass flow meter and thermocouples are outlined in Table 3-3.

Table 3-3: Specification of experimental devices

	Temperature	Pressure	Flow rate
Company	Omega	Omega	Omega
Type	T-Type AWG#28	PX304-050A5V	FMA 3307
Range	-270°C to +400°C	0-50 psig	0 -2000 ml/min nitrogen
Input		12-30 VDC	0-12/15 VDC
Output		0.5-5.5 VDC	0 -5 VDC
response time	Still air 10 s Still Water 0.4 s		
Accuracy	Greater of 1°C or 0.75%		± 1.5% full scale
Repeatability			±0.5% full scale

3.7.1 Mass Flow Rate

An Omega mass flow meter (model FMA-3107) was used to measure the rate of butane uptake. The device measured the flow rate by applying a low electrical current to the flow at one end of the device and measured the heat distribution at the other end (Omega, 2007). This device was calibrated to measure the flow rate of steam corresponding to atmospheric pressure and density of nitrogen gas. A voltage of 0-5 V was output to the circuit board 1. The output voltage is converted to volumetric flow rate using the following equations.

$$V_{N_2} = \frac{VDC}{5} \cdot 2000 \qquad (3\text{-}6)$$

where V_{N2} is the volumetric flow rate corresponding to nitrogen gas under atmospheric pressure, VDC is the voltage output by the flow meter. The flow rate of other gas can be corrected using the correction factor provided by Omega Engineering. The manufacturer's correction factor for butane gas is 0.26. The volumetric flow rate of butane uptake was converted to mass flow rate by multiplying the volumetric flow rate of butane at atmospheric pressure by the density of butane at atmospheric pressure.

$$m_{sup} = V_s @ P_{atm} \cdot \rho_s @ P_{atm} \qquad (3\text{-}7)$$

where m_{sup} is the mass flow rate of solvent uptake, V_s @ P_{atm} is the volumetric flow rate of solvent at atmospheric pressure, and ρ_s @ P_{atm} is the density of the solvent at atmospheric pressure.

4.0 Results and Discussions

Five experiments were conducted to investigate the effect of permeability, low percentage volume of connate water and solvent condensation on the production rate, on solvent chamber growth and on the net solvent requirement in VAPEX. The summary of the experiments conducted is given in Table 4-1.

Table 4-1: Properties of experiments conducted

Experiment Number	Diameter of Glass beads (mm)	Porosity	Permeability ($x10^{12}m^2$)	Percent Connate Water	Average Experiment pressure (psig)	Solvent Condensation
1	1.19	0.38	1123	No	15	No
2	1.19	0.38	1123	7%	14	No
3	0.59	0.39	300	No	14	No
4	0.59	0.39	300	5%	13.5	No
5	1.19	0.38	1123	No	16	Yes

All experiments were conducted using 23 kg/m.s Cold Lake bitumen and instrument grade n-butane as solvent. The objectives were to:

1) Compare production history of experiments #1 and #3 with previous literature data (Oduntan, 2001) to verify the feasibility of the apparatus design.

2) Examine the effect of low percentage volume of connate water on the production rate of VAPEX by comparing results experiments #1 and #3 with that of experiments #2 and #4

3) Finally, the production history of experiment #5 was compared to that of experiment #1 to investigate the enhancement in the live oil production rate and the solvent chamber growth by encouraging solvent condensation at the solvent bitumen interface.

4.1 Determination of Chamber Spreading Velocity

Live oil is referred to as the diluted mixture of oil and solvent. Previous literature indicates that live oil production is constant over 80-85% of the experiment run time. This period of time is referred to as the chamber spreading phase. The concept of a chamber spreading phase is not unique to VAPEX; it is a frequently documented phenomenon in SAGD (Butler,

1991). In theory, the chamber spreading phase is a pseudo-steady state phenomenon observed as the bitumen-solvent interface advances sideways at a constant rate.

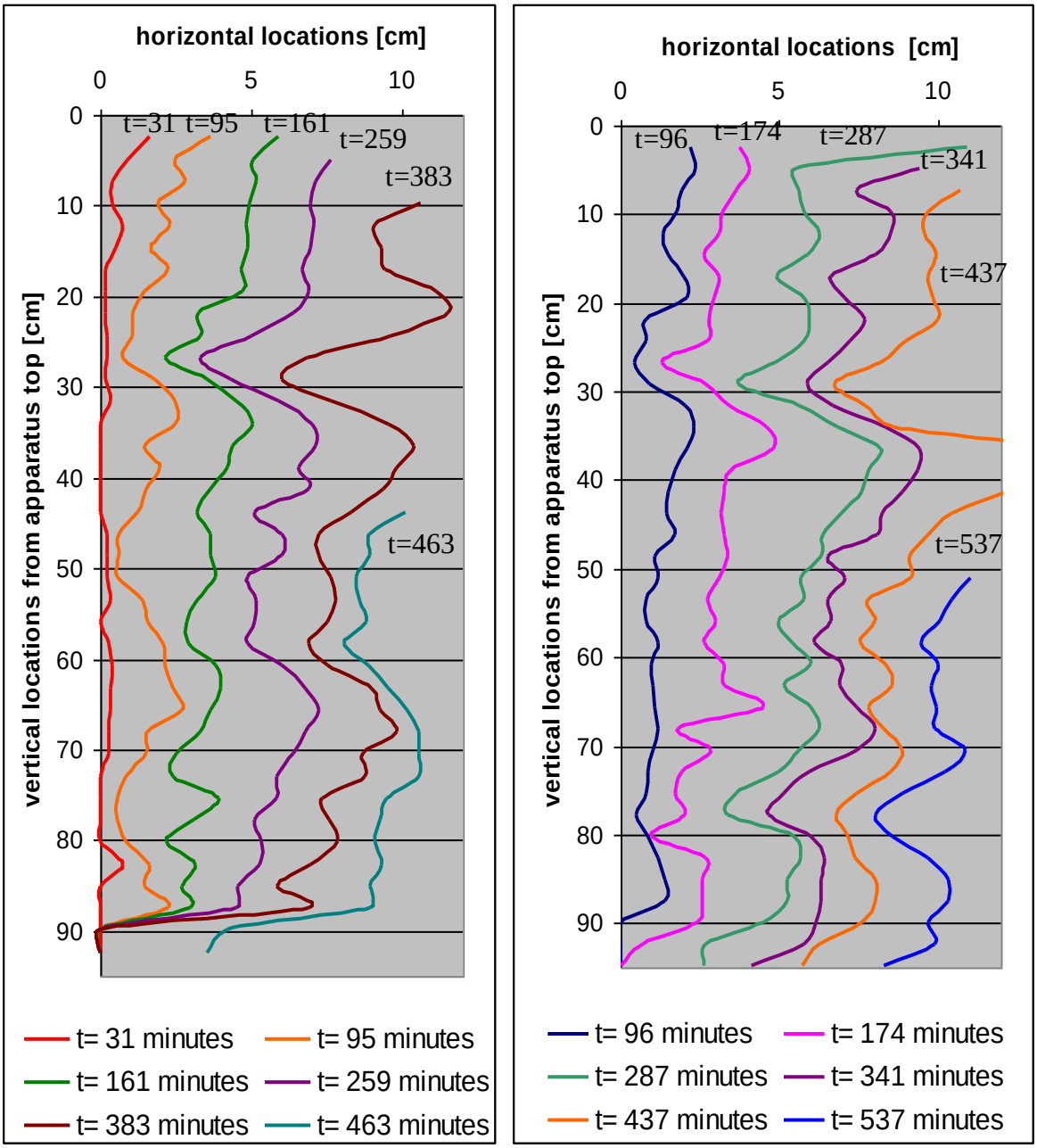

a) b)

Figure 4-1: Bitumen- solvent interface position at specific times for a) experiment #1 without connate water and b) experiment #2 with connate water

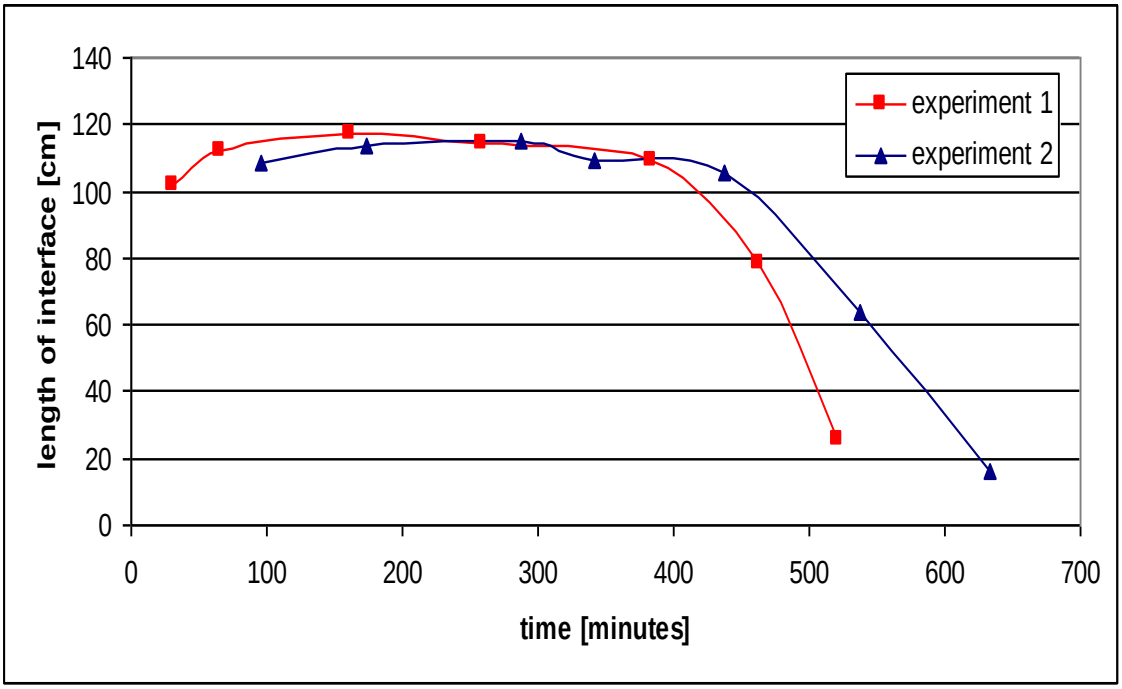

Figure 4-2: Length of interfaces versus time in experiments #1 and #2

A set of systematic criteria in determining the chamber spreading phase applicable to all experiments was defined. Theoretically, the production rate of VAPEX is determined by mass transfer and gravity drainage. Therefore, the height of interface and the length of interface have major impacts on the live oil production rate. The bitumen solvent interface profiles for experiments #1 and #2 are shown in Figure 4-1a and Figure 4-1b. At approximately 400 minutes, the peak of bitumen-solvent interface dropped below 90% of the apparatus height. In addition, the lengths of interfaces versus time plotted in Figure 4-2 indicated that the lengths of interfaces were constant until approximately 400 - 430 minutes. After that time, the lengths of interfaces decreased rapidly. The rapid decrease in production rates is due to the decreased surface area available for mass transfer, which is consistent with the instantaneous live oil production rates plotted in Figure 4-3 and Figure 4-4. The initial instantaneous live oil production rates were approximately 1.1 cm^3/min for both experiments, and at 200 minutes the instantaneous rate peaked at approximately 1.3 cm^3/min and it slowly decreasing. At approximately 400-450 minutes, the instantaneous live oil production rates had dropped below the initial 1.1 cm^3/min, suggesting the live oil production rates begun to level off.

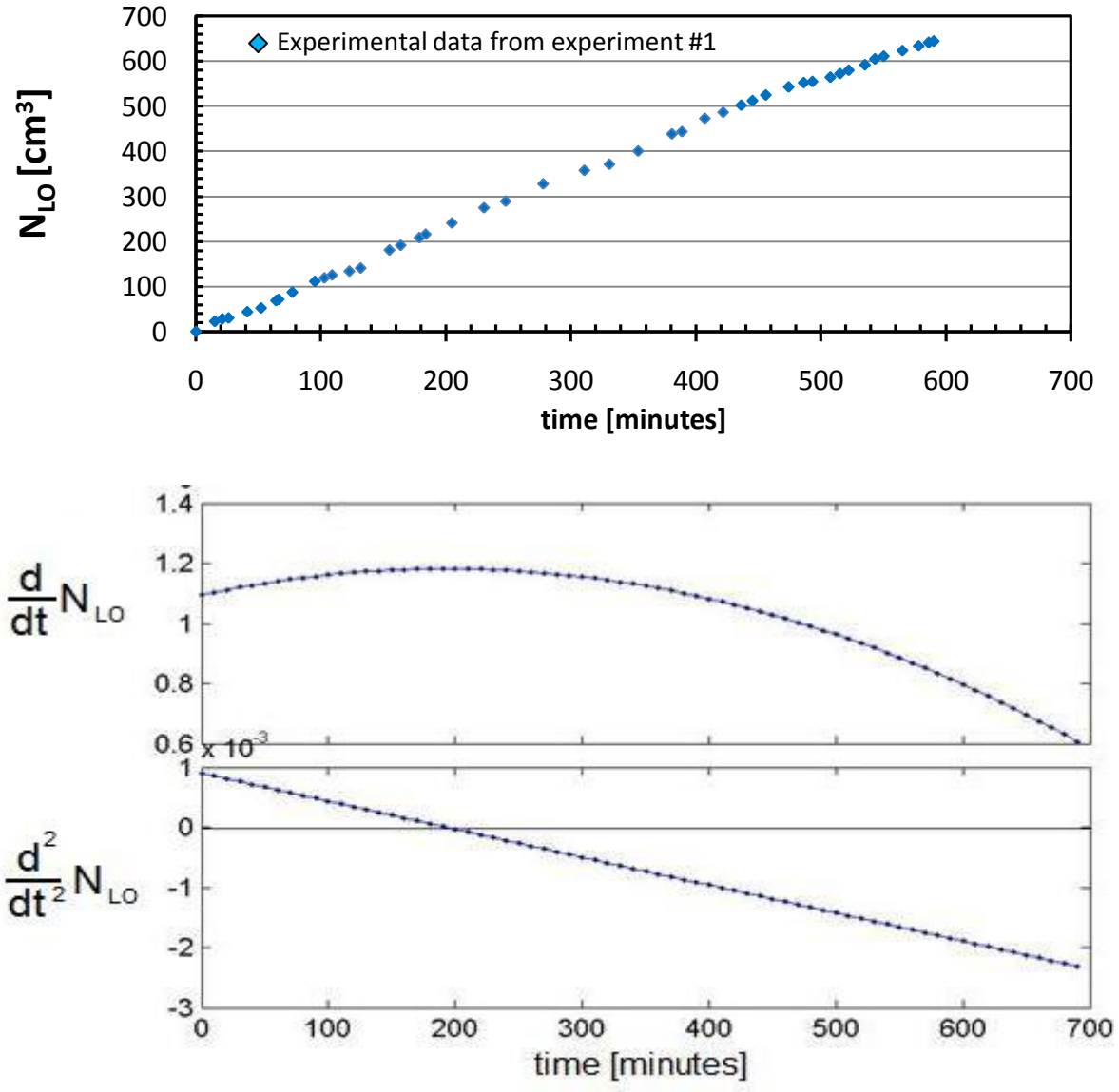

Figure 4-3: Live oil production history, instantaneous production rate and deceleration of the production rate for experiment #1

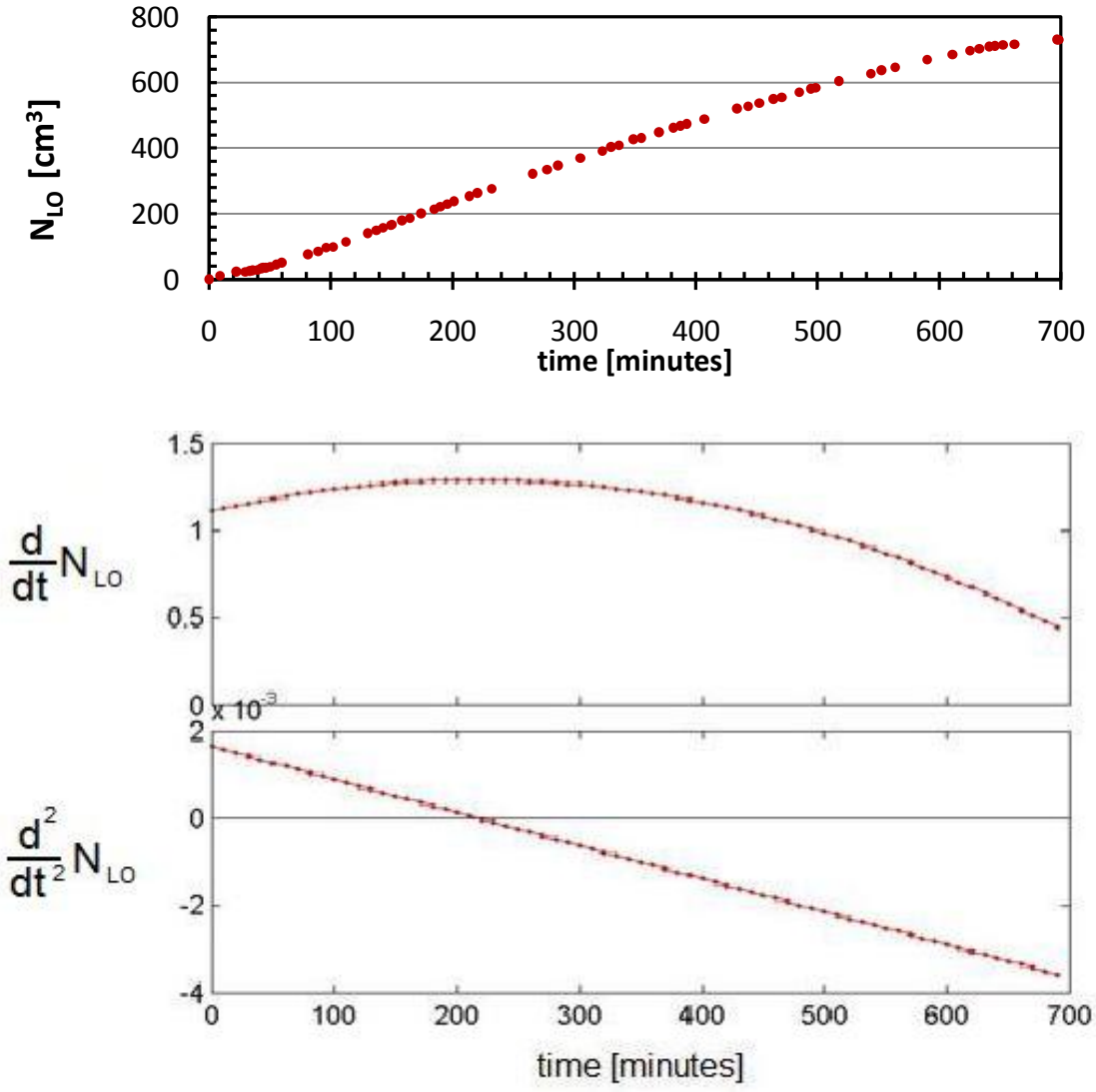

Figure 4-4: Live oil production history, instantaneous live oil production rate, and deceleration of the instantaneous live oil production rate for experiment #2

The apparatus used a vertical line source to distribute the solvent along the interface; however, the live oil production was rather unstable at the beginning of the experiments.

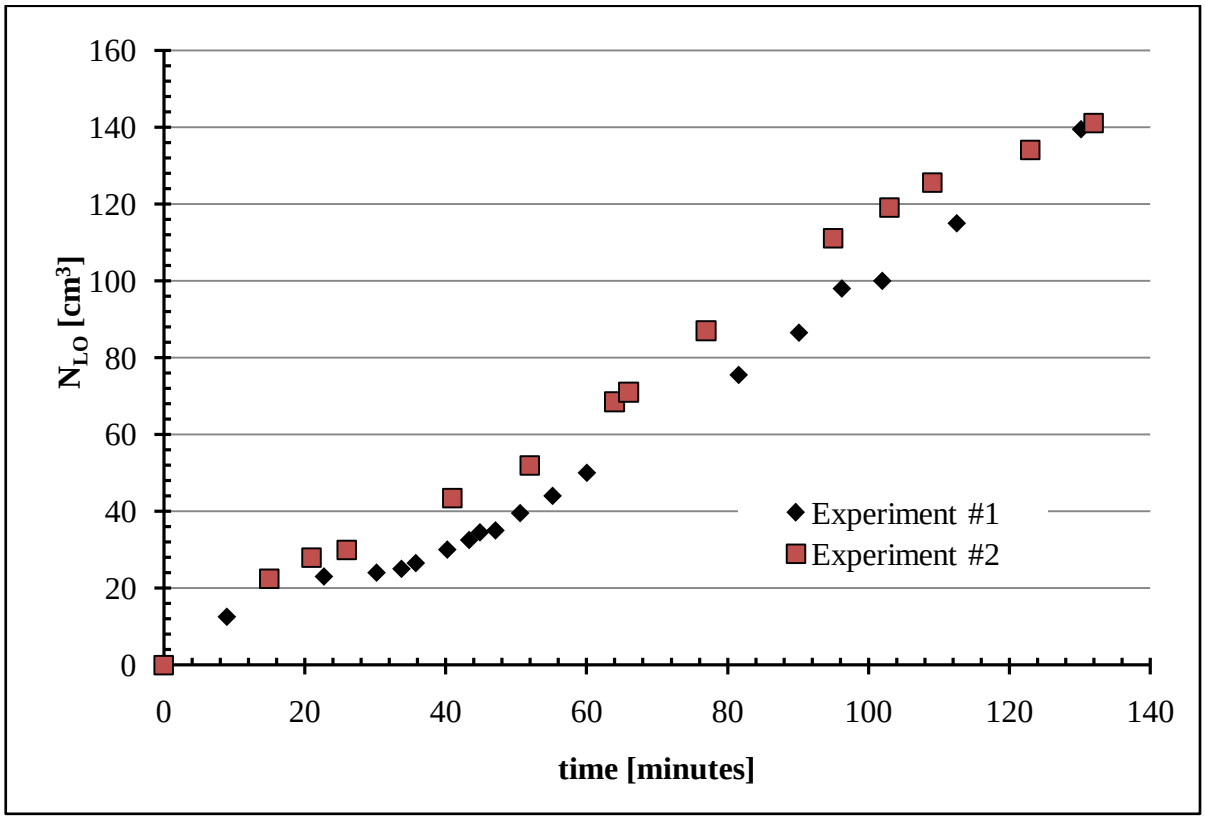

Figure 4-5: Production histories for experiments #1 (without connate water) and #2 (with connate water) from t = 0 min to t = 130 min

Figure 4-5 indicates that the live oil production histories of experiments #1 and #2 were not the same until t = 100 min. The instability in the production histories is because the bitumen-solvent interfaces were not yet well developed during this period of time. The calculations for the production rates and the solvent chamber growth assumed the chamber spreading phase began at t = 100 min to eliminate all the uncertainties. The chamber spreading phases for all experiments were determined using the following criteria:

1) Chamber spreading phase began at t = 100 minutes
2) Chamber spreading phase ended when the length of interface began to drop rapidly

Table 4-2: Length of chamber spreading phase for experiments #1 - #4

Experiment Number	Length of Chamber spreading phase (minutes)	Total experimental time (minutes)	Percent time of chamber spreading phase (%)
1	425	586	72.5%
2	450	698	64.4%
3	860	1221	70.7%
4	750	1451	51.6%

Table 4-2 summarizes the traced length of chamber spreading phase for experiments #1 to #4. For experiments #1 and #2, conducted with 1.19 mm glass beads, the chamber spreading phase ended approximately after 425 and 450 minutes; for experiments #3 and #4, the chamber spreading phase ended approximately after 860 and 750 minutes, respectively. Experiments #1 and #3 were for conditions without connate water and the chamber spreading phase ended at approximately 73% and 71% of the experimental time, approximately 8% and 20% greater than the chamber spreading time in experiments #2 and #4 that had a packing with 7% and 5% connate water respectively.

4.2 VAPEX without Solvent Condensation

Four VAPEX experiments with no solvent condensation were conducted using the new apparatus design. The analysis of the results focused in 3 different areas:

1) Validating the feasibility of the new apparatus design with packing in the annulus
2) Determining the effect of connate water on the production rate, on the horizontal interface advancement velocities and on the net solvent requirement in VAPEX
3) Determining the effect of permeability on the solvent chamber growth and on the net solvent requirement in VAPEX

4.3 Validating the Feasibility of Apparatus Design

The feasibility and the ability of the new apparatus design in replicating the experimental results from previous research (Oduntan, 2001) was investigated first.

Oduntan (2001) investigated the effect of permeability and the height of pay zone on the live oil production rate in unconsolidated model using a rectangular channel apparatus design with permeability ranging from $25x10^{-12}$ m^2 to $1.92x10^{-10}$ m^2 and the pay zone height varied from 21 cm to 247 cm height. The live oil production rate was found to be proportional to the square root of permeability and the height for unconsolidated media. Oduntan concluded that the live oil production rate of a system with $1.36x10^{-10}$ m^2 permeability and a 45^o dip angle can be predicted by the following correlation.

$$Q_{LO} = 0.0014 L_{pz}^{0.55} \qquad (4\text{-}1)$$

where Q_{LO} [m^3/h.m] is the volumetric production flow rate per hour per unit width and L_{pz} is the thickness of the pay zone [m]. The predicted live oil production rate will be scaled to the experimental properties used in experiments #1 and #3.

Table 4-3: Comparison of live oil production rates from experiment #1 and #3 to predicted production rates calculated using Oduntan's scale up correlation.

Exp. #	L [cm]	W [cm]	K [$10^{12}m^2$]	ϕ	Q_{exp} [cm^3/min]	$Q_{predicted}$ [cm^3/min]	$\frac{Q_{exp} - Q_{predicted}}{Q_{exp}}$
1	1.01	0.64	1123	0.38	1.15	1.03	10.4 %
3	1.01	0.64	300	0.39	0.658	0.554	15.7 %

The difference between the experimental live oil production rate and the predicted live oil production rate is less than 16% in both cases. The variation may be due to the difference in the apparatus set up, the material used in the experiments and the slightly different experimental conditions. The comparisons verified the feasibility of the new apparatus design in producing experimental results that were comparable to results from previous literatures.

4.4 Effect of Connate Water in VAPEX

Most heavy oil reservoirs contain a certain percentage of pore volume of water. The effect of connate water on VAPEX has not been completely investigated. Das (1995) conducted two experiments to compare the bitumen production rate in systems with 12% and 16% water saturation. It was observed that the connate water saturation reduced the bitumen production

rate and suggested that bitumen production rate is proportional to the square root of bitumen saturation.

The following section focuses on investigating the effect of connate water on live oil production rate, on solvent chamber growth and on the net solvent requirement in the system. Four experiments were conducted using two sizes of glass beads, 1.19 mm and BT3 (diameter = 590 μm). The details of the experiments conducted are summarized in Table 4-1. In short, experiments #1 and #3 were saturated with 100% bitumen; experiments #2 and #4 were for conditions of 7% and 5% connate water saturation, respectively.

4.4.1 Live Oil and Bitumen Production Rate

The production histories for experiments #1 and #2 are plotted in Figure 4-6. Experiments #1 and #2 were conducted in 1.123×10^{-9} m^2 unconsolidated porous media, and saturated without connate water and 7% connate water respectively.

The chamber spreading phase was determined to end at 425 minutes and 450 minutes, respectively. The live oil production rates during the chamber spreading phase for the two experiments were 1.15 and 1.26 ml/min. The variation in live oil production rate between the two experiments was less than 10%. Similar results were obtained from experiments #3 and #4. The permeability of experiments #3 and #4 was calculated to be 300×10^{-12} m^2. Experiment #3 had no connate water and experiment #4 had 5% connate water. The difference in live oil production rate between the two experiments was approximately 14%. The discrepancies in the live oil production rates between the experiments with and without connate water were too small to indicate that a small percentage volume of connate water would affect the live oil production rate of VAPEX.

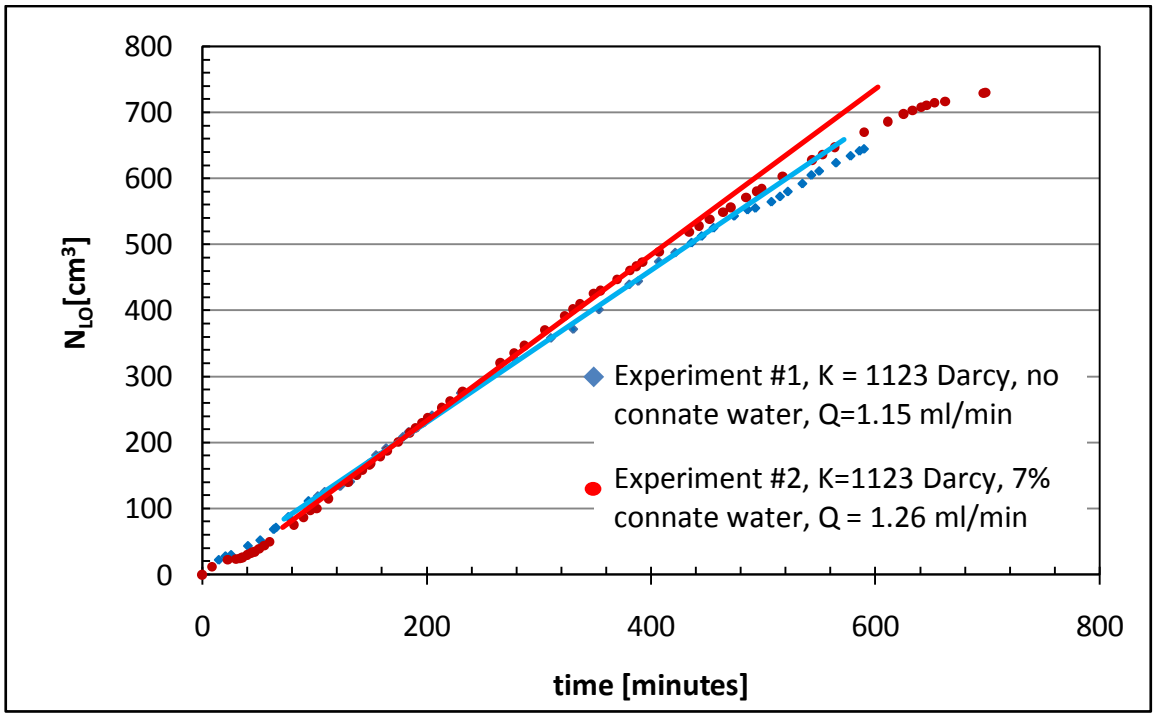

Figure 4-6: Live oil production history for experiments #1 and #2

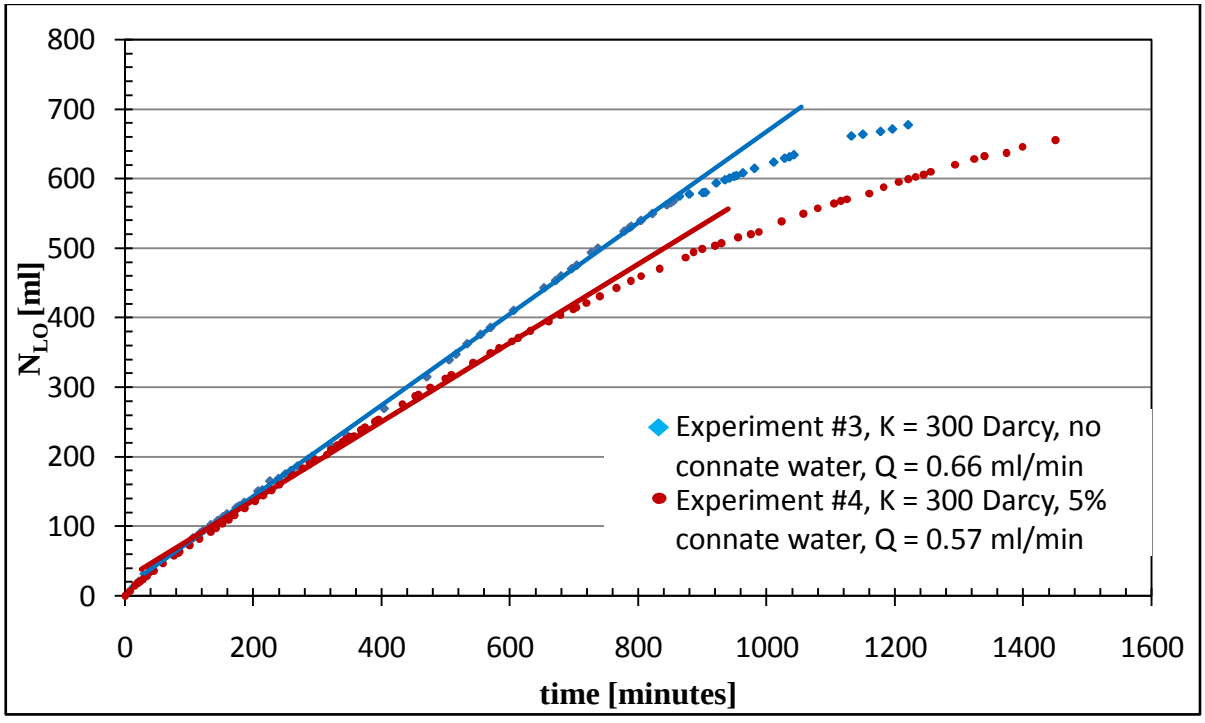

Figure 4-7: Live oil production history for experiments #3 and #4

4.4.2 Bitumen Production Rate

Bitumen produced during the experiments was weighed several times until all solvent was liberated. The production history for bitumen is plotted in Figure 4-8. The bitumen production rates for experiments #1 and #2 were 0.754 g/min and 0.749 g/min respectively. The variation between the 2 experiments was less than 1%. This difference is not significant.

The bitumen production rate during the chamber spreading phase for experiment #3 was 0.35 g/min and it is approximately 14% higher than that of experiment #4. The higher production rate is probably the result of higher initial oil saturation in experiment #3. According to the scale-up production model from Das (1995), the effect of 5% and 7% connate water corresponds to 2.5% and 3.5% differences in bitumen production rates. The difference in bitumen production rates between the two configurations of the experiments is too small to be significant.

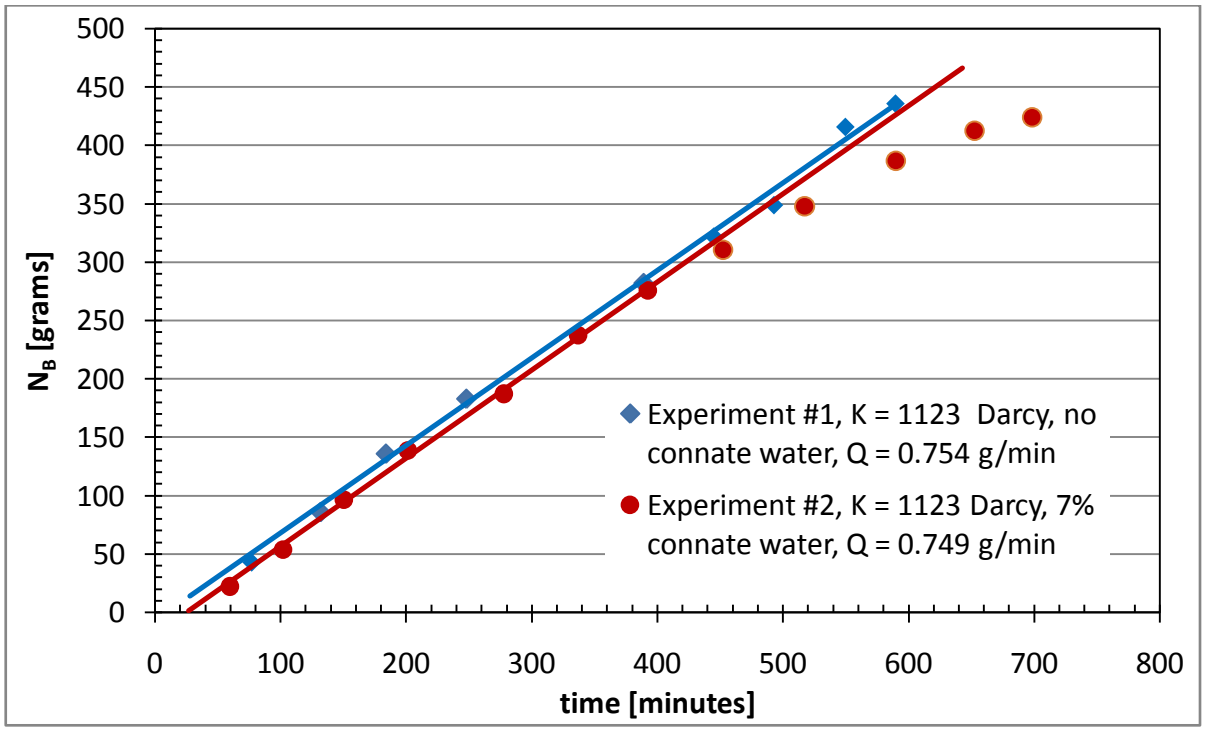

Figure 4-8: Bitumen production history of experiments #1 and #2

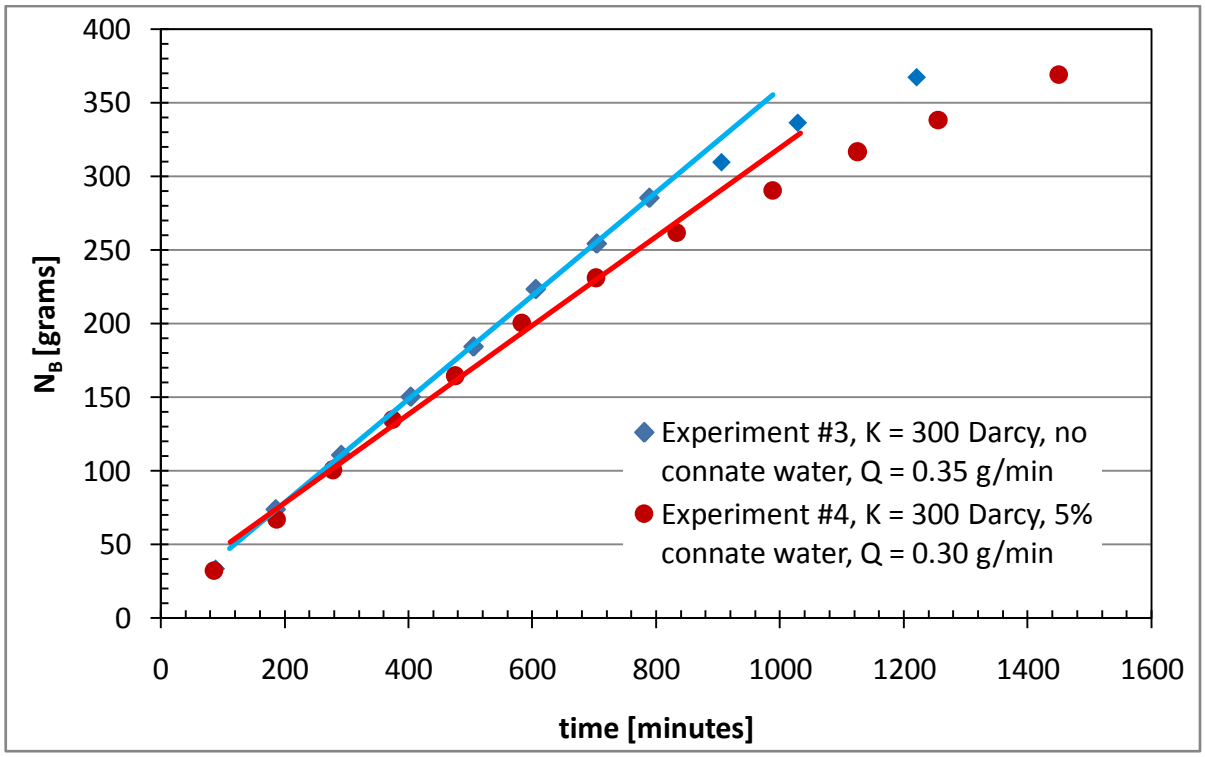

Figure 4-9: Bitumen production history of experiments #3 and #4

4.4.3 Horizontal Interface Advancement

The solvent–bitumen interfaces for experiments #1 and #2 are plotted in Figure 4-1a and Figure 4-1b. In both cases, the interface evolved as per the characteristic VAPEX shape (Oduntan, 2001; Chatzis, 2002; James, 2003). The horizontal locations of the interface profile were extracted at every 2.5 cm vertical location to calculate the velocity of the interface advancement during the chamber spreading phase.

The horizontal interface velocities are plotted in Figure 4-10. In all four experiments, the top 10 cm of the the appratus advanced faster than the rest, perhaps due to channeling near the top. Also interesting to note is that the interface advancement in experiments #3 and #4, with the low permeability were more steady than in the high permeability experiments. The average horizontal advancement velocities were calculated from 15 cm to 85 cm from the top of the apparatus to eliminate the channelling and the capillarity effects. The average horizontal interface advancement velocities for experiments #1 and #2 were 0.0173 cm/min and 0.018 cm/min respectively. The horizontal interface advancement velocities for experiments #3 and #4 were 0.0077 cm/min and 0.0076 cm/min respectively. The

discrepancy was less than 4% for experiments #1 and #2; and less than 2% for experiments #3 and #4. The difference was insignificant; hence, the average horizontal advancement velocities were independent of water saturation for low percentage connate water systems.

It is also observed the advancement of interface in experiments #3 and #4 (Figure 4-10b) is more uniform than that of experiments #1 and #2 (Figure 4-10a). This may be due to the inconsistency in the packing of glass beads, creating heterogeneity.

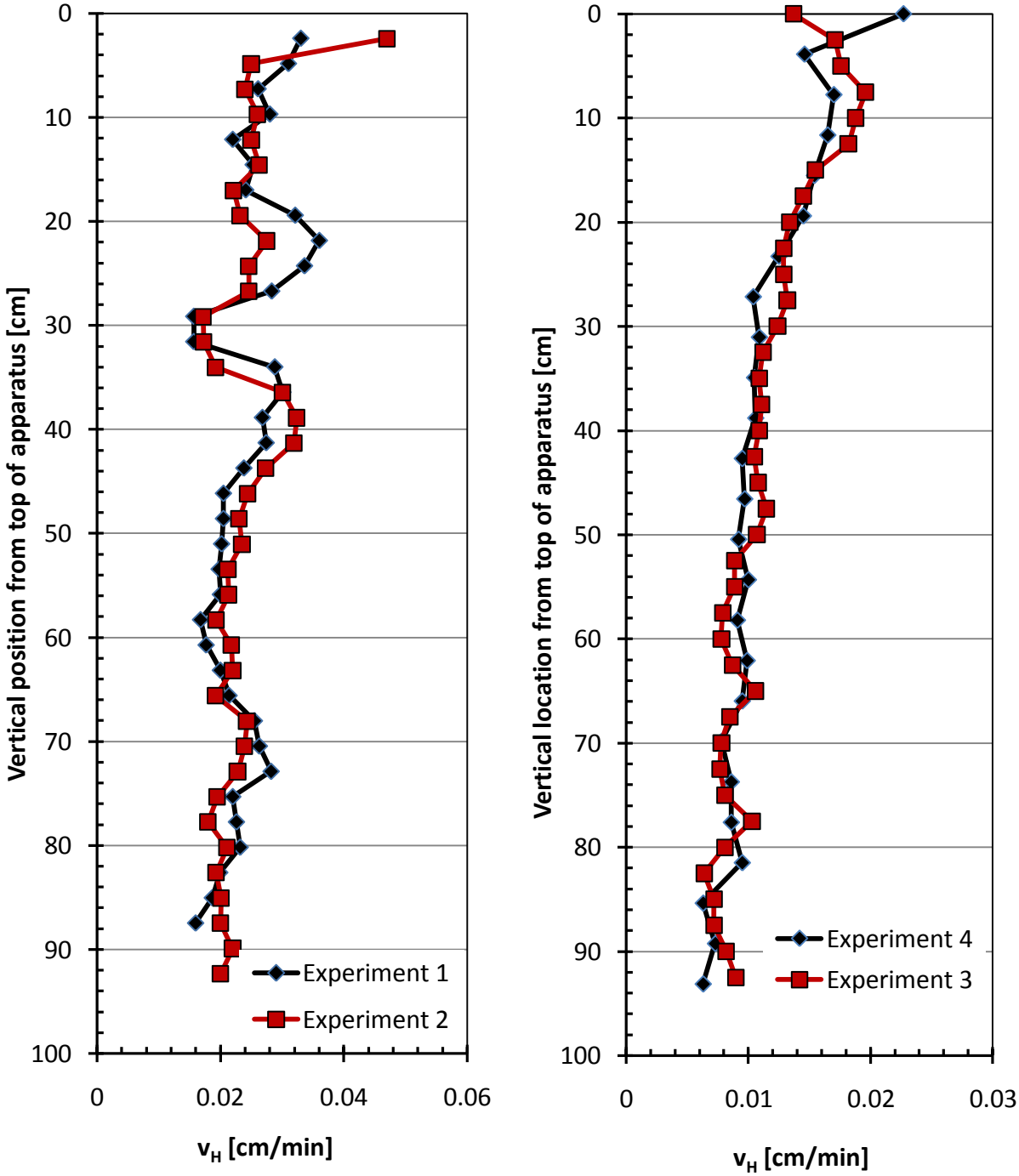

a) b)

Figure 4-10: Horizontal interface advancement velocities in various vertical position for a) experiments #1 (no connate water) and #2 (7% connate water) with $k=1.123\times10^{-9}$ m^2 b) experiments #3 (no connate water) and #4 (5% connate water) with $k=3\times10^{-10}$ m^2

4.4.4 Solvent Mass Balance

The mass fraction of solvent in live oil was measured and calculated as described in section 3.6.3. For experiments #1 and #2 the mass fraction of solvent were 0.25 and 0.30, respectively; the mass fraction for experiments #3 and #4 were 0.38 and 0.35, respectively.

The system pressure and the butane uptake for experiment #3 are shown in Figure 4-11. Experiment #3 was conducted with k = $3x10^{-10}$ m^2 and with no connate water. The total experimental time was 1221 minutes.

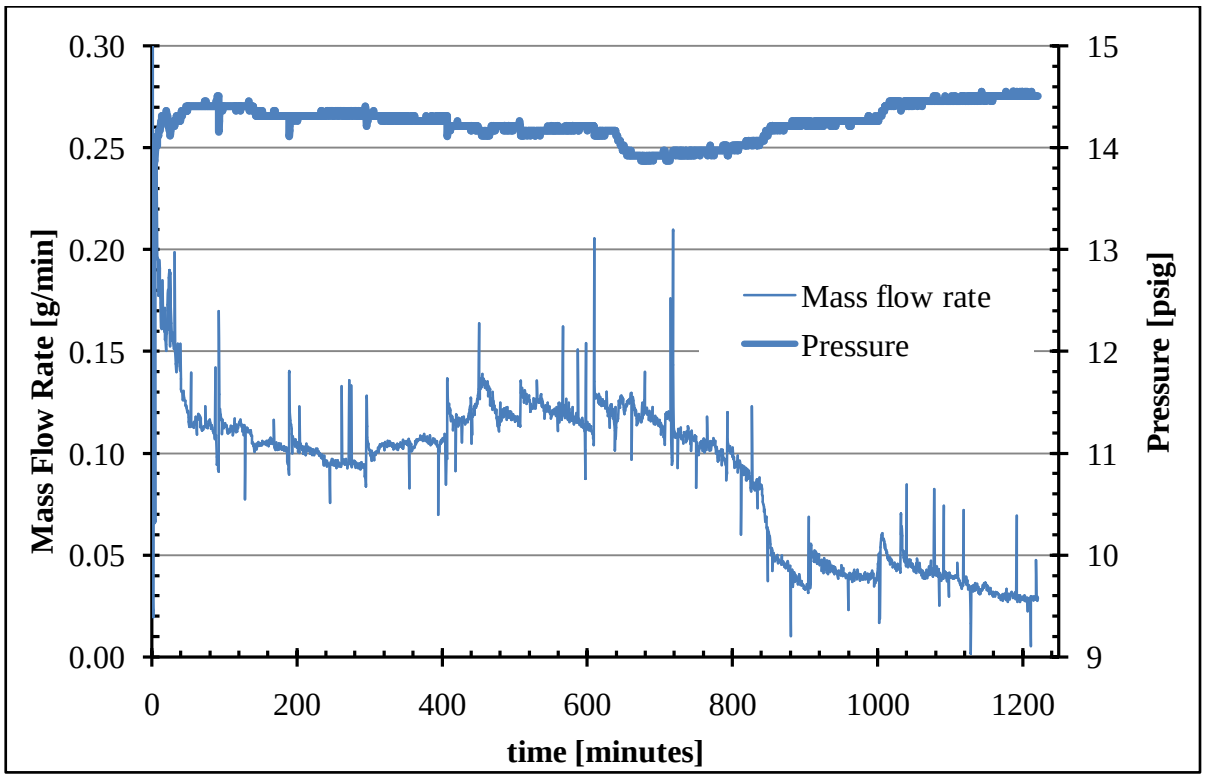

Figure 4-11: Mass flow rate of butane and the pressure of the system versus time for experiment #3 (k = $3x10^{-10}$ m^2, no connate water)

The system pressure was maintained at a constant pressure of 16 psig (110.3 kPa). The uptake of butane was constant at approximately 0.22 g/min during the chamber spreading phase. The sharp increase in the solvent uptake in Figure 4-11, was the result of pressure depletion when emptying the live oil collection cylinder. Theoretically, the solvent is needed for two processes in VAPEX:

1) The majority of the solvent uptake is used to dilute the bitumen through mass transfer.
2) The remaining solvent is used to fill up the emptied pore space after the bitumen has been drained

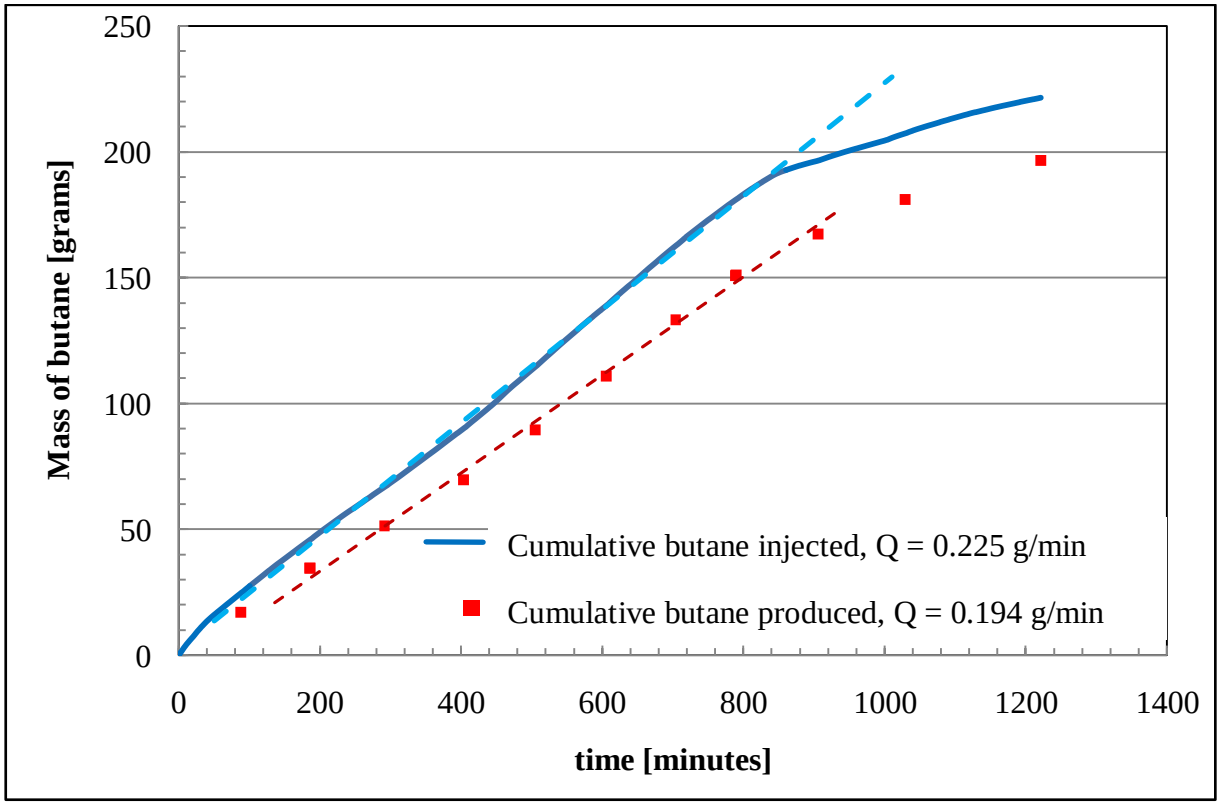

Figure 4-12: Cumulative butane injection and production results of experiment #3

The cumulative butane injection and cumulative butane production for experiment #3 are plotted in Figure 4-12. The injection and production rates of butane during chamber spreading phase were 0.225 g/min and 0.194 g/min, indicating that over 85% of solvent injected during chamber spreading phase was produced with the live oil. For experiment #3, over 85% and 7% of butane injected was produced from the live oil and during the gas blowdown phase of the apparatus respectively. The total solvent loss during the process is approximately 8% of the total butane injection. Table 4-4 summarizes the butane requirement for the experiments #1 - #4. Similar results were obtained from experiment #4. With connate water, over 87% of solvent was produced from the live oil and approximately 6% of the solvent was recovered during the blowdown process. These results indicate that

the solvent requirements for system with and without connate water in VAPEX are about the same.

Table 4-4: Solvent requirements for experiments #1 - #4

Experiment Number	Total solvent uptake [g]	Solvent produced during bitumen production [g]	Solvent produced during blowdown [g]	Total bitumen produced [g]	% of butane injected remained in apparatus
1	167	122	8.6	461	22
2	250	184.6	16.6	431	20
3	230	196	16.4	367	8
4	206	180	11.4	368	7

4.5 Effect of permeability in VAPEX

The effect of permeability to the live oil and bitumen production in VAPEX is well understood. Previous literatures concluded that bitumen and live oil production rate is proportional to the square root of permeability (Oduntan 2001, Butler and Mokrys 1989). The following section focuses on the effect of permeability on the solvent chamber growth and on the net solvent requirement.

4.5.1 Horizontal Interface Advancement

The horizontal interface advancement velocities for all experiments were evaluated in the previous section. The production rate and horizontal interface advancement velocity are summarized in Table 4-5. The average horizontal interface velocities versus permeability plotted in Figure 4-13 showed the horizontal average interface velocity is proportional to $\sqrt{K}$. This observation is similar to Oduntan's scale-up model for live oil production. The horizontal velocity is an important parameter in estimating the live oil production rate of the system during the chamber spreading phase.

Table 4-5: Horizontal interface advancement for experiment 1-4

Experiment Number	k [$x10^{12}$ m^2]	Q_{LO} [cm^3/min]	Q_B [g/min]	v_H [cm/min]
1	1123	1.15 ml/min	0.754 g/min	0.018 cm/min
2	1123	1.25 ml/min	0.749 g/min	0.0173 cm/min
3	325	0.66 ml/min	0.350g/min	0.0077 cm/min
4	276	0.56 ml/min	0.300 g/min	0.0076 cm/min

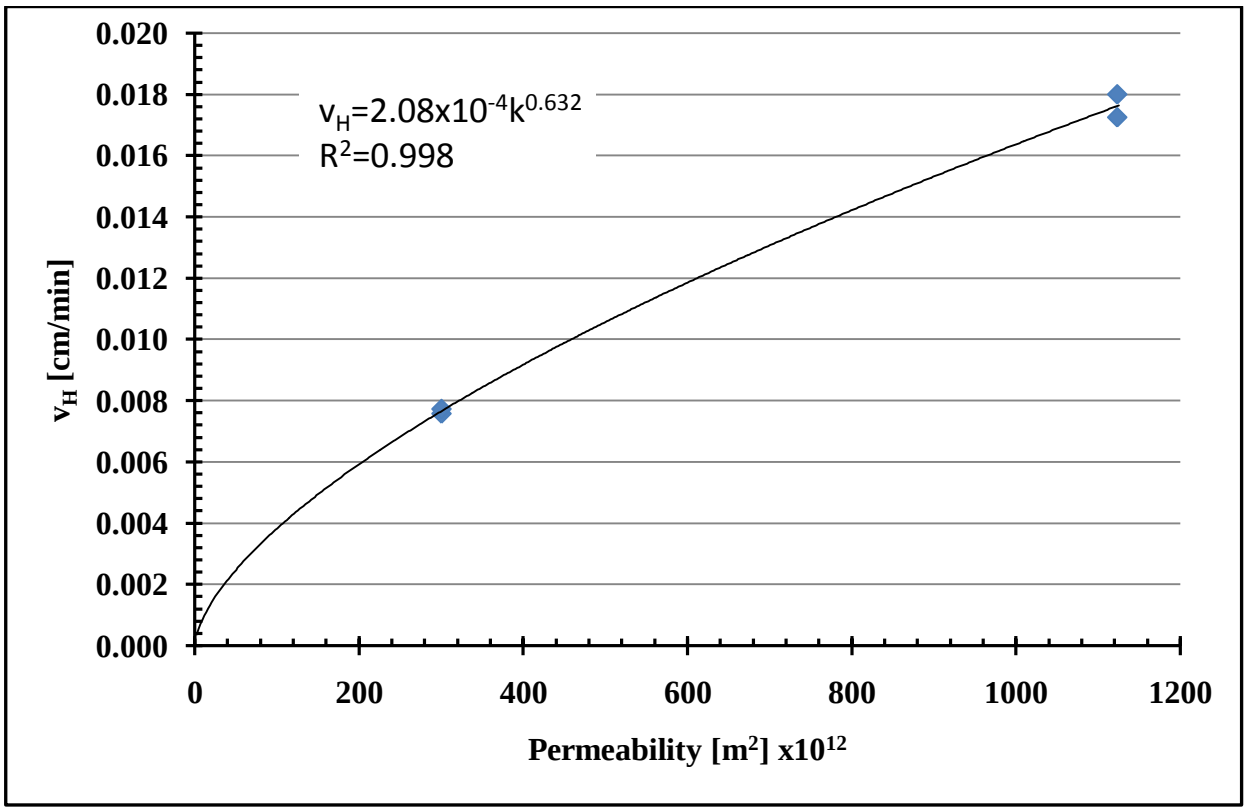

Figure 4-13: The average horizontal interface velocity versus permeability

4.5.2 Solvent Mass Balance

The solvent requirement in the experiments is summarized in Table 4-4. As shown in Table 4-4, at low permeability, over 85% of the solvent was recovered in the live oil produced; and only 74% of solvent was recovered in live oil at high permeability. Furthermore, approximately 8% and 6% of solvent was lost in experiments #3 and #4, compared to 20% and 22% in experiments #1 and #2.

It was also observed that the mass fraction of solvent increases as the permeability decreases. The significant increase in the mass fraction of solvent is believed to be the result of the longer exposure time for bitumen to be exposed to the solvent. The mass fractions of solvent for experiments #1 - #4 are plotted is Figure 4-13.

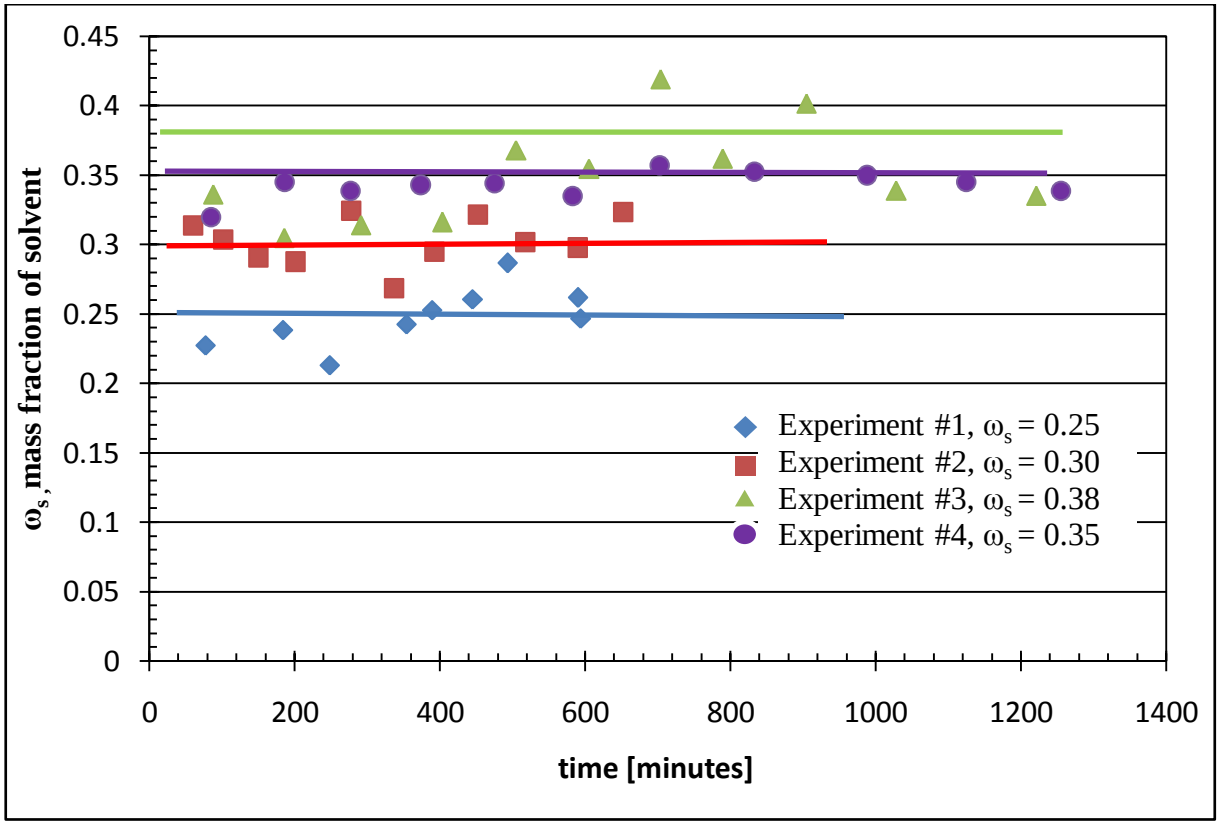

Figure 4-14: Mass fraction of solvent in experiment #1 - #4

4.6 Results for Warm VAPEX Experiment

A preliminary warm VAPEX experiment was conducted to investigate the effect of solvent condensation on the live oil production rate, on the solvent chamber growth and on the solvent requirement using the new apparatus design. The experiment was conducted using 1.19 mm glass beads with approximately 38% porosity and permeability of approximately 1123×10^{-12} m^2. The system was 100% oil saturated without connate water. The properties of the unconsolidated model were identical to experiment #1 to allow a direct comparison between the two experiments. The water bath was maintained at approximately 23^{o}C, while the ambient temperature was fluctuating between 20^{o}C to 21^{o}C.

4.6.1 Production Histories

The experiment was stopped at 352 minutes experimental time because the ambient temperature rose above 21°C.

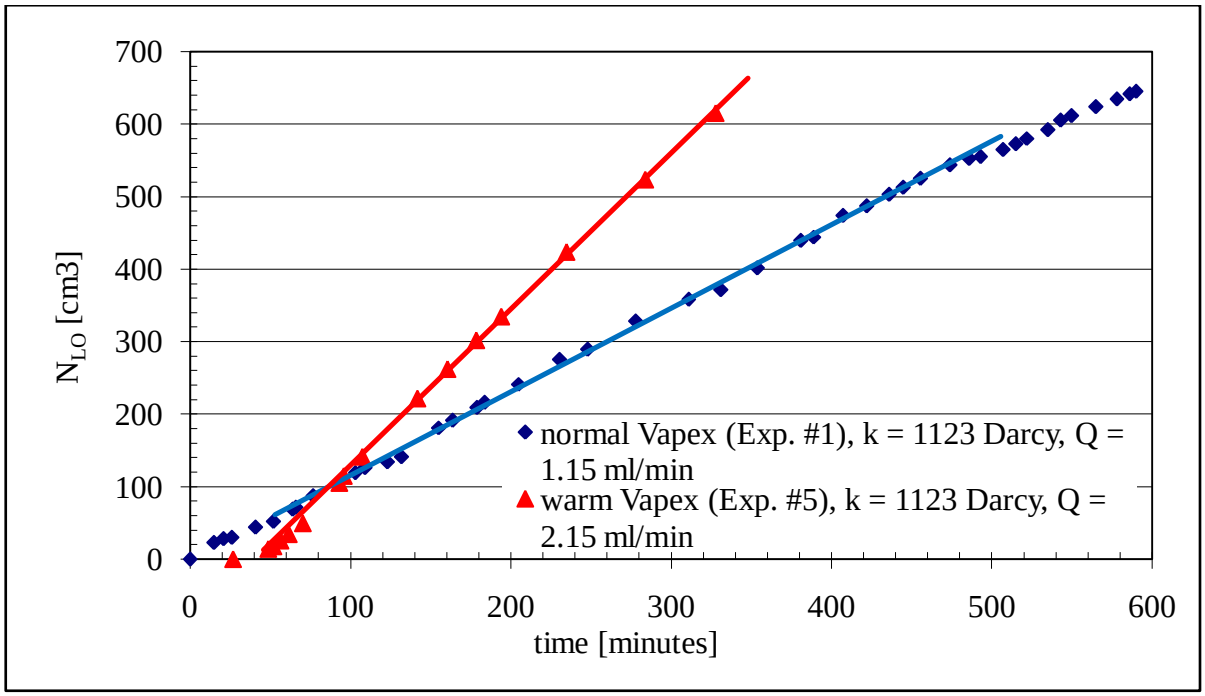

Figure 4-15: Cumulative live oil production versus time for experiments #1 and #5

The live oil production histories of experiments #1 and #5 are plotted in Figure 4-15. The steady-state live oil production rates for experiments #1 and #5 were 1.15 ml/min and 2.16 ml/min, respectively. The live oil production rate increased 87% in experiment #5 compared to experiment #1. The increase is perhaps because of the significant increase in the mass fraction of solvent from 0.25 in experiment #1 to 0.6 in experiment #5.

The bitumen production rate is shown in Figure 4-16. The bitumen production rate increased from 0.72 g/min in experiment #1 to 0.98 g/min in experiment #5. This corresponds to an increase of 36%. The production rate was calculated based on the weight of produced bitumen. The comparison is inadequate because asphaltene precipitation was observed in experiment #5 but not in experiment #1. Asphaltene are the highest molecular weight components in heavy oil; hence, the increase in the volumetric bitumen production rate

should be more significant. Solvent condensation not only increased the bitumen production rate in VAPEX but also improved the quality of the bitumen produced.

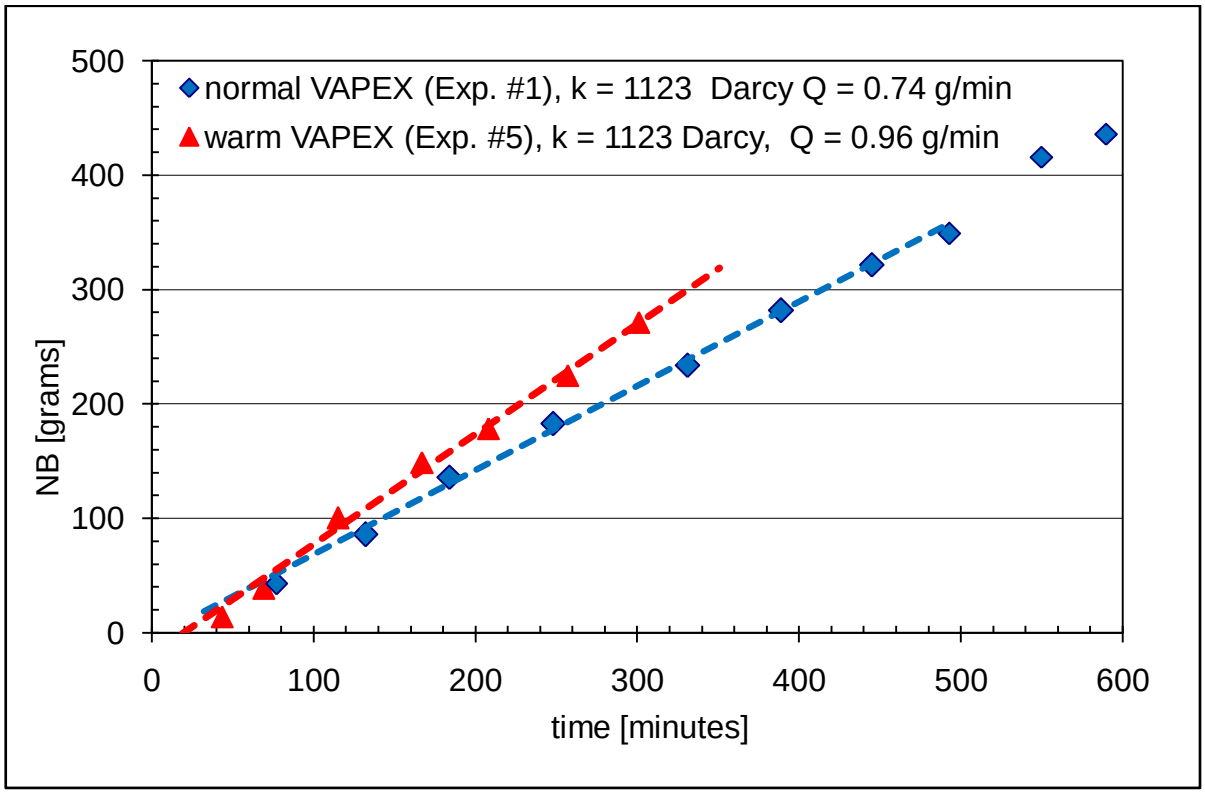

Figure 4-16: Cumulative bitumen production versus time for experiments #1 and #5

4.6.2 Interface Advancement

The bitumen-solvent interface for the warm VAPEX experiment was traced and analyzed as described in section 3.6.4. The bitumen solvent interface profile for warm VAPEX experiment is plotted in Figure 4-17. The profile indicates that the bitumen solvent advancement increases near the bottom of the apparatus. This is different from the characteristic VAPEX interface shown in experiment #1. The reason for such phenomenon is still under investigation.

The horizontal interface advancement velocity versus vertical height for experiment 1 and 5 are plotted in Figure 4-18. It was evident that the advancement for experiment #5 was greater than experiment #1. The average horizontal advancement velocity for experiment #5 was 0.0309 cm/min, 30% higher than experiment #1.

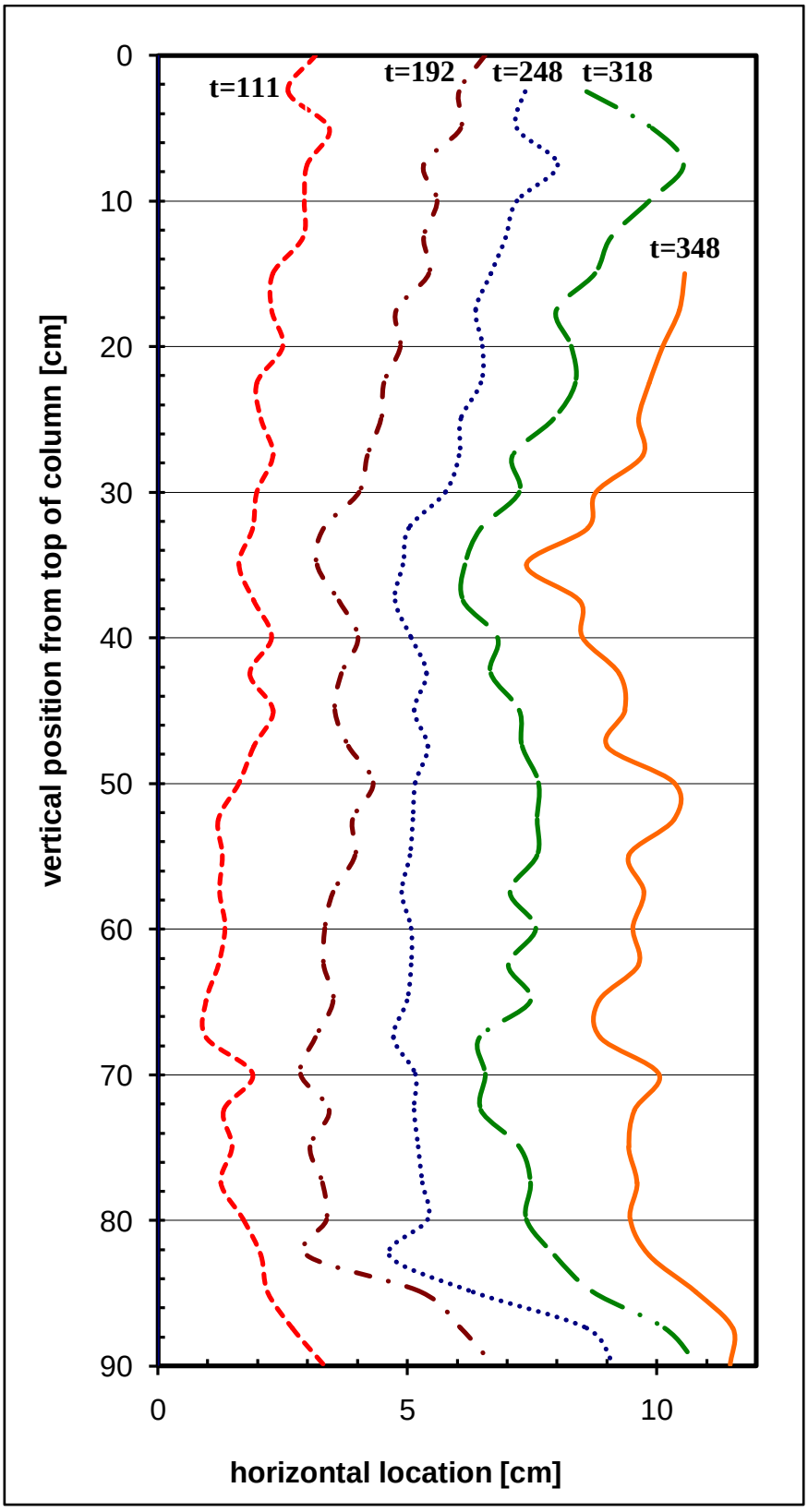

Figure 4-17: Bitumen solvent interfaces for warm VAPEX experiment

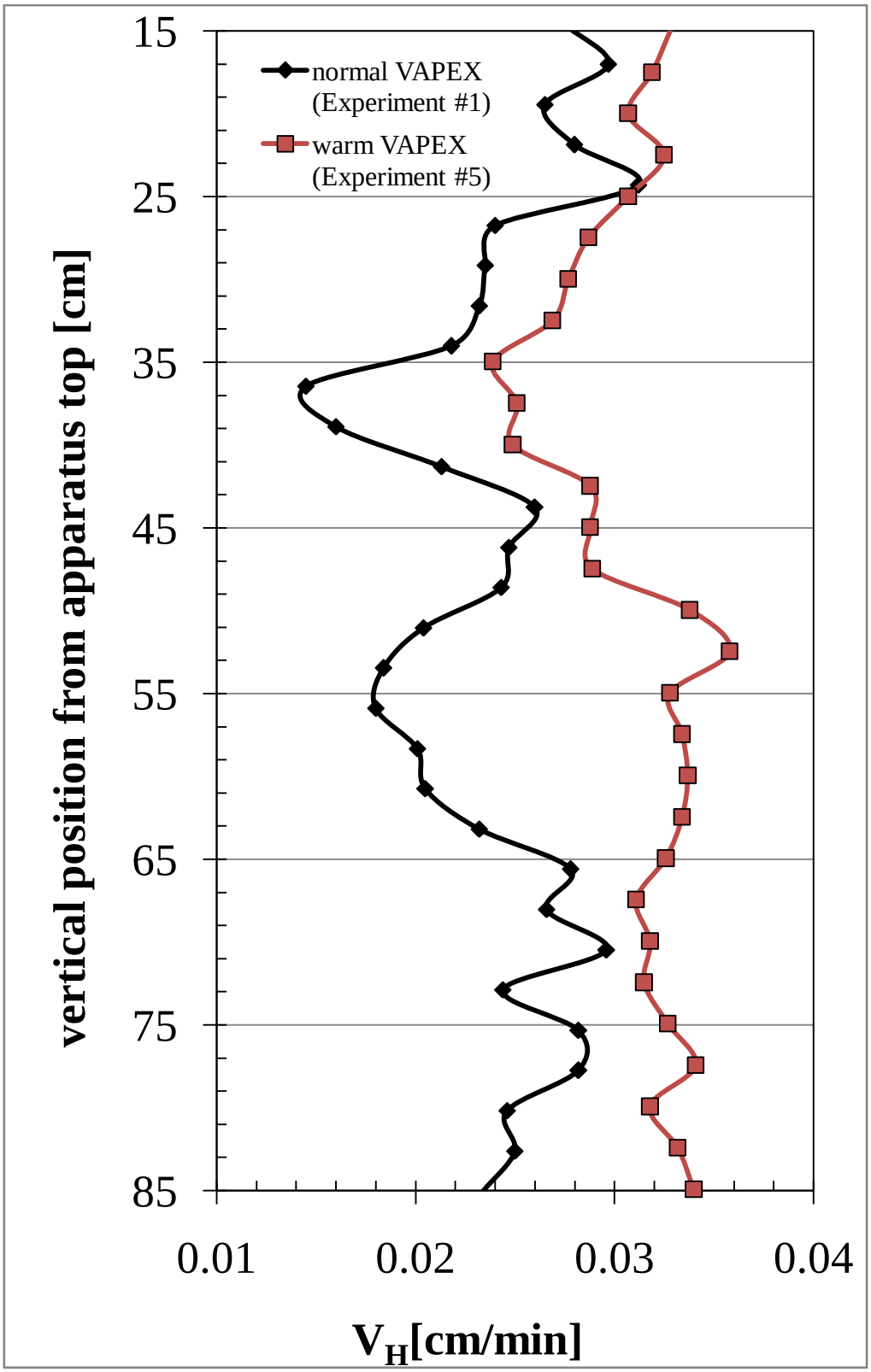

Figure 4-18: Horizontal interface advancement velocity versus vertical height for experiment #1 (normal VAPEX) and experiment #5 (warm VAPEX)

4.6.3 Mass Balance of Solvent

The mass fraction of solvent in live oil increased by 140% (from $\omega_s = 0.25$ in experiment #1 to $\omega_s = 0.60$ in experiment #5). This increase the results from solvent condensation in the gas injection tube and in the swept area, due to heat transfer between the apparatus and the surroundings. Theoretically, at reservoir conditions, solvent condensation is minimal in the swept area because the heat transfer between the swept area and surroundings is minimal by comparison to labratory experiments. Solvent condensation in the swept area is undesirable because it creates a restriction for solvent transport to the solvent bitumen interface. James et. al. (2007) conducted a set of experiments to study the solvent chamber growth in warm VAPEX experiments using glass micromodels. The solvent supply and the apparatus were held at the same temperature as the apparatus to enhance solvent condensation. The observed horizontal interface velocities in the warm VAPEX micromodel experiments were 4 times greater than that of the normal VAPEX experiment in the same mircomodel. The enhancement observed by James et. al. (2007) in glass micromodels is significantly higher than the enhancement observed in this experiment involving the permeability unconsolidated glass beads. The difference may be due to the difference in the porous media characteristic between the glass micromodels and the glass bead packing. It is also believed that the enhancement in the horizontal interface velocity will increase if the solvent condensation in the swept area is minimized.

The solvent uptake and the pressure of the system for the warm VAPEX experiment (experiment #5) is shown in Figure 4-19. The system showed similar behaviour compared to the normal VAPEX. The solvent uptake was relatively constant at 0.4 g/min; almost double that of normal VAPEX experiment (experiment #1). The high solvent uptake caused a significant increase in the mass fraction of solvent in the live oil and in the production rate.

The total solvent uptake for the experiment was calculated to be 245 g. The solvent produced in live oil was 189 g and the mass of solvent recovered during blowdown was 34 g. The total solvent produced during experiment #5 was 223.6 g. Over 77% and 14% of the uptake solvent was produced in the live oil and during blowdown of the apparatus.

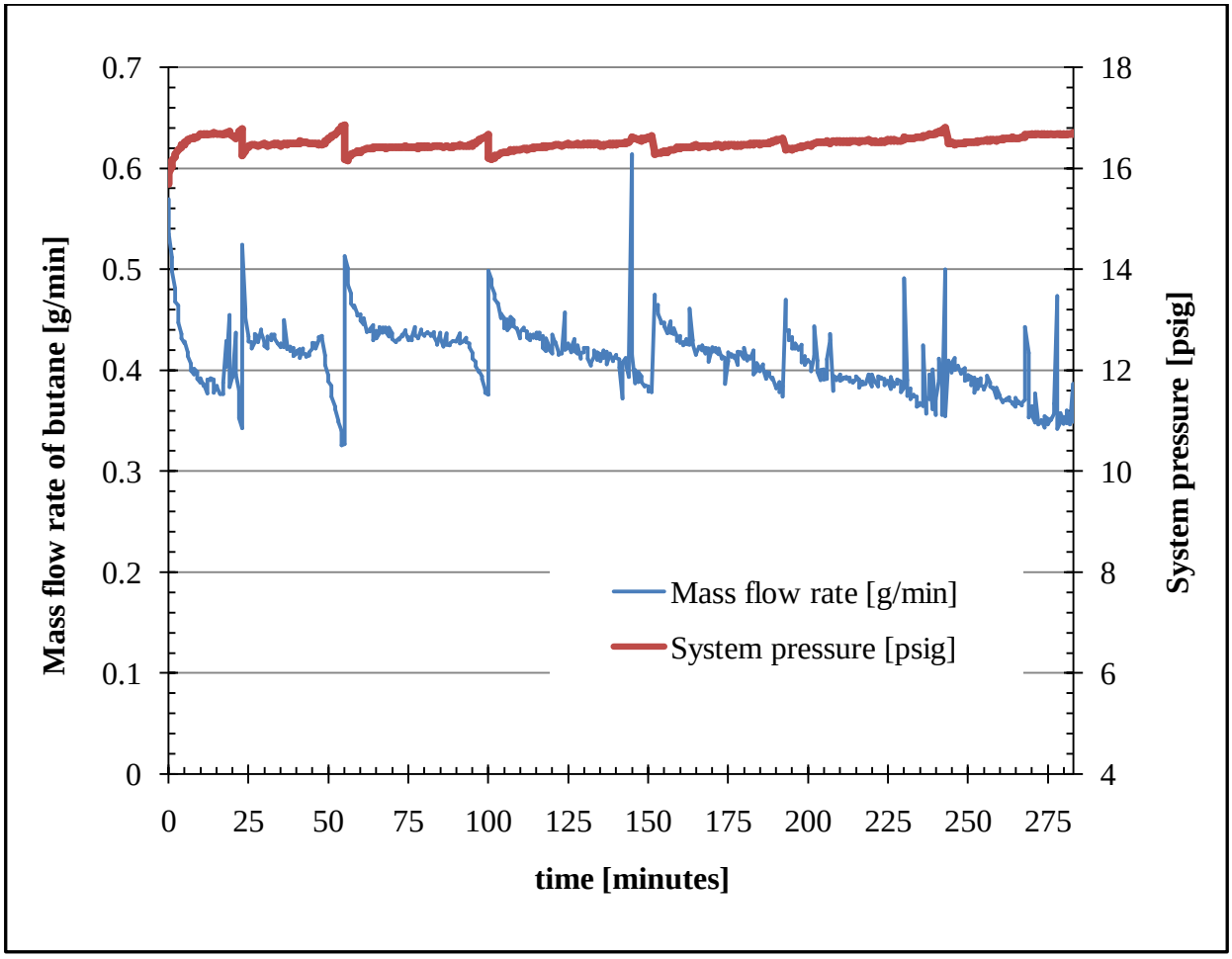

Figure 4-19: Mass flow rate of butane and system pressure for experiment #5 (warm VAPEX experiment)

5.0 Numerical Modeling of VAPEX

Previous attempts were made in modeling the VAPEX process using various of numerical simulation tools (Das 2005, Kapadia et. al. 2006). The most common tool is a very popular commercial reservoir modelling software, CMG-STARS® (STARS, CMG Modeling). The advantages of such a tool are that it is simple to use and it is readily available; the disadvantage is the limited access to the governing equations and the algorithm used in the numerical simulation.

Other attempts in modelling the VAPEX process involved separating the live oil phase and the bitumen phase into two liquid phases. This method only applies the fluid flow equation to the diluted live oil and required a predefined moving boundary condition in describing the advancement of the bitumen solvent interface (Butler and Mokrys, 1989; Kapadia et. al., 2006).

The goal of this thesis is to develop a numerical model that describes the VAPEX process realistically. Both the bitumen and the live oil are treated as one liquid phase and the fluid flow equation is applied throughout the liquid phase. A numerical simulation was run based on the conditions of experiment #3. The simulated production history and the solvent chamber growth were compared to the results of experiment #3 to validate the numerical model.

5.1 Development of the Numerical Model

The numerical simulation of VAPEX was carried-out using Comsol 3.3 (Comsol 3.3, Comsol), which is a commercial finite element software with predefined engineering and mathematical equations. The advantages of Comsol include flexibility and powerful functionality in conducting complex 2-D and 3-D numerical simulation. The software uses a simple graphic user interface to define the control volume of the simulated system. Furthermore, the predefined equations can be combined and modified to suit the needs of the problem analyzed.

5.1.1 Governing Equations and Assumptions

Theoretically, two mechanisms occur in VAPEX:

1) Mass transfer of solvent into bitumen
2) Gravity drainage of the diluted bitumen (live oil)

The bitumen and live oil are treated as one liquid phase in the new numerical model instead of defining a separate bitumen phase and a separate live oil phase defined by solvent concentration. Most of the numerical and mathematical models developed for VAPEX assumed the bitumen to be a stationary phase and only applies the fluid flow equation to the live oil phase. Although the viscosity of bitumen is over four to five orders of magnitude higher than the viscosity of live oil, it is not static as assumed in most mathematical models. In reality, bitumen is moving extremely slowly. The numerical model was built on the idea that both bitumen and live oil flow in the porous media and the rate of drainage depends on the solvent concentration. Hence, the fluid flow equation was applied throughout the control volume to describe the drainage of both bitumen and live oil simultaneously. Several assumptions were made to simplify the development of the numerical model and the calculations involved in the numerical simulations (see Appendix B for the detailed derivation of the governing equations):

1) Constant density in the oil phase:

   The density of oil is a function of solvent concentration, as discuss in later section 5.2.1. The effect of density change on the overall calculation of the numerical simulation is minimal compared to that of viscosity reduction. Furthermore, the dependence of density on solvent concentration will increase the number of iterations required exponentially. Therefore, density of the liquid phase is assumed to be constant at 0.8 g/cm^3.

2) The fluid flow equation in the gaseous phase was neglected:

   The pressure change and density of the gaseous phase is negligible compared to that of the liquid phase; therefore the flow equation (Darcy's equation) for the gaseous phase is eliminated.

3) D_m, D_L , D_T, $\mu_o(\omega_s)$ are tabulated from correlations

The above are the core assumptions made during the development of the numerical model. Additional assumptions made in defining the variables used in the numerical model will be discussed in the later sections. The mass transfer of solvent is governed by the convective diffusion equation for a variable saturation system. The original convective – diffusion equation can only be applied to a fully saturated system. The derivation of convective-dispersion equation for variable saturation conditions in a non reactive system is as follows:

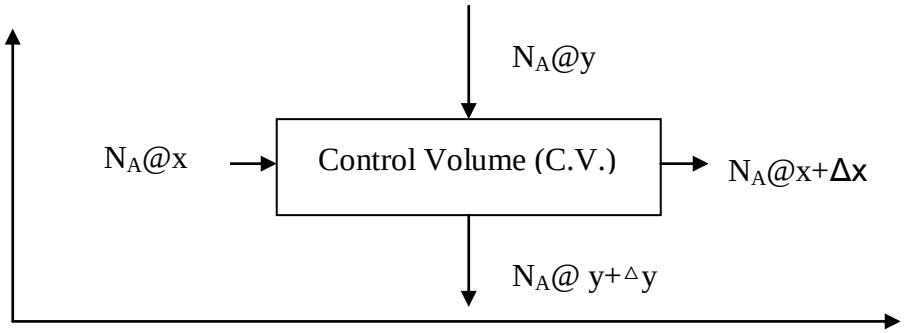

Rate of accumulation of solvent within C.V. per unit volume	=	Rate of transfer of solvent into C.V. across C.S. per unit volume	-	Rate of transfer of solvent out of C.V. across C.S. per unit volume	+	Rate of interphase transfer of solvent within C.V. per unit

$$\frac{\partial(\rho_o \omega_s S_o \emptyset)}{\partial t} = \frac{\partial N_{Sx}}{\partial x} + \frac{\partial N_{Sy}}{\partial y} + \vec{J}_m \quad (5\text{-}1)$$

$$\frac{\partial(\rho_o \omega_s S_o \emptyset)}{\partial t} = \nabla \cdot N_S + \vec{J}_m \quad (5\text{-}2)$$

$$\overrightarrow{N_S} = (\rho_o \omega_s \vec{v}_o - \emptyset S_o D_{SB} \rho_o \nabla \omega_s) \quad (5\text{-}3)$$

$$\frac{\partial(\rho_o \omega_s \emptyset S_o)}{\partial t} - \nabla \cdot (\rho_o \omega_s \overrightarrow{v_o} - \emptyset S_o D_{SB} \rho_o \nabla \omega_s) = \vec{J}_m \quad (5\text{-}4)$$

where ω_s is the mass fraction of solvent in oil, v_o is the Darcy's velocity of oil phase and ρ_o is the density of oil phase. $\vec{J}_m$ is the interphase mass flux, D_{SB} is the hydrodynamic dispersion coefficient, ϕ is the porosity of the system and S is the oil saturation. The above equation describes the mass transfer of solvent in a variable saturation system. This equation

is commonly used to describe the solute transport in groundwater flow, where saturation of the liquid phase varies in the system.

The equations used are the predefined convective-diffusion equation in the chemical engineering module in Comsol. The predefined equation has to be modified to suit the governing equations stated above. The predefined convective diffusion equation in Comsol is as follows:

$$\delta_{st}\frac{\partial c}{\partial t} + \nabla \cdot (-D\nabla c + \vec{v}c) = R \tag{5-5}$$

The above equation is only applicable for fully saturated system, where δ_{st}, D, v and R are the input parameters in Comsol. This equation will need to be modified in order to describe the mass transfer mechanism in VAPEX. If the density is considered constant then the time derivative in Equation (5-4) is expanded to the following.

$$\emptyset\frac{\partial(\omega_s S)}{\partial t} = \emptyset\left[S\frac{\partial \omega_s}{\partial t} + \omega_s\frac{\partial S}{\partial t}\right] \tag{5-6}$$

$$\emptyset\left[S\frac{\partial \omega_s}{\partial t} + \omega_s\frac{\partial S}{\partial t}\right] + \nabla \cdot (-\emptyset S D_{SB}\nabla\omega_s + \omega_s\overrightarrow{v_o}) = \vec{J}_m \tag{5-7}$$

According to Equation (5-7), the input parameters δ_{st}, D, v and R in Comsol equal to the following values:

Table 5-1: Input parameters in Comsol for the convective diffusion equation

Parameters in Comsol	Corresponding terms in physical model
D	$\phi S_o D_{SB}$
v_o	v_o
δ_{st}	ϕS
R	$-\emptyset\omega_s\frac{\partial S}{\partial t} + \frac{\overrightarrow{J_m}}{\rho_o}$
c	ω_s

where ϕ is porosity, S is the oil saturation, D_{SB} is hydrodynamic dispersion, v is Darcy's velocity and J_m is interphase mass transfer flux. The Darcy's velocity and the oil saturation is

calculated by the Darcy's equation. The gravity drainage of the oil phase and the oil saturation in the control volume are governed by the continuity equation:

$$\emptyset \frac{\partial \rho_o S_o}{\partial t} + \nabla \cdot \overrightarrow{\rho_o v_o} = 0 \tag{5-8}$$

$$\overrightarrow{v_o} = -\frac{k_o}{\mu_o}(\nabla P - \rho_o \vec{g}) \tag{5-9}$$

Combining Equation (5-8) and Equation (5-9), the continuity equation for the oil phase becomes:

$$\emptyset \frac{\partial S_o}{\partial t} + \nabla \cdot \left[-\frac{k_o}{\mu_o}(\nabla P_o - \rho_o \vec{g}) \right] = 0 \tag{5-10}$$

$$\emptyset \frac{\partial S_g}{\partial t} + \nabla \cdot \left[-\frac{k_g}{\mu_g}(\nabla P_g - \rho_g \vec{g}) \right] = 0 \tag{5-11}$$

Equation (5-8) is the continuity equation of the oil phase, Equation (5-9) is the Darcy's equation for the oil phase. Equation (5-10) and Equation (5-11) describe the gravity drainage of oil phase and the flow of gaseous phase in the porous media, respectively. S_o and S_g are the oil saturation and solvent saturation of the control volume, respectively. In theory,

$$S_o + S_g = 1 \tag{5-12}$$

k_o is the effective permeability of oil phase, which $k_o = k \cdot k_{ro}(S_{eo})$. k is the absolute permeability of the porous media, and k_{ro} is the relative permeability of oil and it is a function of oil saturation. Similarly, $k_g = k \cdot k_{rg}(S_{eg})$, where k_{rg} is the relative permeability of butane gas in the porous media as a function of gas saturation. S_{eo} and S_{eg} are the effective saturation of oil and gas, respectively. The effective oil saturation is defined in Equation (5-14). ρ_o and ρ_g are the density of oil and gas, respectively. ϕ is the porosity of the porous media. P_c is the capillary pressure and g is the acceleration due to gravity. μ_w and μ_g are the viscosity of oil and gas respectively, noting that the viscosity of oil is a function of concentration of butane. Earlier assumptions stated that the pressure change and density of the gaseous phase is negligible compared to the liquid phase; hence Equation (5-10) is neglected and Equation (5-12) is used to describe the gas saturation.

The predefined Darcy's equation under the earth science module in Comsol is stated as follows:

$$\delta_{st} C_p \frac{\partial P_o}{\partial t} + \nabla \cdot \left[\delta_k \frac{\kappa}{\mu} (\nabla P_o + \rho_o \vec{g} \nabla D) \right] = \delta_Q Q \qquad (5\text{-}13)$$

where the time scaling factor (δ_{ts}), the flux scaling factor (δ_k), the source scaling factor (δ_Q), storage term (C_p), permeability (κ), viscosity (μ), fluid density (ρ_f) and, the source term (Q) are input parameters. The acceleration due to gravity (g) and the downward distance of the model (D) are predefined values. P_o is the pressure of the oil phase in VAPEX. ρ_f is the density of liquid, μ is the viscosity of liquid and it is a function of solvent mass fraction . κ is the effective permeability and k is the absolute permeability, where $k = k_o \cdot k_{ro}(S_{eo})$. δ_{ts} is the time scaling factor, where $\delta_{ts} = 0$ is for steady state system and $\delta_{ts} = 1$ is for transient system. δ_k is the flux scaling factor and $\delta_k = 1$. δ_Q is the source scaling factor and Q is the source term. Both $\delta_{ts} = 0$ and Q=0. k_{ro} is the relative permeability of the oil phase. Corey's correlation is used to describe the relative permeability of the oil phase in the numerical model, $k_{ro} = S_{eo}^4$, where S_{eo} is the effective saturation of the oil phase defined by :

$$S_{eo} = \left(\frac{S_o - S_{or}}{1 - S_{or}} \right) \qquad (5\text{-}14)$$

Comsol evaluates the pressure distribution in the liquid phase; however, it does not evaluate the liquid saturation in the control volume. The storage term (C_p) was modified to calculate the change in effective oil saturation:

$$C_p \frac{\partial P_o}{\partial t} = \emptyset (1 - S_r) \frac{\partial S_{eo}}{\partial P_0} \frac{\partial P_o}{\partial t} \qquad (5\text{-}15)$$

Therefore,

$$C_p = \emptyset (1 - S_r) \frac{\partial S_{eo}}{\partial P_0} = -\emptyset (1 - S_r) \frac{1}{\rho_o \vec{g}} \frac{\partial S_{eo}}{\partial H_p}$$

The storage term (C_p) is function of porosity (ϕ), residual oil saturation (S_r) and the derivative of effective oil saturation and pressure. The effective oil saturation (S_{eo}) and storage term (C_p) can be expressed as a function of capillary pressure head (H_p) using the Van Genuchten correlations:

$$\theta = \begin{cases} \emptyset + S_{eo} \emptyset (1 - S_r); & Hp < 0 \\ \emptyset & Hp \geq 0 \end{cases} \qquad (5\text{-}16)$$

$$S_{eo} = \begin{cases} \dfrac{1}{[1 + |\alpha \cdot Hp|^n]^m} & Hp < 0 \\ 1 & Hp \geq 0 \end{cases} \qquad (5\text{-}17)$$

$$C_p = \begin{cases} \dfrac{\alpha m}{1-m} \dfrac{\emptyset(1 - S_r)}{\rho_o \vec{g}} S_{eo}^{\frac{1}{m}} \left(1 - S_{eo}^{\frac{1}{m}}\right)^m & Hp < 0 \\ 0 & Hp \geq 0 \end{cases} \qquad (5\text{-}18)$$

H_p is the capillary pressure head, where $H_p = \frac{P_g - P_o}{\rho_o \vec{g}}$, θ is the fluid fraction of oil, S_r is the residual oil saturation. The variables α, n and m are parameters of the Van Genuchten model for a bitumen-butane fluid-pair system. Consider constant density, the continuity equation for the oil phase is as follows:

$$-\emptyset(1 - S_r) \frac{1}{\rho_o \vec{g}} \frac{\partial S_{eo}}{\partial H_p} \frac{\partial P_o}{\partial t} + \nabla \cdot \left[\frac{k_o k_{ro}}{\mu(\omega_s)} (\nabla P_o + \rho_o \vec{g} \nabla D)\right] = 0 \qquad (5\text{-}19)$$

where the variables input in Equation (5-13) is summarized in Table 5-2:

Table 5-2: Inputted variables in Comsol for the continuity equation

Parameters in Comsol	Corresponding terms in physical model
C_p	$\emptyset(1 - S_r) \frac{\partial S_{eo}}{\partial P_0}$ or $-\emptyset(1 - S_r) \frac{1}{\rho_o \vec{g}} \frac{\partial S_{eo}}{\partial H_p}$ using van Genuchten correlation $\frac{\alpha m}{1-m} \frac{\emptyset(1 - S_r)}{\rho_o \vec{g}} S_{eo}^{\frac{1}{m}} \left(1 - S_{eo}^{\frac{1}{m}}\right)^m$
v_o	v_o
δ_{st}	1
δ_k	1
δ_Q	0
κ	$k_o k_{ro}$
ρ_f	ρ_o
μ_o	$\mu_o(\omega_s)$
D	y-axis

5.2 Determining the Variables Used in the Numerical Model

The following section discusses the method used in calculating the variables used in the numerical simulation. Some of the variables are approximated based on the limited data available.

5.2.1 Density of liquid phase

The numerical simulation assumed constant density throughout the control volume. This simplified the convection-diffusion equation and eliminated an additional variable in the iterations. In reality, the density of the oil phase is a function of concentration.

$$\frac{1}{\rho_{mix}} = \frac{\omega_s}{\rho_s} + \frac{(1-\omega_s)}{\rho_B} \qquad \textbf{(5-20)}$$

where ρ_{mix} is density of live oil, ρ_s and ρ_B are density of butane and bitumen, respectively. ω_s is the solvent mass fraction. The maximum mass fraction of butane in the live oil produced in experiment #3 is 0.38. The density of bitumen and liquid butane are 980 kg/m^3 and 600 kg/m^3 respectively, the density of live oil as a function of solvent mass fraction is plotted in Figure 5-1.

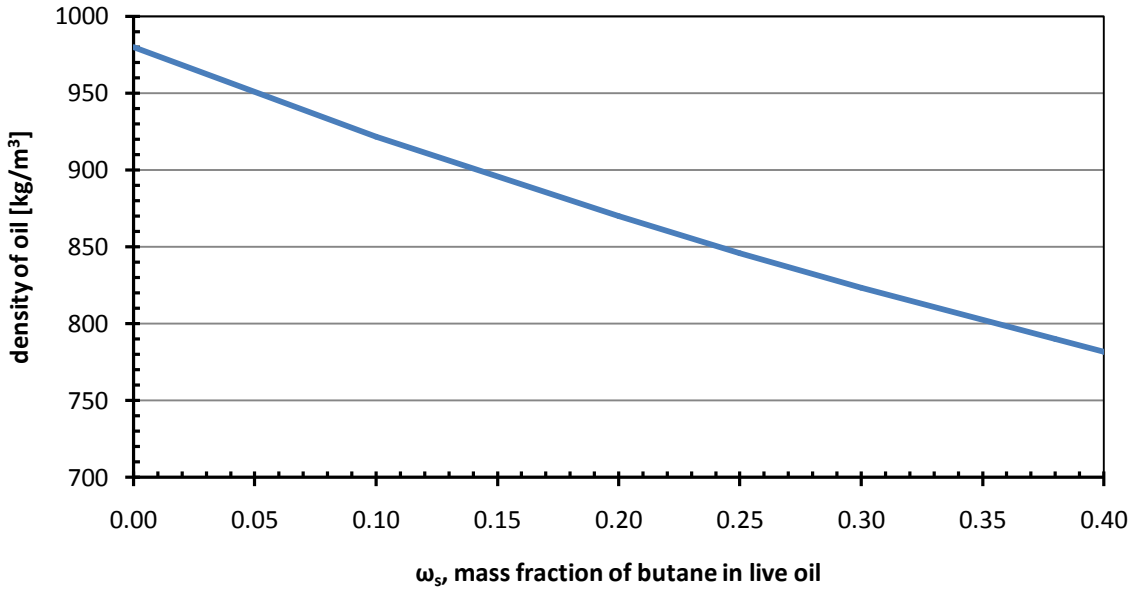

Figure 5-1: Density reduction as a function of solvent concentration

In the system of equations described in section 5.1.1, the density is applied in Darcy's equation to calculate the flow of oil phase. Considering the maximum solvent mass fraction of 0.38 in experiment #3, it is fair to assume the majority of the flowing oil is live oil at the maximum solvent mass fraction. Therefore, the constant density for the oil phase is assumed to be 0.8 g/cm^3 at maximum solvent mass fraction.

5.2.2 Viscosity Calculation

The mechanism of VAPEX is to reduce the viscosity of the bitumen using light hydrocarbon as solvent and produce the diluted live oil by gravity drainage. The magnitude of viscosity reduction can be estimated using Shu's correlation (Shu, 1984) for mixture of bitumen with light hydrocarbon. Given the initial viscosity (μ_B) and density (ρ_B) of bitumen is 23.2 kg/m.s and 980 kg/m^3 , respectively; the viscosity (μ_s) and density (ρ_s) of liquid butane is 1.71x10^{-4} kg/m.s and 600 kg/m^3, respectively. The viscosity of the live oil (μ_{mix}) can be calculated using the following equations:

$$\mu_{mix} = \mu_s^{f_s} \mu_B^{f_B} \tag{5-21}$$

where,

$$f_B = \frac{\alpha C_{VB}}{\alpha C_{VB} + \alpha C_{VS}} \tag{5-22}$$

$$f_s + f_B = 1$$

$$C_{Vs} + C_{VB} = 1$$

$$\alpha = \frac{17.04 \Delta\rho^{0.5237} \rho_B^{3.2745} \rho_s^{1.6316}}{\ln\left(\frac{\mu_B}{\mu_s}\right)} \tag{5-23}$$

where f_B and f_s are the compositional factors for bitumen and solvent, respectively. C_{VB} and C_{VS} are the volume fraction for bitumen and solvent, respectively.

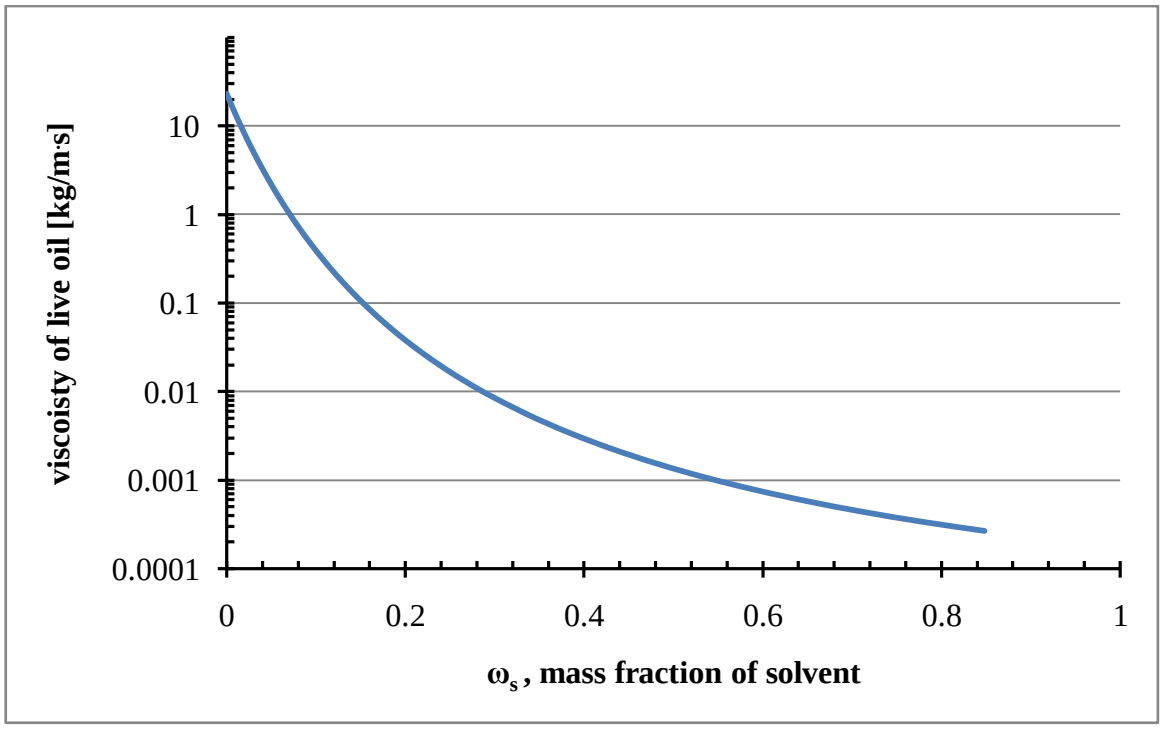

Figure 5-2: Oil viscosity as a function of solvent mass fraction

The oil viscosity reduction as a function of solvent mass fraction is plotted in Figure 5-2. This figure indicates that the majority of the oil viscosity reduction occurs between $\omega_s = 0$ to $\omega_s = 0.2$, where the viscosity is reduced from 23.2 kg/m.s to 0.036 kg/m.s. The maximum mass fraction of solvent in experiment #3 was 0.38 with a viscosity of 0.004 kg/m.s. The viscosity reduction between $\omega_s = 0$ to $\omega_s = 0.2$ corresponds to over 99% of the overall oil viscosity reduction in the experiment.

5.2.3 Capillary Pressure Curve

The numerical model used the capillary pressure versus saturation curve to evaluate the saturation of liquid. During the numerical simulation, both bitumen and live oil exist in the control volume. The capillary pressure curves for bitumen and live oil differ, because the interfacial tension between oil and butane is a function of butane concentration. Das (1995) stated that the interface tension of bitumen decreases from 34 dyne/cm to 18 dyne/cm as the solvent mass fraction increases from $\omega_s = 0$ to $\omega_s = 0.38$. The almost 50% decrease in the oil reduction interfacial tension cannot be neglected, when simulating gravity drainage phenomena with capillary pressure incorporated in the modelling.

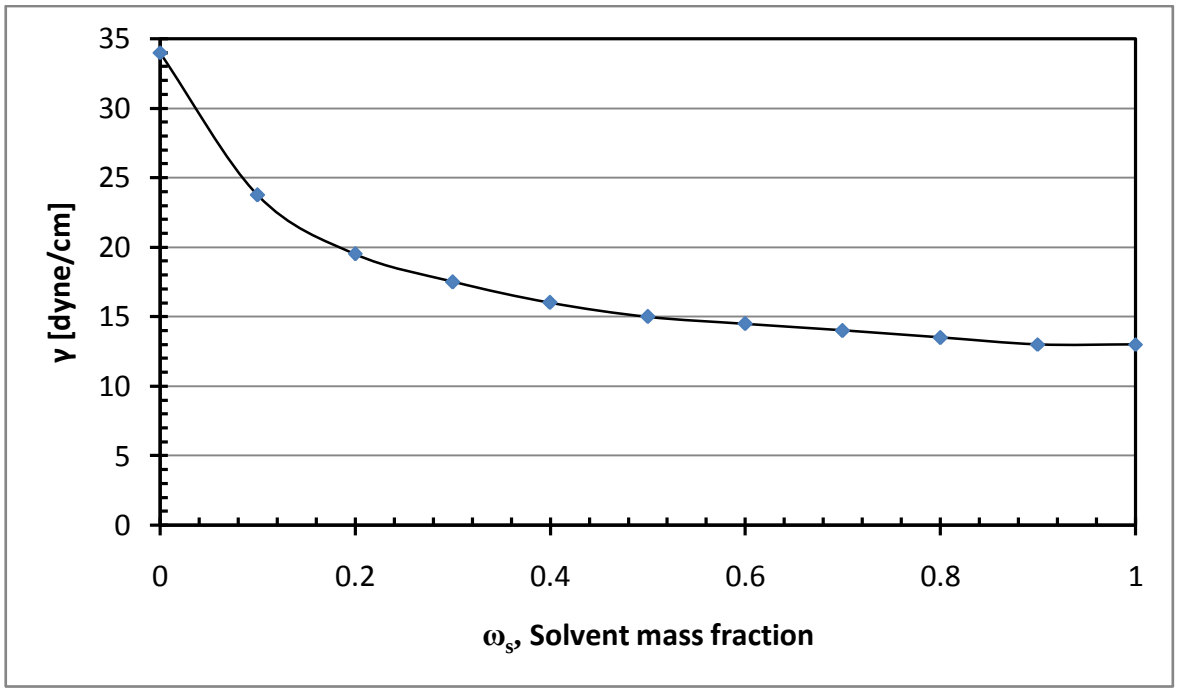

Figure 5-3: Interfacial tension of bitumen and butane mixture (adapted from Das (1995))

The scaling of capillary pressure curve of a particular porous medium in accomplished using the following relation:

$$\frac{P_{c1}}{P_{c2}} = \frac{\gamma_1}{\gamma_2}\sqrt{\frac{k_2}{k_1}} \qquad (5\text{-}24)$$

where, γ is the interfacial tension of the oil-solvent interface. The capillary pressure of the system is a function of interfacial tension and permeability; therefore, the capillary pressure values will change as the solvent mass fraction increases. This affects the capillary pressure curves that were used to evaluate the oil saturation in the particular position of the system. The problem with the capillary pressure curves as a function of solvent mass fraction in Comsol® is that this requires continuous iterations during the numerical simulation. In addition to evaluating the oil saturation of the system, the first derivative of the capillary pressure curve is a part of Darcy's equation; hence, having the capillary pressure curve as a function of solvent concentration increases the memory requirement exponentially. In order to differentiate the live oil and the bitumen in the oil phase without increasing the amount of iterations in the simulation, a step function was used. The capillary pressure curve for

bitumen was used for the oil phase for conditions of $\omega_s < 0.2$ and the capillary pressure curve for live oil was employed for the oil phase for conditions of $\omega_s \geq 0.2$.

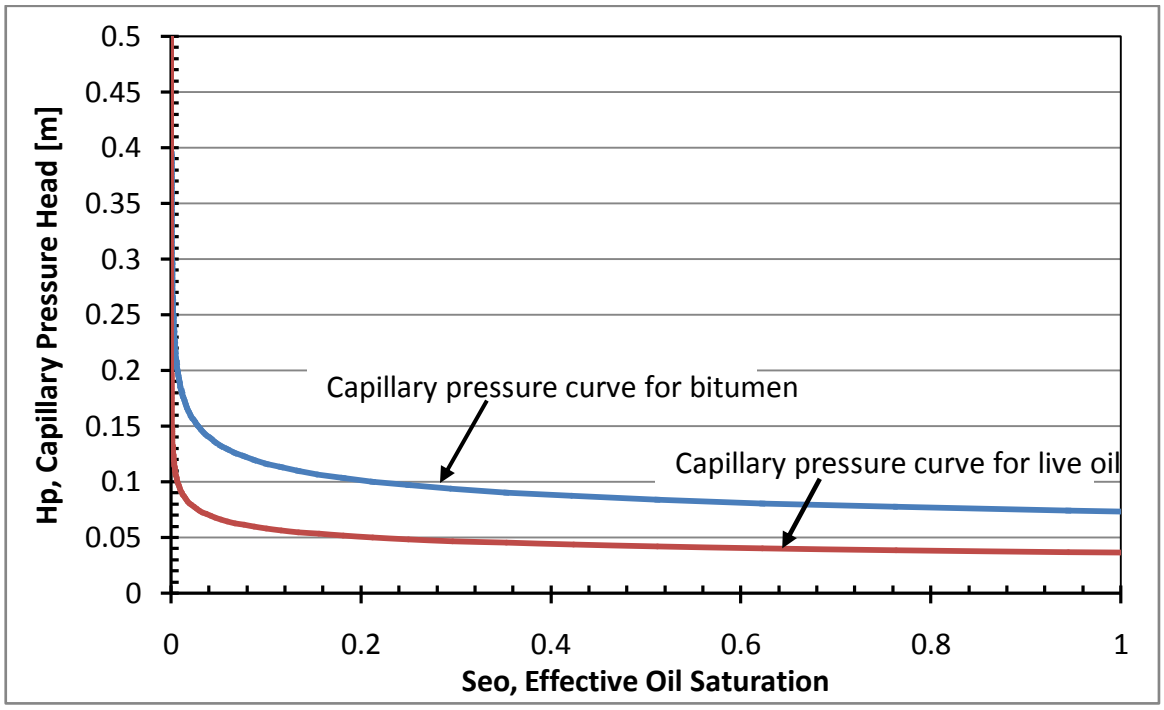

Figure 5-4: Capillary pressure curves for bitumen (ω_s = 0) and live oil (ω_s = 0.38) for permeability of 300 Darcy and porosity of 0.39

The capillary pressure curves for bitumen ($\omega_s = 0$) and live oil ($\omega_s = 0.38$), respectively for a 300 Darcy unconsolidated glass beads porous media is plotted in Figure 5-4. The capillary pressure was calculated based on the Pc versus S_{eo} curve of water-air drainage system (Ioannidis et. al., 2006) and scaled to the interfacial tension of bitumen and live oil for a permeability of 300 D system using Equation (5-24). As discussed in the previous section, the majority of the viscosity reduction occurs between $\omega_s = 0$ and $\omega_s = 0.2$. In the modelling, it is assumed that the capillary pressure curve for bitumen is applied to the liquid phase with $\omega_s < 0.2$ and the capillary pressure curve for live oil is applied to the liquid phase with $\omega_s \geq 0.2$. The step change in the capillary pressure curve reduced the number of iterations required but still enabled the numerical model to distinguish the difference between the bitumen phase and the live oil phase in finite volume element as it is drained by gravity. The disadvantage is that this method compromised the accuracy of the numerical modelling.

The capillary pressure data were defined by the van Genuchten correlation for capillary pressure versus saturation. The van Genuchten correlation is outlined in section 5.1.1. The capillary pressure curves shown in Figure 5-4 were curve fitted values using the van Genuchten correlation. The variables in van Genuchten correlation for the two curves are summarized in Table 5-3.

Table 5-3: The variables of the capillary pressure curves used in the numerical simulation

Parameter values	α	n	m	conditions
Bitumen Pc versus S_{eo} curve	11	10	0.89	$\omega_s < 0.2$
Live oil Pc versus S_{eo} curve	22	10	0.89	$\omega_s \geq 0.2$

5.2.4 Diffusion and Dispersion

The mass transfer mechanism of VAPEX involves both diffusion and dispersion of solvent in bitumen. James et. al. (2003) used a 1-D diffusion model to evaluate the diffusivity of solvent into bitumen. It was concluded that molecular diffusivity is a function of solvent concentration. For this simulation, the variation in molecular diffusivity is insignificant since the system is dispersion dominated; furthermore, having molecular diffusion as a function of solvent concentration increases the number of iterations required in the numerical simulation. For the current numerical model, the diffusivity is assumed to be a constant value of $5x10^{-10}$ m^2/s, and the dispersion coefficient values are determined based on the Peclet number.

When two miscible fluids are injected simultaneously into the porous medium, pore scale mixing of the two fluids occurs. This is called dispersion. Boustani and Maini (2001) stated that dispersion is significant to the mass transfer mechanism of VAPEX and cannot be neglected.

$$D_{SB} = D_i + D_m \qquad (5\text{-}25)$$

where D_{SB} is the hydrodynamic dispersion coefficient of the system, and it is combination of mechanical dispersion (D_i) and molecular diffusion (D_m). The mechanic dispersion can be

divided into two components (Perkins and Johnston,1963), longitudinal dispersion (D_L) and transverse dispersion (D_T). Longitudinal dispersion describes dispersion along the direction of fluid flow, while transverse dispersion describes dispersion perpendicular to the direction of fluid flow. Both longitudinal and transverse coefficients depend on velocity:

$$D_L = \alpha_L v_{pv} \tag{5-26}$$

$$D_T = \alpha_T v_{pv} \tag{5-27}$$

where α_L and α_T are the longitudinal and transverse dispersivities respectively, and v_{pv} is the interstitial velocity of the system. In a 2-D control volume, the hydrodynamic dispersion coefficient can be expressed using the velocity in the x and y direction (Donaldson et. al., 1998).

$$D_{xx} = \frac{\alpha_L v_{pvx}^2 + \alpha_T v_{pvy}^2}{\sqrt{v_{pvx}^2 + v_{pvy}^2}} + D_m \tag{5-28}$$

$$D_{yy} = \frac{\alpha_T v_{pvx}^2 + \alpha_L v_{pvy}^2}{\sqrt{v_{pvx}^2 + v_{pvy}^2}} + D_m \tag{5-29}$$

$$D_{xy} = \frac{(\alpha_L - \alpha_T) v_{pvx} v_{pvy}}{\sqrt{v_{pvx}^2 + v_{pvy}^2}} + D_m \tag{5-30}$$

where v_{pvx} and v_{pvy} is the interstitial velocity in the x and y direction. The longitudinal coefficient for VAPEX can be estimated by the Peclet number correlation using Figure 2-6. The Peclet number is a dimensionless number that relates the rate of convection to the rate of mass transfer by molecular diffusion. The Peclet number (Pe) is expressed as follows:

$$Pe = \frac{\vec{v}_{pv} D_p}{D_m} \tag{5-31}$$

The Peclet number is a function of velocity, diffusivity and particle size. The molecular diffusivity (D_m) and the average particle size (D_p) were assumed to be 5×10^{-10} m^2/s and 0.590 mm respectively. Although the velocity of the system was unknown, the initial guess can be estimated using Darcy's equation for gravity drainage. The permeability in the numerical model was 3×10^{-10} m^2. The density and viscosity of the live oil were 800 kg/m^3

and 0.004 kg/m.s, respectively (assuming maximum solvent mass fraction ω_s = 0.38). The maximum interstitial velocity during gravity drainage for live oil was calculated to be 1.37×10^{-3} m/min. The interstitial velocity was used to estimate the initial guess for longitudinal dispersion. Equation (5-26) states the longitudinal dispersion as a function of longitudinal dispersion coefficient and velocity. The longitudinal dispersion coefficient was back calculated by the velocity estimated using the method described above.

The value of transverse dispersion is typically 24 times less than that of longitudinal dispersion (Dullien, 1992). The transverse dispersion coefficient for the numerical simulation is $\alpha_T = \alpha_L/24$. The dispersion coefficients estimated above were used to run the 1st numerical simulation. The velocity calculated by the numerical simulation was used to recalculate the dispersion coefficient using the same method, until the velocity used to calculate the dispersion coefficients and velocity evaluated by the numerical simulation were identical.

5.2.5 Mass Transfer Coefficient

As the diluted bitumen drains out of the control volume, the emptied pores are filled by the solvent (Li, 2007). The mass exchange between the gaseous phase and liquid phase is described by the mass transfer correlation (J_m) in the variable saturation convection - diffusion equation. Assuming linear driving force, the mass transfer correlation is:

$$\vec{J}_m = K_m a_i \rho_o (\omega_{smax} - \omega_s) \tag{5-32}$$

where K_m is the mass transfer coefficient, a_i is the specific interfacial area and ω_{smax} is the maximum solvent mass fraction. The convection diffusion equation (Equation (5-4)) then becomes:

$$\frac{\partial(\rho_o \omega_s \emptyset S)}{\partial t} - \nabla(\rho_o \omega_s \overrightarrow{v_o} - \emptyset S D_{SB-o} \rho_o \nabla \omega_s) = K_m a_i \rho_o (\omega_{smax} - \omega_s) \tag{5-33}$$

Assuming constant density, the above becomes:

$$\frac{\partial(\omega_s \emptyset S)}{\partial t} - \nabla(\omega_s \overrightarrow{v_o} - \emptyset S D_{SB} \nabla \omega_s) = K_m a_i(\omega_{smax} - \omega_s) \quad (5\text{-}34)$$

The product of $K_m a_i$ is referred to as the mass transfer rate coefficient (Powers et al., 2006). The value of the mass transfer rate coefficient can be estimated using the modified Sherwood number. The modified Sherwood number is a dimensionless number that relates the length scale to the diffusive boundary layer thickness. The modified Sherwood number is expressed as follows (Miller et. al.,1990):

$$Sh^* = \frac{K\alpha_i D_{pz}^2}{D_m} \quad (5\text{-}35)$$

In addition to Equation (5-35), the modified Sherwood number can be estimated using an empirical correlation. However, no research exists on the empirical correlation for mass transfer of butane into bitumen in the VAPEX process. For the purpose of this numerical simulation, the empirical correlation for the dissolution of non aqueous phase liquid (NAPL) from a region with high initial saturation was used to calculate the modified Sherwood number of the system (Nambi and Powers, 2003).

$$Sh^* = 37.15 Re'^{0.6} S_n^{1.24} \quad (5\text{-}36)$$

$$Re' = \frac{\rho_o v_{pv} D_p}{\mu} \quad (5\text{-}37)$$

where S_n is the saturation of the non-aqueous phase, Re□ is the interstitial Reynolds number. In NAPL dissolution, water is the wetting phase and NAPL is the non wetting phase; however, in VAPEX, oil is the wetting phase and solvent in the non wetting phase. Therefore, S_n in Equation (5-36) refers to the solvent saturation. The Reynolds number is calculated using the interstitial velocity calculated from the previous section. The viscosity and density of the fluid are assumed to be 800 kg/m^3 and 0.004 kg⁄m.s respectively (assuming ω_{smax}). The modified Sherwood number was estimated using Equation (5-36) and the interstitial velocity evaluated by the numerical model. The mass transfer coefficient was then calculated to be $0.28S_s^{1.24}$ using Equation (5-35). The mass transfer correlation was estimated to be described by:

$$\frac{\vec{J}_m}{\rho_o} = 0.28 S_s^{1.24}(\omega_{smax} - \omega_s) \qquad \text{valid for } S_{eo}<0.55 \qquad (5\text{-}38)$$

The mass transfer correlation is only valid when the saturation of diluted bitumen is less than 0.55. The pervious sections stated that in order to reduce the number of iterations required in the numerical simulation, the effect of solvent mass fraction on the capillary pressure curve is simplified into a step function. The assumption was made to simplify the calculation required by the numerical model; however, this also introduced other issues to the calculations.

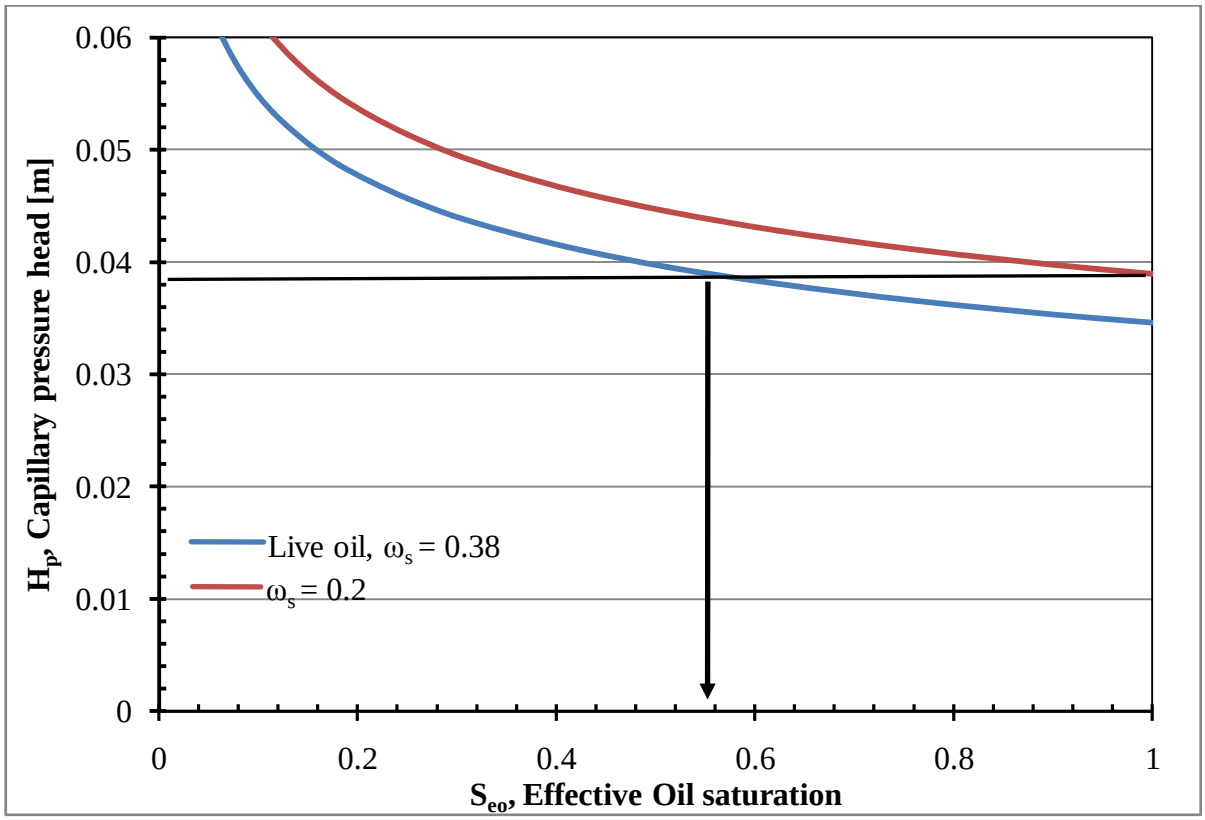

Figure 5-5: The capillary pressure curves for live oil and ω_s=0.2

The solid line in Figure 5-5 is the capillary pressure curve for live oil used in the numerical model and the dotted line is the capillary pressure curves for bitumen with solvent mass fraction of 0.2. At H_p = 0.038 m, the oil saturation calculated by the capillary pressure curve of live oil is approximately 0.55. With the same Hp, the oil saturation is evaluated to be fully saturated using the capillary pressure curve for bitumen with ω_s = 0.2. The variation suggests parts of the oil phase was drained ahead of time due to the simplification of the step function

in the capillary pressure curve. As a result, the mass transfer correlation is only applied to the elements where the oil saturation is less than 0.55.

5.2.6 Subdomain, Boundary and Initial Conditions

Comsol 3.3® uses a graphic user interface (GUI) to model the problem analyzed. The GUI is simple to use and enables modeling of complex geometry. The analysis of the VAPEX model is conducted using a 2-D rectangular control volume, constructed of 1 sub-domain and five boundaries. The subdomain represents the control volume of the porous media. The dimension of the modelled control volume is 2 cm wide by 100 cm height. The y axis is the vertical axis with gravity acting in the "-y" direction. The permeability and porosity values are $3x10^{-10}$ m^2 and 0.39 respectively.

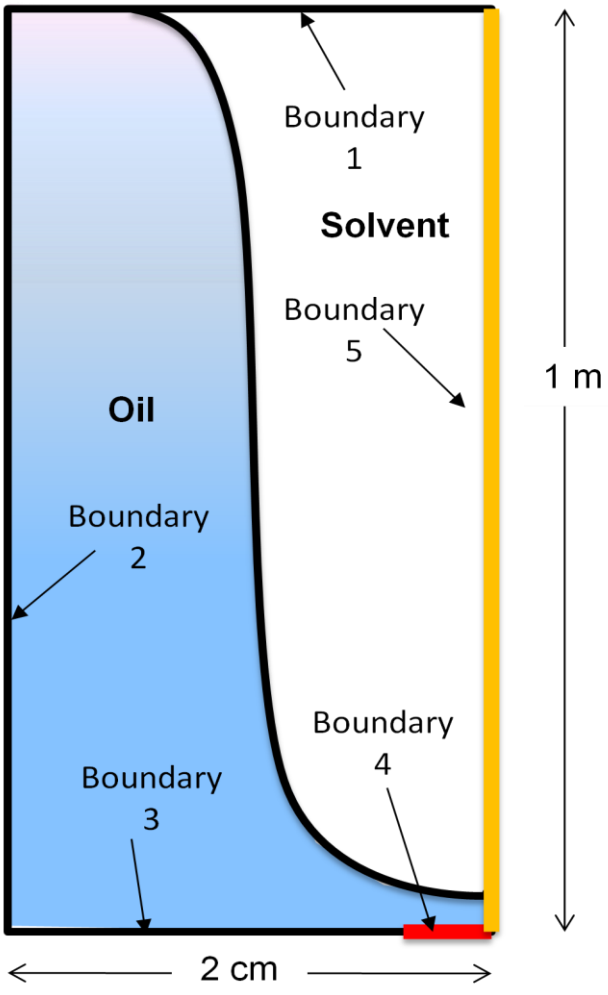

Figure 5-6: Control volume of the numerical model

Initially, the control volume is assumed to be saturated with 100% bitumen. At t > 0, boundary 5 is exposed to solvent with maximum mass fraction of 0.38 and boundary 4 is opened for drainage. The maximum mass fraction of 0.38 corresponds to the average maximum mass fraction measured from experiment #3. Boundary #4 is 0.5 cm wide to mimic the opening that connects the apparatus to the collection cylinder. Since both the apparatus and the collection cylinder operate at identical system pressure, the effect of butane pressure on the system is negligible. In theory, at t > 0, butane begins diffusing into the bitumen through boundary 5 and reduces the viscosity of the bitumen. Once the bitumen becomes mobile, it is drained out of the porous medium through boundary 4. As a result, the boundary condition for boundary 5 is maximum solvent mass fraction ($\omega_s = 0.38$) and the boundary condition for boundary 4 is $P_o = 0$ psig to mimic the line source and oil production opening of the experiments.

Table 5-4: Boundary and initial conditions in Comsol®

	Darcy's equation	**Mass transfer equation**
Boundary Conditions		
Boundary 1	Symmetry/zero flux	Insulated/Symmetry
Boundary 2	Symmetry/zero flux	Insulated/Symmetry
Boundary 3	Symmetry/zero flux	Insulated/Symmetry
Boundary 4	$P_o = 0$ (production opening)	Insulated/Symmetry
Boundary 5	Symmetry/zero flux	$\omega_s = 0.38$
Initial Conditions	$P_o = \rho_o g H$	$\omega_s = 0$

5.2.7 Mesh Configurations

Comsol 3.3 is a finite element analysis tool. Once all variables are input into the system, the sudomain is discretized into small elements. Typically, smaller mesh size produces more accurate numerical simulation; however, there is a limit to the mesh size used in the numerical model. Smaller mesh size in the subdomain increases the number of elements in the numerical simulation. This will in turn increase the calculation time and memory requirement of the numerical model. To further understand the effect of mesh size on the numerical simulation result, two simulations were run with 1mm (horizontal) by 10 mm

(vertical) and 0.67 mm (horizontal) by 6.7 mm (vertical) mesh size to study the effect of the mesh size on the precision and accuracy of the numerical simulation. Results are presented and discussed in section 5.4.3.

5.3 Method in Analyzing the Numerical Results

The developed numerical model evaluates the liquid saturation, the solvent concentration and the liquid velocity for each element and output the numerical results at 5 minute-intervals. The output data were analyzed before they were compared to the results from experiment #3. The analysis of the numerical results focused on the velocity of the liquid phase, the bitumen production history, and the solvent chamber growth.

5.3.1 Determining the Chamber Spreading Phase

The bitumen production rate and horizontal interface velocities were evaluated at the chamber spreading phase; therefore, it was necessary to develop a set of criteria to determine the chamber spreading phase for the numerical simulation that is comparable to that of experiment #3. The criteria in determining the chamber spreading phase for experiment #3 was:

1) The chamber spreading phase begins at t = 100 minutes
2) The chamber spreading phase ends when the length of interface decreases rapidly

The first criterion is applicable to the numerical simulation, because data were outputted every 5 minutes; hence, data extraction starting from t=100 minutes was not difficult. The second criterion is not applicable when analyzing the numerical simulation results, because it is very difficult to evaluate the length of interface in the numerical model. According to the analysis in section 4.1, the height of the interface is also an indication of the end of the chamber spreading phase. So for the numerical simulation, the criteria in determining the chamber spreading phase are:

1) The chamber spreading phase begins at t = 100 minutes
2) The chamber spreading phase ends when the height of interface drops below 0.95 m

5.3.2 Velocity of the Liquid Phase

The numerical model calculates the velocity of the liquid phase using the 2-D Darcy's equation. The liquid velocity is critical in estimating the dispersion coefficient and the mass transfer rate coefficient of the numerical simulation as discussed in sections 5.2.4 and 5.2.5.

To verify the feasibility of the velocity value used to estimate the dispersion coefficient and the mass transfer rate coefficient, the maximum velocity of the liquid phase during the chamber spreading phase was measured every 20 cm vertically starting at 20 cm from the top of the control volume at 25-minute intervals. The average of the maximum velocity value computed was used to recalculate the dispersion coefficient and the mass transfer rate coefficient, until the velocity value used in the estimation agreed with that of the numerical simulations.

5.3.3 Bitumen Production Rate

The numerical model evaluates and outputs the liquid saturation of each element of the meshes every five minutes. The liquid saturation of the control volume is calculated using the following equation:

$$S_L = \frac{\int S_w dA}{\int dA} = \frac{\int S_w dA}{A} \qquad (5\text{-}39)$$

where S_L is the average liquid saturation of the control volume, S_w is the liquid saturation of the element of mesh calculated by the numerical model, A is the area of the control volume. The dimension of the subdomain of the numerical model is 2 cm by 100 cm. Equation (5-39) was entered into Comsol to evaluate the average liquid saturation (S_L) at specific time. The porosity of the system is 39%. With an initial oil saturation of 100%, the cumulative bitumen production is calculated as follows:

$$N_B = V_i \rho_B (1 - S_L) \qquad (5\text{-}40)$$

Where N_B is the cumulative mass production of bitumen per 1cm depth with one side production, ρ_B is the density of bitumen (980 kg/m^3). V_i is initial volume of oil in the control volume. The bitumen saturation is recorded every 25 minutes. The cumulative mass production of bitumen is plotted against time to evaluate the bitumen production rate of the numerical simulation.

5.3.4 Solvent Chamber Growth

The numerical simulation results were extracted to create an interface profile. The horizontal interface location was measured at every 10 cm vertically, at 25-minute intervals. The data extracted were used to create an interface profile similar to that of the experimental model. Using the horizontal location extracted, the horizontal interface velocity can be calculated using method described in section 3.6.4.

5.4 Results and Discussions

Two numerical simulations were conducted using the developed numerical model for VAPEX. Both numerical simulations performed were based on the conditions of experiment #3, with varied mesh size varied to investigate the effect of mesh size on the numerical simulation results. Simulation #1 used a larger mesh size of 1 mm wide by 10 mm long and simulation #2 used a smaller mesh size of 0.67 mm wide by 6.7 mm long.

5.4.1 Bitumen Production Histories

The production history for each numerical simulation is shown in Figure 5-7. The cumulative bitumen production is based on 1 cm depth and one side production. The steady state bitumen production rates were evaluated between 100 to 200 minutes for simulation #1 and 100 to 225 minutes for simulation #2. The simulated results are in qualitative agreement with the experimentally measured production history, in that the simulated data of cumulative bitumen production is a linear function of time.

The steady state bitumen production rates for simulation #1 and simulation #2 were 0.276 g/min and 0.25 g/min per cm depth with 1 side production. The steady state bitumen production rate of experiment #3 was 0.273 g/min per cm depth for one side production. The difference in the bitumen production rates between the two simulations and experiment #3 is less than 10%. This indicates that the numerical model developed can successfully simulate the bitumen production history of the VAPEX experiment.

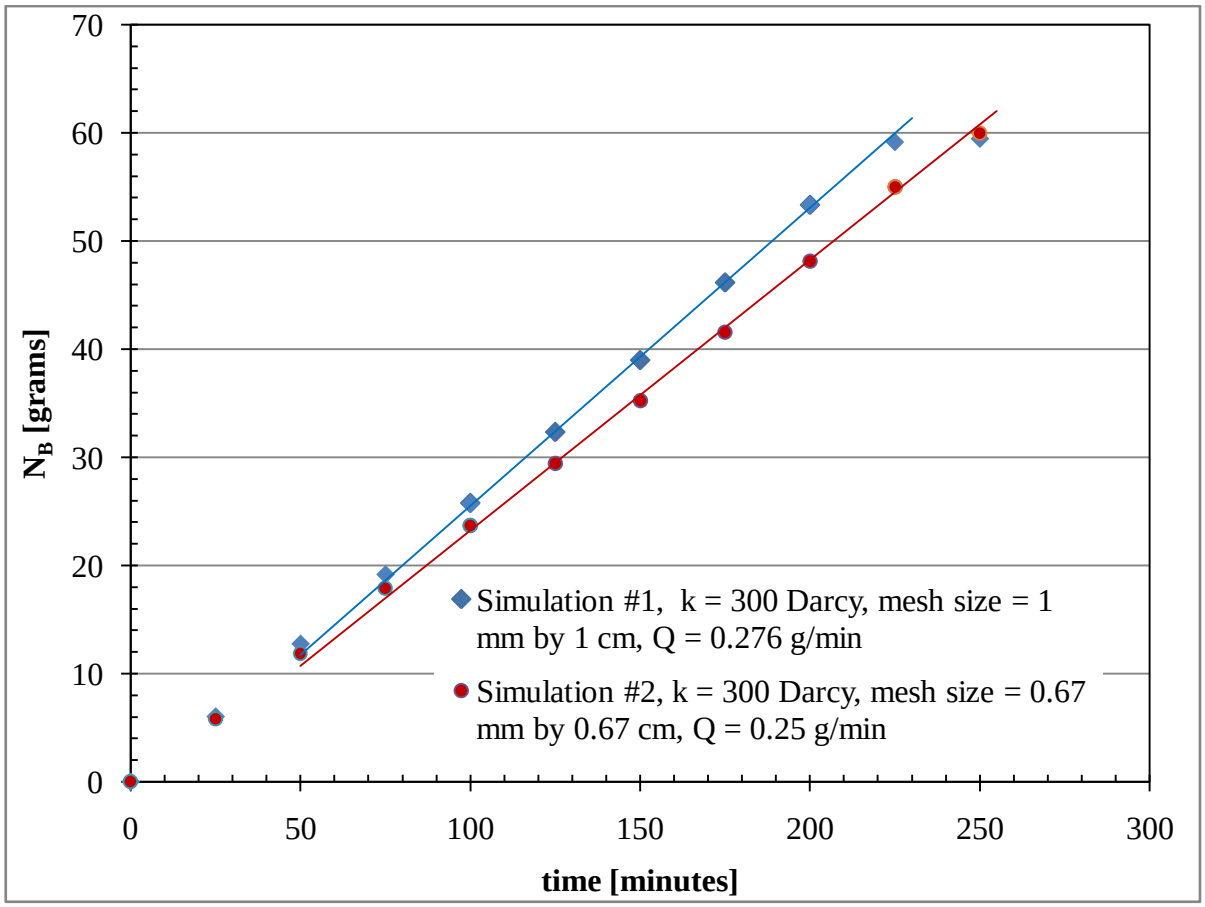

Figure 5-7: Production histories of simulations #1 and simulation #2

5.4.2 Interface Advancement

One of the goals in developing the numerical simulation is to mimic the solvent chamber growth in the experiments. The horizontal interface position of the simulations were extracted every 10 cm vertically at 25 minute-intervals. Figure 5-8a and Figure 5-8b are the interface profile extracted from the numerical simulations. They were then compared to the interface profile of experiment #3. The simulation results show no channelling near the top of the control volume. In VAPEX, channelling near the top of the apparatus only occurs due to the uneven packing of glass beads. In the numerical simulation, properties of the unconsolidated model were uniform; so channelling near the top of the apparatus did not exist.

The horizontal interface velocities during the chamber spreading phase of the simulations are plotted in Figure 5-9. Results show the interface velocities were very constant throughout the

pay zone. The average horizontal interface velocities for simulations #1 and #2 were 0.00874 cm/min and 0.0076 cm/min respectively. Average horizontal interface velocity for experiment #3 was 0.0078 cm/min. The difference in the horizontal interface velocity between the simulation and the experiment is less than 12%, which is insignificant. Results from the evaluation of the VAPEX interface profile indicate that this numerical model can successfully simulate the solvent chamber growth of experiment #3.

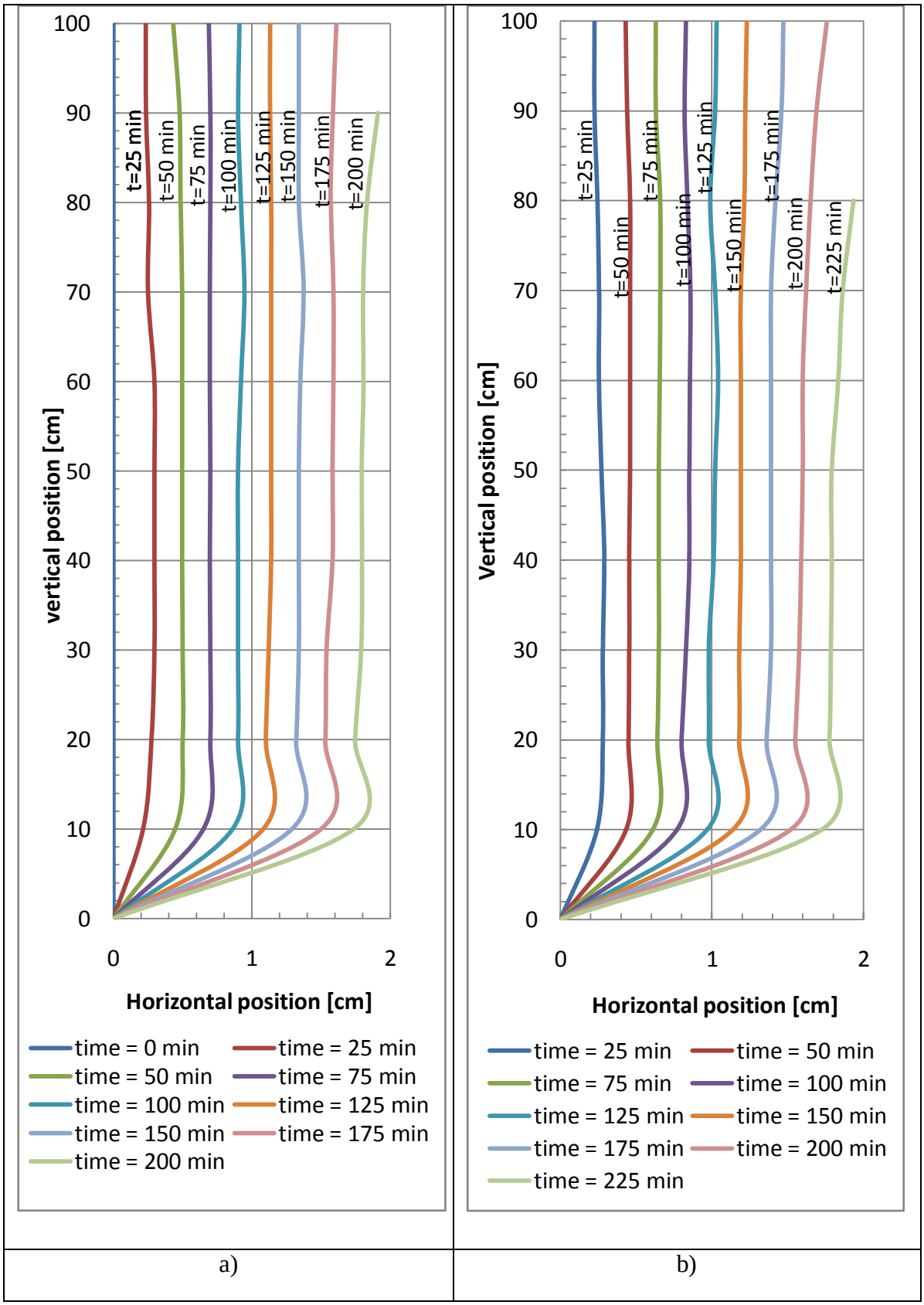

a) b)

Figure 5-8: Interface profiles for a) simulation #1 and b) simulation #2

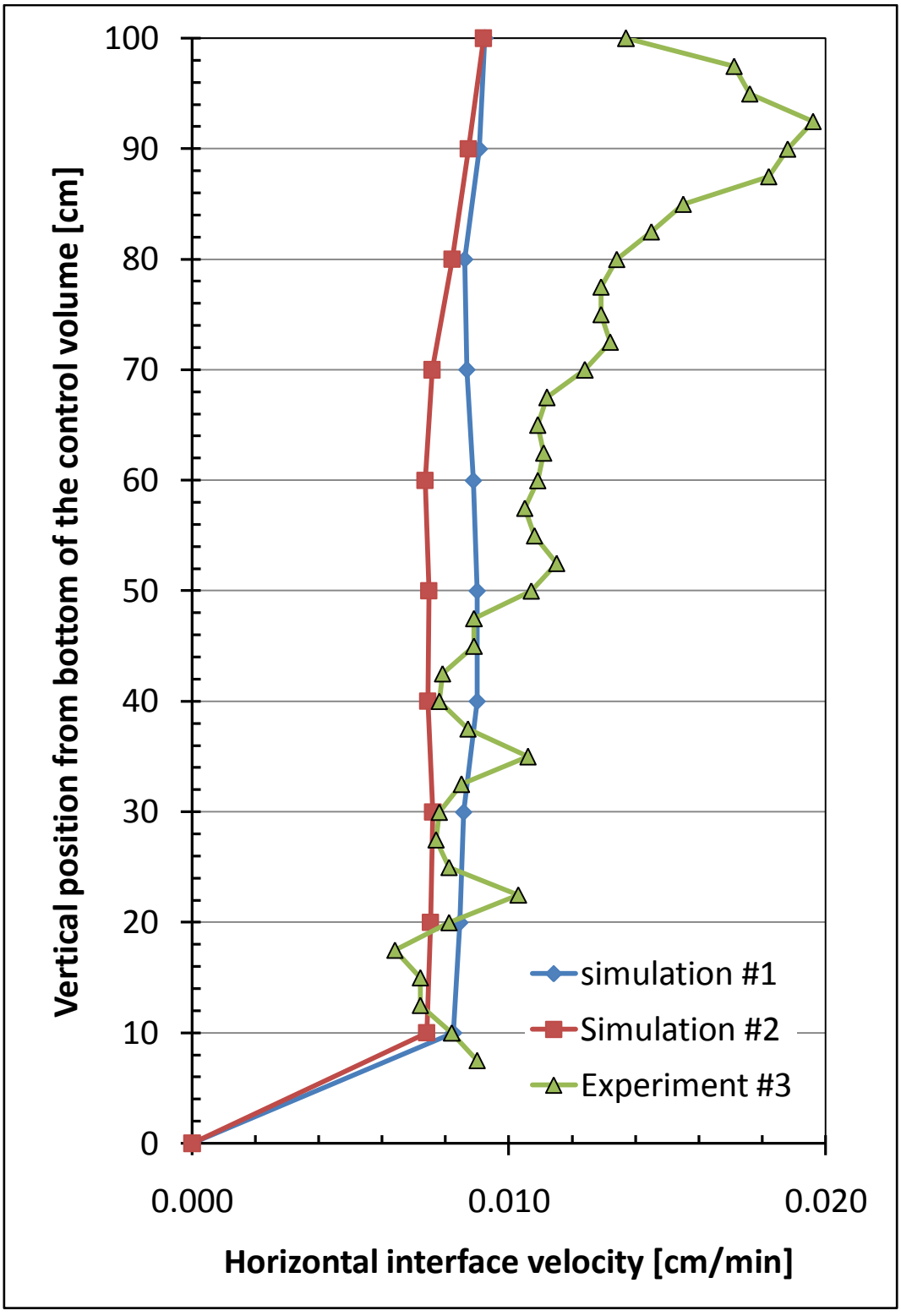

Figure 5-9: Horizontal interface velocities for simulation #1 (mesh size of 1mm by 10mm), simulation #2 (mesh size of 0.67mm by 6.7mm) and experiment #3 (k = $3x10^{-10}$ m^2, no connate water)

5.4.3 Effect of Mesh Size

Two numerical simulations of experiment #3 were conducted using different mesh configuration to study the effect of mesh size on the numerical simulations results. Simulation #1 was conducted with 1 mm by 1 cm mesh size and simulation #2 was conducted with 0.67 mm by 6.7 mm mesh size. Theoretically, smaller mesh size would result in more accurate numerical simulation; however, the minimum size of the mesh is restricted. Smaller mesh size resulted in larger number of elements and increased the number of computation required in the simulation. For example, Simulation # 1 has a total of 2000 elements and approximately 16000 degrees of freedom; the number of meshes increased 125% to 4500 elements in simulation #2 and the degrees of freedom increased to approximately 37000, which is more than double of that of simulation #1. Decreasing in the mesh size increases the memory requirement significantly. Furthermore, run time of simulation #1 was less than 8 hrs, while the runtime of simulation #2 was over 2 days.

The steady state bitumen production rates for simulations #1 and #2 were 0.276 g/min and 0.250 g/min respectively. The bitumen production rate from simulation #1 was approximately 10% larger than that of simulation #2. The horizontal interface velocities for simulations #1 and #2 were 0.0087 cm/min and 0.0076 cm/min respectively, where the horizontal interface velocity for simulation #1 is 13% greater than that of simuation #2. Both the bitumen production rate and the horizontal interface velocity for simulation #1 are greater then that of simulation #2. The reason can be accounted for by a higher numerical dispersion in simulation #1 than in simulation #2.

Numerical dispersion happens when solvent diffuses into an element, and it is immediately dispersed throughout the element due the averaging of element properties. As a result, the larger mesh size, the greater the numerical dispersion and less accurate the numerical simulation. The effect of numerical dispersion on simulation #2, with the smaller mesh size, is less than that of simulation #1; hence, it is fair to conclude the simulation results from simulation #2 are more accurate than that of simulation #1. This also explains why both the bitumen production rate and the horizontal interface velocity for simulation #1 were larger than those of simulation #2 by 12%.

5.5 Recommendations on Improving the Numerical Model

The results from the numerical model indicate that the current model is capable of replicating the experimental results within a 12% difference. The accuracy of the numerical model depends on the quality of the input variables. In additional to mesh size, other factors that may improve the numerical model include: 1) capillary pressure curve, 2) diffusivity and dispersion coefficient, 3) mass transfer rate coefficient, and 4) Mesh Configuration

1) **Capillary pressure curve**

   Capillary pressure curve is critical to the algorithm of the numerical model. It is used to evaluate the liquid saturation of the system. The capillary pressure curves used in this model were calculated based on the capillary pressure curve of a water air drainage system and scaled to the interfacial tension of bitumen and live oil. The capillary pressure data calculated were curve-fitted into van Genuchten correlations to describe the capillary pressure curve in the numerical model. The scaling and the curve-fittings of the water air capillary pressure curve to describe the bitumen drainage affect the accuracy of the capillary pressure curve inputted. In addition, the step function used in distinguishing the bitumen and live oil capillary pressure curves also contribute to the error in the oil saturation calculation. Instead of curve fitting the capillary pressure curve using van Genuchten correlation, another option is to analyze the capillary pressure data graphically using a spiral curve, to reduce the inaccuracy in the capillary pressure data due to curve fitting of data.

2) **Diffusivity and Dispersion coefficient**

   First, the diffusivity used in the numerical model is a constant value. This assumption contradicts the observation made by James et. al. (2004). James et. al. (2004) concluded the diffusivity of butane into bitumen is a function of solvent concentration.

   Second, the dispersion coefficients were estimated using Perkins and Johnson (1963) correlation for dispersion, which is generally applied to a fully saturated system. Although the effect of variable saturation on dispersion in has not been investigated, the effect of variable saturation on dispersion in groundwater solute transport showed that dispersion increases as the saturation of aqueous phase decreases (Nosier et. al.,

2006). This observation may explain the fact that the bitumen production rate from simulation #2 is less than the bitumen production rate from experiment #3.

3) **Mass transfer rate coefficient**

   The mass transfer rate coefficient was estimated using empirical correlation of the modified Sherwood number from NAPL dissolution in water, which was not an ideal representation of the VAPEX process. The effect of such assumption has not been investigated. The mass transfer rate should be found experimentally for the VAPEX problem.

4) **Mesh configuration**

   A quick study was conducted to understand the effect of mesh size on the production history and the solvent chamber growth of the numerical model. The disadvantage of the mesh configuration of the current numerical model is the inability to simulate a very large VAPEX system. In field operation, the dimension of the control volume is in the magnitude of kilometres rather than in millimetres. If the mesh size remains 1 mm by 1 cm or 0.67 mm by 6.7 mm, the total number of element and the total degrees of freedom will be exponential. A suggestion in minimizing such problem is to introduce a variable mesh configuration to the numerical model. The idea is to have smaller size meshes near the interface and larger size meshes in the bitumen and the swept area. The variable mesh configuration should enable the system to have the larger size meshes in the swept area and the bitumen phase, where mass transfer and gravity drainage is minimal, but also have confined meshes near the interface, where mass transfer and gravity drainage is crucial.

The above are factors that may affect the accuracy of the numerical simulation model. Further studies and experiments are required to improve the data inputted into the numerical model; hence, improve the results of the numerical simulation.

6.0 Conclusions

- A new apparatus with packing in an annulus was designed and built. The new apparatus offered superior pressure handling capability and a visible outer surface to study the solvent chamber growth. Production histories indicate the production rates obtained using the new apparatus agree within 16% of those predicted using Oduntan's scale up model. The results verified that the new apparatus for conducting VAPEX experiments is feasible in replicating experimental results obtained with the rectangular packing design.
- Live oil and bitumen production histories, and the solvent chamber growth analysis indicate that the effect of a small value of connate water saturation (i.e. $S_w < 0.07$) on VAPEX is insignificant
- Results from the warm VAPEX experiment show the live oil production rate to double and the bitumen production rate improved by 30% when solvent condensation occurs. The horizontal interface velocity also increased by 38%. In addition, asphaltene precipitation was observed during the warm VAPEX experiment, indicating in-situ upgrading of bitumen during the recovery process. It is believed that the enhancement in the bitumen production rate and horizontal interface velocity will improve if better insulation is applied to the apparatus to avoid solvent condensation in the swept area.
- A new 2-D numerical model of VAPEX was developed using Comsol 3.3. The new numerical design assumed both bitumen and live oil as one liquid phase. The numerical model developed is capable in modeling the production history and the solvent chamber growth of the experiments.
- Two simulations with two different mesh configurations were conducted based on the properties of the experiment #3 to validate the feasibility of the numerical model developed. Bitumen production rates and the horizontal interface velocities agree within 15% of that of experiment #3. The results are expected to improve as more accurate data are imputed into the model.
- The variation of mesh configuration in the numerical simulations (conducted using mesh size of 1 mm by 1 cm and 0.67 mm by 6.7 mm) indicates the effect of mesh

size on the bitumen production rate and horizontal interface velocity is approximately 15%. The difference is due to the larger numerical dispersion that occurs in the larger mesh size.

7.0 Recommendations

The thesis revealed the effect of connate water and solvent condensation on the live oil and bitumen production, the solvent chamber growth and the solvent requirements in VAPEX. Further research is necessary before VAPEX can be applied to commercial use. Such research should include:

- Conducting additional experiments to investigate the effect of a high percentage volume of connate water on the production history and solvent chamber growth of VAPEX.
- Designing a better insulation for the apparatus to improve the quality of the warm VAPEX experiments results by reducing the solvent condensation in the swept area.
- Investigating the effect of in-situ upgrading on bitumen viscosity in warm VAPEX experiments.
- Improving the quality of the numerical simulation results by following the recommendations stated in section 5.5.

References

Azin, R., Kharrat, R. & Ghotbi, C. (2005). *Applicability of the VAPEX process to Iranian oil reservoirs*, SEP 92720.

Boustani, A. and Maini, B.B., (2001) *The Role of Diffusion and Convective Dispersion in Vapour Extraction Process*, JCPT, 40(1)

Boustani, A. (2001). Investigation of Interfacial Mass Transfer in Vapour Extraction Process, University of Calgary, Calgary, Alberta, Canada

Butler, R.M. & Mokrys, I.J. (1989). *Solvent analog model of steam-assisted gravity drainage,* AOSTRA Journal of Research, 5(1), 17-32.

Butler, R.M. *Thermal recovery of oil and bitumen,* Prentice-Hall, Englewood Cliffs, NJ, (1991).

Butler, R.M. & Mokrys, I.J. (1991). *A new process (VAPEX) for recovering heavy oils using hot water and hydrocarbon vapour*, JCPT, 30(1), 97-106.

Butler, R.M. & Mokrys, I.J. (1993). *Recovery of heavy oils using vaporized hydrocarbon solvents: further development of the VAPEX process*, JCPT, 32(6), 56-62.

Chatzis, I. (2002). *Pore scale mechanisms of heavy oil recovery using the VAPEX process*, Paper 2002-198, presented at the Petroleum Society's Canadian International Petroleum Conference 2002, Calgary, Alberta, Canada, 11-13 June, 2002.

Chatzis, I. (2005). *Fundamentals of Petroleum Production*, ChE 614 Class Notes, Dept. of Chemical Engineering, University of Waterloo, Ontario, Canada

Das, S.K. (1995). *In situ recovery of heavy oil and bitumen using vaporized hydrocarbon solvents*, PhD thesis, The University of Calgary, Alberta, Canada.

Das, S.K. (1998). *VAPEX: an efficient process for the recovery of heavy oil and bitumen*, SPE J. 50941, 232-237.

Das, S.K. & Butler, R.M. (1998). *Mechanism of the vapor extraction process for heavy oil and bitumen*, Journal of Petroleum Science and Engineering, 21, 43-59.

Das, S. (2005). *Diffusion and Dispersion in the Simulation of VAPEX Process*, SPE 97924

Donaldson, J. H., Istok, J. D. and O'Reilly K. T. (1998). *Dissolved Gas Transport in the Presence of Trapped Gas Phase: Experimental Evaluation of Two Dimensional Kinetic Model*. Ground water, 36(1),133-142

Dullien, F.A.L. (1992). *Porous Media – Fluid Transport and Pore Structure*, Second Edition, AcademicPress, San Diego.

Dusseault, M.B. (2006). *Future trends in oil and gas industry, Canadian heavy oil resources and new production technologies*, GEOMEC Oil Fields Geomechanics International, available online: www.geomec.com/products/essays/essay01.doc, (Accessed on 13 Feb 2007).

Friedrich, K. (2006).*The effect of non-condensable gas on VAPEX process*, M.A.Sc. Thesis, University of Waterloo, Waterloo, Ontario, Canada.

Ioannidis, M., Chatzis, I., Lemaire , C. & Perunarkilli, R. (2006). *Unsaturated Hydrualic Conductivity from Nuclear Magnetic Resonance Measurements*, Water Resources Research (42), W07201

James, L.A. (2003). *A closer look at VAPEX*, M.A.Sc. Thesis, University of Waterloo, Waterloo, Ontario, Canada.

James, L. & Chatzis, I. (2004). *Details of gravity drainage of heavy oil during vapour extraction*, presented at the International Society of Core Analysis, held in Abu Dhabi, UAE, 5-9 October, 2004.

James, L., Rezaei, N., & Chatzis, I. (2007). *VAPEX, Warm VAPEX, and Hybrid VAPEX – The State of Enhanced Oil Recovery for In-Situ Heavy Oils in Canada,* Paper 2007-200 in the proceedings of Canadian International Petroleum Conference 2001, Calgary, Alberta, Canada, June 12-14, 2007.

Jin, W., (1999). *Heavy Oil Recovery Uisng the Vapex Process*, M.A.Sc. Thesis, University of Waterloo, Waterloo, Ontario, Canada

Kapadia R. , Upreti, S. , Lohi, A., & Chatzis, I. (2006). *Determination of Gas Dispersion in Vapor Extraction of Heavy Oil and Bitumen*, Journal of Petroleum Science and Engineering, 51, 214-222.

Karmaker, K. and Maini, B.B. (2003). *Applicability of Vapour Extraction Process to Problematic Viscous Oil Reservoirs*, SPE 84034, presented at the SPE annual Technical Conference and Exhibition, Denver, Colorado, October 5-8, 2003

Li, T. M. W. (2004). *Recovery of Source Non-aqueous Phase Liquids from Groundwater Using Supersaturated Water Injection,* M.A.Sc. Thesis, University of Waterloo, Waterloo, Ontario, Canada

Luo, P. and Gu, Y. (2005). Effects of Asphaltene Content and Solvent Concentration on Heavy Oil Viscosity, SPE 97778

Miller, C., Poirier-McNeill, & Mayer, A. (1990). Dissolution of Trapped Nonaqueous Phase Liquids: Mass Transfer Characteristics, Water Resources Research, 26(11), 2783-2796

Nambi, I. & Power, S. (2003). *Mass transfer correlations for nonaqueous phase liquid dissolution from regions with high initial saturations,* Water Resources Research, 39(2), 1030

Nosier, S. A., El-Khiary, M. I., Nasr, M. A. & Mubarak, A. A. (2006). *Diffusion Controlled Corrosion in Gas Sparged Systems*, Chem Biochem. Eng., 20(1), 47-53

Oduntan, A.R. (2001). Heavy Oil Recovery Using the VAPEX Process: Scale-Up and Mass Transfer Issues, M.A.Sc. Thesis, University of Waterloo, Waterloo, Ontario, Canada.

Oduntan, A.R., Chatzis, I., Smith, J. & Lohi, A. (2001). *Heavy oil recovery using the VAPEX process: scale-up and the mass transfer issues*, Paper 2001-127 in the proceedings of Canadian International Petroleum Conference 2001, Calgary, Alberta, Canada, June 12-14.

Perkins, T. K. and Johnston, O.C., (1963). A Review of Diffusion and Dispersion in Porous media. SPE Reprint Series, Miscible Displacement, pp. 77-91

Ramakrishnan, Venkatesh (2003). *In-situ Recovery of Heavy Oil by VAPEX using Propane*, M.A.Sc. Thesis, University of Waterloo, Waterloo, Ontario, Canada

Scion Image, Scion Corporation, Frederick, Maryland, USA.

Sedaee Sola, B. & Rashidi, F. (2006). *Application of the SAGD to an Iranian carbonate heavy-oil reservoir*, SPE 100533.

Shu, W.R. (1984). *A Viscosity Correlation for Mixtures of Heavy Oil, Bitumen and Petroleum Fraction*, SPE, 24(3), 277-282.

Singhal, A.K., Das, S.K., Leggitt, S.M., Kasraie, M. & Ito, Y. (1996). *Screening of reservoirs for exploitation by application of steam assisted gravity drainage/VAPEX processes*, SPE 37144.

STARS, Computer Modeling Group (CMG) Ltd., Calgary, Alberta, Canada.

Upreti, S.R., and Mehrotra, A.K. (2002). *Diffusivity of CO_2, CH_4, C_2H_6 and N_2 in Athabasca Bitumen*, The Canadian Journal of Chemical Engineering, 80, 116-125.

Wen, Y. & Kantzas (2006) A. *Evaluation of Heavy Oil/ Bitumen – Solvent Mixture Viscosity Model*, JCPT, 45(4)

Yazdani, A. & Maini, B.B. (2005). *Effects of drainage height and grain size on production rates in the VAPEX process: experimental study*, SPE Reservoir Evaluation and Engineering, SPE 89409.

Zhang, Y.P., Hyndman, C.L., and Maini, B.B., (2000). *Measurement of Gas Diffusivity in Heavy Oils*, Journal of Petroleum Science and Engineering, 25, 37-47.

Zhang, H., Luo, G., Gu, Y. (2006). Physical Modeling of Heavy Oil Production Rate in a Vapour Extraction Process. *Proceedings: Canadian International Petroleum Conference*, Calgary, AB, June 13-15, 2006, Paper 2006-142.

Appendix A: Apparatus Design Calculations

Apparatus Design Calculation:

For outer tube:

The apparatus is a thick wall pressure vessel, the calculation is as follows (Ugural and Fenster, 2003):

$$\sigma_\theta = \frac{a^2 P_i}{b^2 - a^2}\left[1 + \left(\frac{b}{r}\right)^2\right]$$

$$\sigma_r = \frac{a^2 P_i}{b^2 - a^2}\left[1 - \left(\frac{b}{r}\right)^2\right]$$

$$\sigma_z = \frac{a^2 P_i}{b^2 - a^2}$$

where σ_θ is hoop stress of the tube

σ_r is radial stress of the tube

σ_z is longitudinal stress of the tube

a is the inner radius of the tube

b is the outer radius of the tube

P_i is the pressure applied

r is the radius of the tube, where the maximum stress occurs at r=a

$$\sigma_{eq} = \sqrt{\sigma_r^2 + \sigma_\theta^2 + \sigma_z^2 - \sigma_r\sigma_\theta - \sigma_r\sigma_z - \sigma_z\sigma_\theta}$$

where σ_{eq} is equivalent stress of the tube,

if $\sigma_{eq} < \sigma_{rupture}$ the design is safe; if $\sigma_{eq} > \sigma_{rupture}$ the design will fail

For the outer cylinder		
a	1.25	in
b	1.5	in
P	100	psi
hoop stress	554.5455	
radial stress	-100	
longitudinal stress	227.2727	
equivalent stress	566.853	
rapture stress	45	kpsi

For 100 psig, $\sigma_{eq} << \sigma_{rupture}$, the outer tube is safe for the apparatus design

Appendix B: Derivation of Governing Equations

The following section discusses the derivation of the governing equations used in the numerical simulation.

Convective Diffusion Equation for a Variable Saturation System:

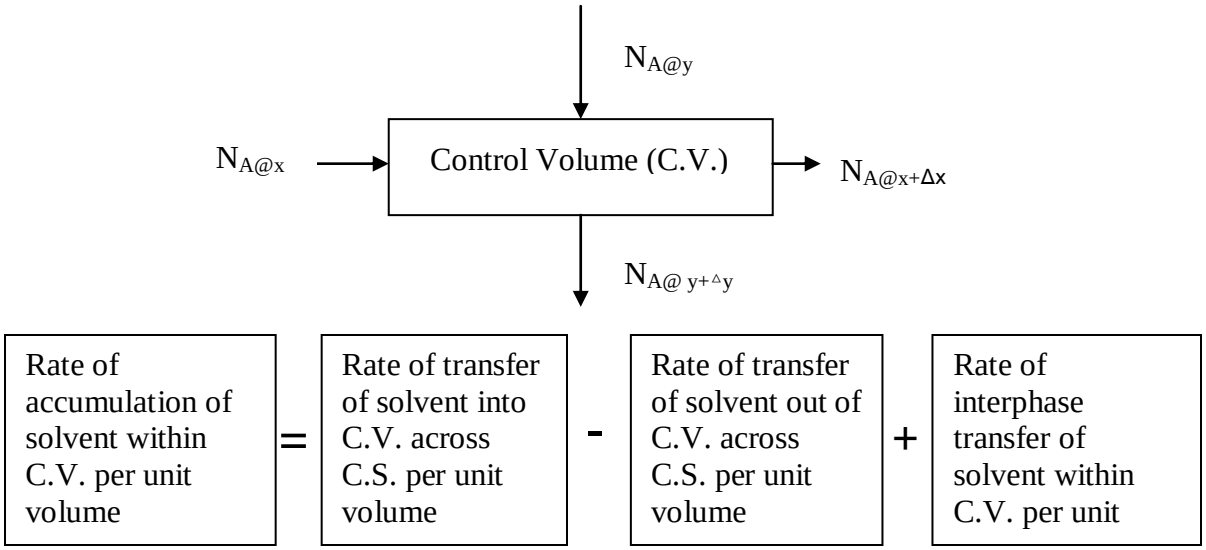

$$\frac{\partial(\rho_o \omega_s S_o \emptyset)}{\partial t} = \frac{\partial N_{Sx}}{\partial x} + \frac{\partial N_{Sy}}{\partial y} + \vec{J}_m \quad \text{(B-1)}$$

$$\frac{\partial(\rho_o \omega_s S_o \emptyset)}{\partial t} = \nabla \cdot N_S + \vec{J}_m \quad \text{(B-2)}$$

$$\overrightarrow{N_S} = (\rho_o \omega_s \vec{v}_o - \emptyset S_o D_{SB} \rho_o \nabla \omega_s) \quad \text{(B-3)}$$

$$\frac{\partial(\rho_o \omega_s \emptyset S)}{\partial t} - \nabla \cdot (\rho_o \omega_s \overrightarrow{v_o} - \emptyset S_o D_{SB}\, \rho_o \nabla \omega_s) = \vec{J}_m \quad \text{(B-4)}$$

The predefined convective diffusion equation for constant saturation system in Comsol is as follows:

$$\delta_{st} \frac{\partial c}{\partial t} + \nabla \cdot (-D \nabla c + \overrightarrow{v_o} c) = R \quad \text{(B-5)}$$

where the time scaling factor (δ_{st}), hydrodynamic dispersion (D), and the Darcy's velocity of oil flow (v_o) and additional variable (R) are the input parameters in Comsol. Equation (B-5) only applies to mass transfer in a constant saturation system; it has to be modified in order to

describe the mass transfer of solvent in VAPEX Equation (B-4). Consider constant oil density and porosity throughout the control volume, Equation (B-4)becomes:

$$\emptyset \frac{\partial(\omega_s S_o)}{\partial t} + \nabla \cdot (-\emptyset S D_{SB} \nabla \omega_s + \omega_s \overrightarrow{v_o}) = \frac{\vec{J}_m}{\rho_o} \quad \text{(B-6)}$$

The time derivative of the Equation (B-6) is expanded as follows:

$$\emptyset \frac{\partial(\omega_s S_o)}{\partial t} = \emptyset \left[S \frac{\partial \omega_s}{\partial t} + \omega_s \frac{\partial S}{\partial t} \right] \quad \text{(B-7)}$$

Hence, Equation (B-2) becomes:

$$\emptyset \left[S_o \frac{\partial \omega_s}{\partial t} + \omega_s \frac{\partial S_o}{\partial t} \right] + \nabla \cdot (-\emptyset S D_{SB} \nabla \omega_s + \omega_s \overrightarrow{v_o}) = \frac{\vec{J}_m}{\rho_o} \quad \text{(B-8)}$$

The input parameters (D, v_o, δ_{st} and R) in Comsol are as follows:

Input parameters in Comsol	Corresponding term in physical model
D	$\phi S_o D_{SB}$
v_o	v_o
δ_{st}	ϕS
R	$-\emptyset \omega_s \frac{\partial S}{\partial t} + \frac{\overrightarrow{J_m}}{\rho_o}$
c	ω_s

Continuity Equation

The following equation is the continuity equation for liquid phase with constant density:

$$\emptyset \frac{\partial S_o}{\partial t} + \nabla \cdot \overrightarrow{v_o} = 0 \quad \text{(B-9)}$$

The velocity of the oil phase is calculated by Darcy's equation:

$$\overrightarrow{v_o} = -\frac{k k_{ro}}{\mu_o} (\nabla P_o - \rho_o \vec{g}) \quad \text{(B-10)}$$

As the result, the continuity equation for the oil phase becomes

$$\emptyset \frac{\partial S_o}{\partial t} + \nabla \cdot \left[-\frac{k k_{ro}}{\mu_o} (\nabla P_o - \rho_o \vec{g}) \right] = 0 \quad \text{(B-11)}$$

The continuity equation for the gas phase is derived using similar method

$$\emptyset \frac{\partial S_s}{\partial t} + \nabla \cdot \overrightarrow{v_g} = 0 \quad \text{(B-12)}$$

$$\overrightarrow{v_g} = -\frac{k k_{rg}}{\mu_g} \left(\nabla P_g - \rho_g \vec{g} \right) \quad \text{(B-13)}$$

$$\emptyset \frac{\partial S_s}{\partial t} + \nabla \cdot \left[-\frac{k k_{rg}}{\mu_g} \left(\nabla P_g - \rho_g \vec{g} \right) \right] = 0 \quad \text{(B-14)}$$

Considering the velocity of solvent is negligible compare to that of the liquid phase, Equation (B-11) is eliminated. The gravity drainage of the control volume is governed by Equation (B-8). The predefined Darcy's equation under the earth science module in Comsol is stated as follows:

$$\delta_{st} C_p \frac{\partial P_o}{\partial t} + \nabla \cdot \left[\delta_k \frac{\kappa}{\mu} (\nabla P_o + \rho_o \vec{g} \nabla D) \right] = \delta_Q Q \quad \text{(B-15)}$$

where time scaling factor (δ_{ts}), flux scaling factor (δ_k), Source Scaling factor (δ_Q), storage term (C_p), permeability (κ), viscosity (μ), fluid density (ρ_f) and, the source term (Q) are input parameters. Comsol evaluates the pressure distribution in the liquid phase; however, it does not evaluate the liquid saturation in the control volume. The storage term (C_p) was modified to calculate the change in effective oil saturation. As a result, the time derivative in Equation (B-12) is modified to incorporate the saturation calculation:

$$C_p \frac{\partial P_o}{\partial t} = \emptyset (1 - S_r) \frac{\partial S_{eo}}{\partial P_0} \frac{\partial P_o}{\partial t} \quad \text{(B-16)}$$

Therefore,

$$C_p = \emptyset (1 - S_r) \frac{\partial S_{eo}}{\partial P_0} = -\emptyset (1 - S_r) \frac{1}{\rho_o \vec{g}} \frac{\partial S_{eo}}{\partial H_p}$$

where, porosity (ϕ) and residual oil saturation (S_r) are predefined values. Hp is the capillary pressure head ($H_p = \frac{P_g - P_o}{\rho_o \vec{g}}$). Hence, the continuity equation becomes

$$\emptyset (1 - S_r) \frac{\partial S_{eo}}{\partial P_0} \frac{\partial P_o}{\partial t} + \nabla \cdot \left[\frac{k_o k_{ro}}{\mu(\omega_s)} (\nabla P_o + \rho_o \vec{g} \nabla D) \right] = 0 \quad \text{(B-17)}$$

Or

$$-\emptyset(1-S_r)\frac{1}{\rho_o\vec{g}}\frac{\partial S_{eo}}{\partial H_p}\frac{\partial P_o}{\partial t}+\nabla\cdot\left[\frac{k_o k_{ro}}{\mu(\omega_s)}(\nabla P_o+\rho_o\vec{g}\nabla D)\right]=0 \qquad \textbf{(B-18)}$$

Equation (B-14) neglected the residual oil saturation in the calculation and only evaluates the effective oil saturation of the control volume.

The inputted variables for the Equation (B-18) are as follows:

Parameter in Comsol	Value inputted
C_p	$\emptyset(1-S_r)\frac{\partial S_{eo}}{\partial P_o}$ *or* $-\emptyset(1-S_r)\frac{1}{\rho_o\vec{g}}\frac{\partial S_{eo}}{\partial H_p}$ using van Genuchten correlation $\frac{\alpha m}{1-m}\frac{\emptyset(1-S_r)}{\rho_o\vec{g}}S_{eo}^{\frac{1}{m}}\left(1-S_{eo}^{\frac{1}{m}}\right)^m$
v_o	v_o
δ_{st}	1
δ_k	1
δ_Q	0
K	$k_o k_{ro}$
ρ_f	ρ_o
μ_o	$\mu_o(\omega_s)$
D	y-axis

Appendix C: Model Report from Comsol

water drainage +diffusion

1. Table of Contents

2. Model Properties

Property	**Value**
Model name	water drainage +diffusion
Author	Sindy Tam
Company	University of Waterloo

Department	Chemical Engineering
Reference	
URL	
Saved date	Aug 9, 2007 4:18:26 PM
Creation date	Aug 20, 2005 6:34:04 PM
COMSOL version	COMSOL 3.3.0.405

File name: D:\Sindy-t\New Folder\mesh analysis\New Folder\K=.3, D include Upv, K=300-5 smaller mesh.mph

Application modes and modules used in this model:

Geom1 (2D)

Darcy's Law (Earth Science Module)

Convection and Diffusion (Chemical Engineering Module)

4. Geom1

Space dimensions: 2D

Independent variables: x, y, z

4.1. **Scalar Expressions**

Name	**Expression**
pin	rhowater*g_w*(1-y)
Hc	(0-pw)/(rhowater*g_w)
Sew	(1+abs(alpha*Hc)^N)^(-M)*(Hc>0)+1*(Hc<=0)
thetaw	(thetar+Sew*(thetas-thetar))*(Hc>0)+thetas*(Hc<=0)
krw	(Sew^4)*(Hc>0)+1*(Hc<=0)

Cp	1/rhowater/g_w*((alpha*M/(1-M)*(thetas-thetar)*Sew^(1/M)*(1-Sew^(1/M))^M))*(Hc>0)
Senw	1-Sew
Try	c*diff(thetaw,t)
alpha	20*(c>0.2)+9*(c<=.2)
source	Kc*Snw^1.24*(Cmax-c)*(Senw>=0.45)
Vpv	abs(v_w)/.395
Upv	abs(u_w)/.395
Tpv	(Upv^2+Vpv^2)^(-0.5)
Sw	thetaw/thetas
Snw	1-Sw

4.2. **Expressions**

4.2.1. Subdomain Expressions

Subdomain	1
kaps	3e-010
thetas	0.395
thetar	0.0395
N	9
L	0.5
M	1-1/N

4.3. Mesh

4.3.1. Mesh Statistics

Number of degrees of freedom	36722

Number of mesh points	4681
Number of elements	4500
Triangular	0
Quadrilateral	4500
Number of boundary elements	360
Number of vertex elements	5
Minimum element quality	0.186
Element area ratio	0.917

4.4. Application Mode: Darcy's Law (w)

Application mode type: Darcy's Law (Earth Science Module)

Application mode name: w

4.4.1. Scalar Variables

Name	Variable	Value	Description
tscale	tscale_w	1e-5	Heaviside scaling factor
g	g_w	9.82*time^2	Gravity
D	D_w	y	Elevation/vertical axis

4.4.2. Application Mode Properties

Property	**Value**
Default element type	Lagrange - Quadratic
Variable	Pressure analysis
Analysis type	Transient
Frame	Frame (xy)
Weak constraints	Off

4.4.3. Variables

Dependent variables: pw

Shape functions: shlag(2,'pw')

Interior boundaries not active

4.4.4. Boundary Settings

Boundary		1-3, 5	4
Type		Zero flux/Symmetry	Pressure

4.4.5. Subdomain Settings

Locked Subdomains: 1

Subdomain		1
Storage term (S)	1	Cp
Saturated permeability (kaps)	m^2	kaps*krw
Density-liquid (rhof)	kg/m^3	rhowater
Viscosity-liquid (eta)	Pa·s	etaw(c)*time

Subdomain initial value		1
Pressure (pw)	Pa	pin

4.5. Application Mode: Convection and Diffusion (chcd)

Application mode type: Convection and Diffusion (Chemical Engineering Module)

Application mode name: chcd

4.5.1. Application Mode Properties

Property	**Value**
Default element type	Lagrange - Quadratic
Analysis type	Transient

Equation form	Conservative
Equilibrium assumption	Off
Frame	Frame (xy)
Weak constraints	Off

4.5.2. Variables

Dependent variables: c

Shape functions: shlag(2,'c')

Interior boundaries not active

4.5.3. Boundary Settings

Boundary		1-3	4
Type		Insulation/Symmetry	Convective flux
Concentration (c0)	mol/m^3	0	0

Boundary	5
Type	Concentration
Concentration (c0)	**Cmax**

4.5.4. Subdomain Settings

Locked Subdomains: 1

Subdomain		1
Diffusion coefficient (D)	m^2/s	**5e-6*thetaw**
Diffusion coefficient (dtensor)	m^2/s	**{{'(Dm+(alphaL*Upv^2+alphaT*Vpv^2)*Tpv)*thetaw','Dm*thetaw';'Dm*thetaw','(Dm+(alphaT*Upv^2+alphaL*Vpv)*Tpv)*thetaw'}}**
dtype		**aniso**

Reaction rate (R)	mol/(m^3·s)	**-Try+source**
Time-scaling coefficient (Dts)	1	**thetaw**
x-velocity (u)	m/s	**u_w**
y-velocity (v)	m/s	**v_w**

5. Constants

Name	**Expression**	**Value**	**Description**
rhowater	850		
time	60		
alphaT	alphaL/24		
alphaL	5.11e-4		
Dm	5e-10*time		
Kc	.284		
Cmax	0.38		

6. Integration Coupling Variables

6.1. Geom1

6.1.1. Source Subdomain: 1

Name	Value
Variable name	Se
Expression	Sew
Order	4
Global	Yes

7. **Interpolation Functions**

7.1. Interpolation Function: etaw

Interpolation method: Cubic Spline

8. Equations

8.1. Point

Dependent variables: pw, c

8.1.1. Point: 1-5

weak term (weak)

0
0

dweak term (dweak)

0
0

constr term (constr)

0
0

8.2. Boundary

Dependent variables: pw, c

8.2.1. Boundary: 1-3

q coefficient

pw	c

0	0
0	0

g coefficient

0
0

h coefficient

pw	c
0	0
0	0

r coefficient

0
0

weak term (weak)

0
0

dweak term (dweak)

0
0

constr term (constr)

0
0

8.2.2. Boundary: 4

q coefficient

pw	c
0	0
-diff(-(nx_chcd*u_c_chcd+ny_chcd*v_c_chcd)*c,pw)	-diff(-(nx_chcd*u_c_chcd+ny_chcd*v_c_chcd)*c,c)

g coefficient

0
-(nx_chcd*u_c_chcd+ny_chcd*v_c_chcd)*c

h coefficient

pw	c
-diff(-pw,pw)	-diff(-pw,c)
0	0

r coefficient

-pw
0

weak term (weak)

0
0

dweak term (dweak)

0
0

constr term (constr)

0
0

8.2.3. Boundary: 5

q coefficient

pw	c
0	0
0	0

g coefficient

0
0

h coefficient

pw	c
0	0
-diff(-c+c0_c_chcd,pw)	-diff(-c+c0_c_chcd,c)

r coefficient

0
-c+c0_c_chcd

weak term (weak)

0
0

dweak term (dweak)

0
0

constr term (constr)

0
0

8.3. Subdomain

Dependent variables: pw, c

8.3.1. Subdomain: 1 [locked]

Diffusion coefficient (c)

Pw	c
-diff(-(kap_w/eta_w*pwx+rhof_w*g_w*kap_w/eta_w*diff(D_w,x)),pwx), -diff(-(kap_w/eta_w*pwy+rhof_w*g_w*kap_w/eta_w*diff(D_w,y)),pwx), -diff(-(kap_w/eta_w*pwx+rhof_w*g_w*kap_w/eta_w*diff(D_w,x)),pwy), -diff(-(kap_w/eta_w*pwy+rhof_w*g_w*kap_w/eta_w*diff(D_w,y)),pwy)	-diff(-(kap_w/eta_w*pwx+rhof_w*g_w*kap_w/eta_w*diff(D_w,x)),cx), -diff(-(kap_w/eta_w*pwy+rhof_w*g_w*kap_w/eta_w*diff(D_w,y)),cx), -diff(-(kap_w/eta_w*pwx+rhof_w*g_w*kap_w/eta_w*diff(D_w,x)),cy), -diff(-(kap_w/eta_w*pwy+rhof_w*g_w*kap_w/eta_w*diff(D_w,y)),cy)
-diff(u_c_chcd*c-Dxx_c_chcd*cx-Dxy_c_chcd*cy,pwx), -diff(v_c_chcd*c-Dyx_c_chcd*cx-Dyy_c_chcd*cy,pwx), -diff(u_c_chcd*c-Dxx_c_chcd*cx-Dxy_c_chcd*cy,pwy), -diff(v_c_chcd*c-Dyx_c_chcd*cx-Dyy_c_chcd*cy,pwy)	-diff(u_c_chcd*c-Dxx_c_chcd*cx-Dxy_c_chcd*cy,cx), -diff(v_c_chcd*c-Dyx_c_chcd*cx-Dyy_c_chcd*cy,cx), -diff(u_c_chcd*c-Dxx_c_chcd*cx-Dxy_c_chcd*cy,cy), -diff(v_c_chcd*c-Dyx_c_chcd*cx-Dyy_c_chcd*cy,cy)

Absorption coefficient (a)

pw	c
0	0
-diff(R_c_chcd,pw)	-diff(R_c_chcd,c)

Source term (f)

0
R_c_chcd

Damping/Mass coefficient (da)

pw	c
Cp+eps	0
0	Dts_c_chcd

Conservative flux convection coeff. (al)

pw	c
-diff(-(kap_w/eta_w*pwx+rhof_w*g_w*kap_w/eta_w*diff(D_w,x)),pw), -diff(-(kap_w/eta_w*pwy+rhof_w*g_w*kap_w/eta_w*diff(D_w,y)),pw)	-diff(-(kap_w/eta_w*pwx+rhof_w*g_w*kap_w/eta_w*diff(D_w,x)),c), -diff(-(kap_w/eta_w*pwy+rhof_w*g_w*kap_w/eta_w*diff(D_w,y)),c)
-diff(u_c_chcd*c-Dxx_c_chcd*cx-Dxy_c_chcd*cy,pw), -diff(v_c_chcd*c-Dyx_c_chcd*cx-Dyy_c_chcd*cy,pw)	-diff(u_c_chcd*c-Dxx_c_chcd*cx-Dxy_c_chcd*cy,c), -diff(v_c_chcd*c-Dyx_c_chcd*cx-Dyy_c_chcd*cy,c)

Convection coefficient (be)

pw	c
0, 0	0, 0
-diff(R_c_chcd,pwx), -diff(R_c_chcd,pwy)	-diff(R_c_chcd,cx), -diff(R_c_chcd,cy)

Conservative flux source term (ga)

-(kap_w/eta_w*pwx+rhof_w*g_w*kap_w/eta_w*diff(D_w,x)), -(kap_w/eta_w*pwy+rhof_w*g_w*kap_w/eta_w*diff(D_w,y))
u_c_chcd*c-Dxx_c_chcd*cx-Dxy_c_chcd*cy, v_c_chcd*c-Dyx_c_chcd*cx-Dyy_c_chcd*cy

weak term (weak)

0
0

dweak term (dweak)

0
0

constr term (constr)

0
0

Ultraweak term (bnd.weak)

0
0

9. Variables

9.1. Point

Name	Description	Expression
rhof_w	Density	rhowater

9.2. Boundary

Name	Description	Expression
nU_w	Normal velocity	u_w * nx_w+v_w * ny_w

flux_w	Outward flux	u_w * nx_w+v_w * ny_w
ndflux_c_chcd	Normal diffusive flux, c	nx_chcd * dflux_c_x_chcd+ny_chcd * dflux_c_y_chcd
ncflux_c_chcd	Normal convective flux, c	nx_chcd * cflux_c_x_chcd+ny_chcd * cflux_c_y_chcd
ntflux_c_chcd	Normal total flux, c	nx_chcd * tflux_c_x_chcd+ny_chcd * tflux_c_y_chcd

9.3. Subdomain

Name	**Description**	**Expression**
S_w	Storage term	Cp * CSs_w
Qs_w	Liquid source	0
K_w	Hydraulic conductivity tensor	Ks_w * CKs_w
Kxx_w	Hydraulic conductivity tensor	K_w
Kxy_w	Hydraulic conductivity tensor	0
Kyx_w	Hydraulic conductivity tensor	0
Kyy_w	Hydraulic conductivity tensor	K_w
kap_w	Permeability tensor	kaps_w * CKs_w
kapxx_w	Permeability tensor	kap_w
kapxy_w	Permeability tensor	0
kapyx_w	Permeability tensor	0
kapyy_w	Permeability tensor	kap_w

gradP_w	Pressure gradient	sqrt(pwx^2+pwy^2)
u_w	x-velocity	-(kapxx_w * (pwx+diff(rhof_w * g_w * D_w,x))+kapxy_w * (pwy+diff(rhof_w * g_w * D_w,y)))/eta_w
v_w	y-velocity	-(kapyx_w * (pwx+diff(rhof_w * g_w * D_w,x))+kapyy_w * (pwy+diff(rhof_w * g_w * D_w,y)))/eta_w
U_w	Velocity field	sqrt(u_w^2+v_w^2)
grad_c_x_chcd	Concentration gradient, c, x component	cx
dflux_c_x_chcd	Diffusive flux, c, x component	-(Dxx_c_chcd * cx+Dxy_c_chcd * cy)
cflux_c_x_chcd	Convective flux, c, x component	c * u_c_chcd
tflux_c_x_chcd	Total flux, c, x component	dflux_c_x_chcd+cflux_c_x_chcd
grad_c_y_chcd	Concentration gradient, c, y component	cy
dflux_c_y_chcd	Diffusive flux, c, y component	-(Dyx_c_chcd * cx+Dyy_c_chcd * cy)
cflux_c_y_chcd	Convective flux, c, y component	c * v_c_chcd
tflux_c_y_chcd	Total flux, c, y component	dflux_c_y_chcd+cflux_c_y_chcd
beta_c_x_chcd	Convective field, c, x component	u_c_chcd
beta_c_y_chcd	Convective field, c, y component	v_c_chcd
grad_c_chcd	Concentration gradient, c	sqrt(grad_c_x_chcd^2+grad_c_y_chcd^2)
dflux_c_chcd	Diffusive flux, c	sqrt(dflux_c_x_chcd^2+dflux_c_y_chcd^2)
cflux_c_chcd	Convective flux, c	sqrt(cflux_c_x_chcd^2+cflux_c_y_chcd^2)
tflux_c_chcd	Total flux, c	sqrt(tflux_c_x_chcd^2+tflux_c_y_chcd^2)

cellPe_c_chcd	Cell Peclet number, c	h * sqrt(beta_c_x_chcd^2+beta_c_y_chcd^2)/Dm_c_chcd
Dm_c_chcd	Mean diffusion coefficient, c	(Dxx_c_chcd * u_c_chcd * u_c_chcd+Dxy_c_chcd * u_c_chcd * v_c_chcd+Dyx_c_chcd * v_c_chcd * u_c_chcd+Dyy_c_chcd * v_c_chcd * v_c_chcd)/(u_c_chcd^2+v_c_chcd^2+eps)
res_c_chcd	Equation residual for c	-(Dxx_c_chcd * cxx+Dxy_c_chcd * cxy-cx * u_c_chcd+Dyx_c_chcd * cyx+Dyy_c_chcd * cyy-cy * v_c_chcd+R_c_chcd)
res_sc_c_chcd	Shock capturing residual for c	cx * u_c_chcd+cy * v_c_chcd-R_c_chcd
da_c_chcd	Total time scale factor, c	Dts_c_chcd